Biodegradable hydrogels based on water-soluble chitosan for cell transplant

Thesis submitted by

Mª Amparo Gámiz González

To obtain the degree of Doctor

at Universitat Politècnica de València

Thesis supervisors:

Prof. Dr. José Luís Gómez Ribelles

Prof. Dr. Ana Vidaurre Garayo

Center for Biomaterials and Tissue Engineering

Universitat Politècnica de València

Universitat Politècnica de València

July 2016

PhD program in Tecnologías para la Salud y el Bienestar,
Universitat Politècnica de València, 2016

PhD Thesis.

Biodegradable hydrogels based on water-soluble chitosan for cell transplant.

Author:

Mª Amparo Gámiz González

Thesis Supervisors:

Prof. Dr. José Luís Gómez Ribelles

Centro de Biomateriales e Ingeniería Tisular

Universitat Politècnica de València

Prof. Dr. Ana Vidaurre Garayo

Centro de Biomateriales e Ingeniería Tisular

Universitat Politècnica de València

The research described in this thesis was carried out at the Center for Biomaterials and Tissue Engineering of the Universitat Politècnica de València, Valencia, Spain.

The work had the financial support by the project MAT2010-21611-C03-01, MAT2013-46467-C4-1-R and the Spanish Ministry through the grant BES-2011-044740 in the FPI program.

A mi familia.

"Cualquier cosa que decidas hacer en la vida,
hay que hacerla con el corazón.
Si no, está vacía."

Joaquín Sabina

Agradecimientos

En primer lugar, quisiera agradecer a José Luis Gómez Ribelles por haberme brindado la oportunidad de formar parte de su equipo de investigación. Aunque no fue siempre fácil, he podido crecer profesionalmente con sus consejos, su apoyo y sus grandes ideas. A Ana Vidaurre Garayo, por orientarme y apoyarme en todo momento, dándole ese toque de paciencia a mi vida. Siempre os agradeceré el haber confiado en mí.

Me gustaría dar las gracias al Servicio de Microscopia, Manolo, José Luis, Merche y Alicia, de la Universitat Politècnica de València. Al Instituto de Tecnología Química, Guillermo y Judit del grupo de Avelino Corma y a Ismael y Pablo del grupo de Jaime Primo. A Estrella del servicio de Resonancia Magnético Nuclear. A Isabel Solana, de la Universitat de València.

Debo agradecer a aquellas personas que han formado parte de este trabajo y que me han guiado y apoyado durante mis estancias en otros centros de investigación. Al Profesor Senentxu Lanceros de la Universidade do Minho y a su grupo: Daniela, Pedro, Clarisse, Juan Alberto y en especial a Vitor Sencadas por su disponibilidad y ayuda incondicional.

A la Profesora Ulrica Edlunde y a la gente del KTH, Laleh, Annas, Parmida, Arturo, Channgan, Robertus, Minha, Veluska, Carmen, Rosana y

Gonzalo, por hacerme sentir como en casa y ayudarme en todo momento.

A los estudiantes que me han acompañado a lo largo del camino, porque el aprendizaje ha sido mutuo, aquí hay un trocito de cada uno de ellos. A Laura Teruel por ser un pilar fundamental en el centro. A Christos Pandis por sus consejos y por su buen humor. A Carmen y Ximo por su paciencia con las células y mis hidrogeles.

A los que día a día me han acompañado, María, Miriam L, Miriam H, Cristina, Marco, Virginia, Sara, Pepe, Laia, Luis Andrés, Clara…, porque aunque ya no están en el centro seguimos compartiendo ideas, risas y noticias. A Manu que todavía seguimos codo con codo formándonos para este mundo tan grande.

A los que todavía me acompañan Álvaro, Silvia, María, Laura, Guillermo, en general a todo el CBIT por compartir ideas, risas en definitiva buenos y no tan buenos momentos.

A los profesores e investigadores del centro por resolver cualquier duda o por simplemente dar ánimo y buenos consejos.

A mis amigos, que siempre están apoyándome, con vosotros la vida es mejor.

Finalmente a mi familia, porque sin ellos hoy no estaría donde estoy. A mi padre, por sus sabios consejos, por ser un gran luchador, gran padre y mejor persona, tú haces que nunca sintamos ese vacío tan grande. A mis hermanos, Jose y Ana por ser un pilar fundamental en mi vida y a mi sobrino, Hugo que nos saca la sonrisa día a día. Pero en especial a mi Madre.

Abstract

The aim of tissue engineering is to develop functional biological substitutes to replace or restore damaged tissues by preparing three-dimensional scaffolds able to accommodate cells plus signaling factors to promote the regeneration of damaged tissue. These materials should be biodegradable and disappear as new tissue is being regenerated. For this reason there is a special interest in developing scaffolds that while providing a favourable environment for cells also possess a degradation rate that can be adapted to the tissue's rate of regeneration. Scaffolds should be porous and possess a pore morphology adapted to the application for which they are designed. They must also be able to hold large quantities of water (hydrogels) while presenting suitable cell/biomaterial interaction (hydrophobic materials in general have better cell adhesion).

The aim of this thesis is to create chitosan-based three-dimensional porous structures with tunable degradation rates with particular interest in fast degradation rate. Hydrogels of block-copolymer networks were prepared to crosslink the chitosan (CHT) or carboxymethyl chitosan (CmCHT) with either a hydrophobic polymer of low molecular weight, such as poly(ε-caprolactone), (PCL) or a hydrophilic polymer such as poly(ethylene

glycol), (PEG). The hypothesis was that the degradation of the cross-linker polymer leaves behind large water-soluble polymer chains (protonated chitosan or carboxymethyl chitosan).

Chitosan is a natural polymer with good biomaterial properties (it is biocompatible, biodegradable and its mechanical properties are similar to those of biological tissues). It provides a suitable environment for cells and has been widely used in different tissue engineering applications. Its biodegradation mechanism gives subproducts that are metabolized by the organism without presenting cytotoxicity. However, in spite of chitosan's favourable properties, the polymer has relatively slow biodegradation times in enzymatic media that contain lysozyme and even slower in hydrolytic conditions.

Chitosan's physical and chemical properties largely depend on its deacetylation degree (DD). In order to analyze these properties, chitosan was synthesized with various DD ranging from 85% to 45%. Water absorption was seen to rise rapidly as deacetylation was reduced. This would appear to contradict the fact that chitin water absorption (low DD) is much lower than that of chitosan. In order to understand this behaviour, it was analyzed the dependence of the degree of network swelling on the parameters determined by the Flory Rhener theory: the water-polymer interaction parameter, the elastic properties of the network and the density of the cross-linking according to the sample's water content. The instability of the crystals during the swelling process was seen to increase as DD was reduced. The rise in water content at low DD values was thus explained by the reduced crystallinity and, therefore, also the network cross-linking density.

The thermal stability of chitosan according to its DD was analysed by thermogravimetry. The polymer's thermal degradation was measured as a

function of its temperature at different heating rates. Different methods were applied to obtain the activation energy. Although activation energy appears to rise when DD is reduced, there is no a clear tendency. The system presented a complex degradation profile, in which activation energy depends on the conversion rate. A degradation model was proposed with two stages associated to the acetylated and deacetylated units of the polymer chain.

Electrospinning was chosen as the porous membrane preparation technique as it provides thin membranes that can be handled with fiber sizes in the order of microns. The membranes obtained were treated with ethanol and cross-linked with gluteraldehyde. The influence of the electrospinning and cross-linking processes on the thermal stability of chitosan was analyzed. The Kissinger model, a non-isoconversional method, was used to calculate the activation energy (E_a) from polymer's thermal degradation subjected to each of the processes. It was shown that E_a values increase after each process in relation to that of the original chitosan.

Chitosan and carboxymethyl chitosan hydrogels covalently cross-linked with short chains of poly(ε-caprolactone), (PCL) and poly(ethylene glycol) (PEG) were synthesized. The PCL was functionalized with terminal aldehyde groups to enable the chemical cross-linking reaction. The formation of networks was confirmed by solubility tests with appropriate solvents for each polymer. Hydrogels that absorbed large quantities of water were obtained, with values that ranged between 90 and 5000%. Thermogravimetryc analysis was used for the study of the thermal stability and showed some interactions between the network components. It was also used to determine the proportion of each polymer in the network. The calorimetric tests together with the DRX analysis of the

crystallinity showed that networks formed by hydrophilic-hydrophobic components (CHT-PCL and CmCHT-PCL) presented phase separation (more apparent in the case of CHT-PCL). However, phase separation was not observed in networks formed by two hydrophilic components (CmCHT-PEG). Studies on the kinetics of hydrolytic and enzymatic biodegradation showed three different systems: CmCHT-PEG system that can be classified as stable hydrogel, CHT-PCL system as semidegradable hydrogel and degradable hydrogels with degradation kinetics in the order of days for the CmCHT-PCL system.

Porous structures of the synthesized hydrogels were prepared by swelling in water with subsequent freezing and lyophilisation. Pore morphology was seen to depend on the composition. The pore sizes and their interconnections were suitable for containing cells.

Finally, biological studies were carried out on porous CmCHT-PCL hydrogels. Fibroblasts were used to analyze cytotoxicity and optimize the seeding process. Mesenchymal stem cells (MSCs) from pig adipose tissue were then cultivated and the results showed that these networks can be used in the organism in tissue engineering applications with degradation times of around a week.

Resumen

La ingeniería tisular tiene como finalidad desarrollar sustitutos biológicos funcionales que reemplacen o restauren los tejidos dañados. Se trata de preparar andamiajes tridimensionales (scaffolds) que sean capaces de albergar células y factores de señalización que favorezcan la regeneración del tejido dañado. Conviene que los materiales sean biodegradables para que vayan desapareciendo a medida que se forma el nuevo tejido. Es por ello que existe un especial interés en el desarrollo de scaffolds que proporcionando un entorno favorable a las células, tengan una tasa de degradación que se adapte a velocidad de regeneración del tejido. Los scaffolds deben ser porosos y poseer una morfología del poro adaptada a la aplicación para la que son diseñados. Deben ser capaces de albergar gran cantidad de agua (hidrogeles) al tiempo que presentan una interacción célula/biomaterial adecuada (en general los materiales hidrófobos presentan mayor adhesión celular).

El objetivo de esta tesis es el de crear estructuras porosas tridimensionales basadas en quitosano con velocidades de degradación ajustables con particular interés en velocidades de degradación altas. Se han preparado hidrogeles de redes de copolimeros en bloque entrecruzando el quitosano,

(CHT) o el carboximetil quitosano, (CmCHT) con un polímero hidrófobo de bajo peso molecular como la poli(ε-caprolactona), (PCL) o bien con un polímero hidrófilo como es el poli(etilenglicol), (PEG). La hipótesis de trabajo fue que la degradación del polímero que actúa como entrecruzador debe dejar grandes cadenas del polímero (quitosano protonado o carboximetil quitosano) que son solubles en agua.

El quitosano es un polímero de origen natural que presenta buenas propiedades como biomaterial, (es biocompatible, biodegradable y sus propiedades mecánicas se asemejan a las de los tejidos biológicos). Se ha utilizado en muchas aplicaciones dentro de la ingeniería de tejidos proporcionando un buen entorno para las células, y su mecanismo de biodegradación da subproductos que son metabolizadas por el organismo sin presentar citotoxicidad. A pesar de las buenas propiedades del quitosano, el polímero presenta tiempos de biodegradación bastante lentos en medio enzimático conteniendo lisozima y aún más lentos en condiciones hidrolíticas.

Las propiedades físico-químicas del quitosano dependen en gran medida del grado de desacetilación, DD. Con el fin de analizar dichas propiedades se ha llevado a cabo la síntesis de quitosano con DD variando entre 85% y el 45%. Se ha comprobado que la absorción de agua aumenta rápidamente a medida que el grado de desacetilación disminuye. Esto parece contradecir el hecho de que la absorción de agua de la quitina (DD bajo) es mucho menor que la de quitosano. Para entender dicho comportamiento se ha analizado la dependencia del grado de hinchado de la red con los parámetros que determina la teoría de Flory Rhener: parámetro de interacción agua-polímero, las propiedades elásticas de la red y la densidad de entrecruzamiento en función del contenido en agua de la muestra. Se comprobó que la inestabilidad de los cristales durante el proceso de

hinchamiento aumenta al disminuir el grado de desacetilación. De esta forma, se explicó el aumento del contenido en agua para valores bajos de DD por la disminución de cristalinidad y, por tanto, de densidad de entrecruzamiento de la red.

La estabilidad térmica del quitosano en función de DD ha sido analizada por TGA. Se ha medido la degradación térmica del polímero en función de la temperatura para varias velocidades de calentamiento. Se han aplicado diferentes métodos para obtener la energía de activación. Aunque parece que la energía de activación aumenta cuando DD disminuye, no hay una tendencia clara. Se ha comprobado que se trata de un sistema complejo en el que la energía de activación depende del grado de conversión. Se ha propuesto un modelo con dos etapas de degradación asociadas a las unidades acetiladas y desacetiladas de la cadena polimérica.

Como técnica de preparación de membranas porosas se ha elegido el electrohilado, ya que permite obtener membranas delgadas y manipulables con tamaños de fibra del orden de micras. Las membranas obtenidas han sido tratadas con etanol y entrecruzadas con glutaraldehído. Se ha analizado la influencia de los procesos de electrohilado y entrecruzamiento en la estabilidad térmica del quitosano. Un método no-isoconversional, el modelo de Kissinger, se ha utilizado para calcular la energía de activación de la degradación térmica del polímero, E_a, sometido a cada uno de los procesos. Se ha comprobado que los valores de E_a aumentan después de cada proceso con respecto a la del quitosano de partida.

Se han sintetizado hidrogeles de quitosano, y carboximetil quitosano entrecruzados covalentemente con cadenas cortas de poli(ε-caprolactona), y poli(etilenglicol). Ha sido necesario funcionalizar la PCL con grupos terminales aldehído para que se pueda producir la reacción de

entrecruzamiento químico. La formación de las redes se ha confirmado mediante ensayos de solubilidad con buenos solventes para cada polímero. En todos los casos se han obtenido hidrogeles que absorben gran cantidad de agua con valores que oscilan entre 90 y 5000%. El análisis de la estabilidad térmica mediante TGA ha revelado las interacciones entre los componentes de la red; además se ha utilizado para determinar la proporción de cada polímero en la red. Los ensayos de calorimetría junto con el análisis de cristalinidad de las redes por DRX revelan que las redes formadas por componentes hidrofílico-hidrofóbico, (CHT-PCL y CmCHT-PCL) presentan separación de fases (más evidente en el caso de CHT-PCL). Sin embargo, no se observa separación de fases en las redes formadas por dos componentes hidrofílico (CmCHT-PEG). Los estudios de las cinéticas de biodegradación tanto hidrolítica como enzimática revelan la obtención de tres sistemas que se pueden clasificar como hidrogeles estables, para los hidrogeles formados por CmCHT-PEG, hidrogeles semidegradables para el sistema CHT-PCL y finalmente hidrogeles degradables con cinéticas de degradación del orden de días, para el sistema CmCHT-PCL.

Se han preparado estructuras porosas mediante el hinchado en agua y la posterior congelación y liofilización. Se ha comprobado que la morfología de los poros depende de la composición. Los tamaños de poro y su interconexión son adecuados para albergar células.

Finalmente se ha llevado a cabo estudios biológicos de los hidrogeles porosos de CmCHT-PCL. Se utilizaron fibroblastos para analizar la citotoxicidad y optimizar el proceso de siembra. Posteriormente se realizaron cultivos con células mesenquimales del tejido adiposo de cerdo (MSCs). Los resultados han revelado que dichas redes pueden ser utilizadas como sistemas de liberación de células en el organismo con tiempos de degradación del orden de una semana.

Resum

L'enginyeria tissular té com a finalitat desenvolupar substituts biològics funcionals que reemplacen o restauren els teixits danyats. Es tracta de preparar suports tridimensionals (esquelets o scaffolds) que siguen capaços d'albergar cèl·lules i factors de senyalització que afavorisquen la regeneració del teixit danyat. Convé que els materials siguen biodegradables perquè vaguen desapareixent a mesura que es forma el nou teixit. És per això que hi ha un interès especial en el desenvolupament d'esquelets que, proporcionant un entorn favorable a les cèl·lules, tinguen una taxa de degradació que s'adapte a la velocitat de regeneració del teixit. Els scaffolds han de ser porosos i han de tenir una morfologia del porus adaptada a l'aplicació per a la qual són dissenyats. Han de ser capaços d'albergar una gran quantitat d'aigua (hidrogels) alhora que presenten una interacció cèl·lula/biomaterial adequada (en general, els materials hidròfobs presenten més adhesió cel·lular).

L'objectiu d'aquesta tesi és crear estructures poroses tridimensionals basades en quitosan amb velocitats de degradació sintonizables amb un interés particular de rutes de degradació altes. S'han preparat hidrogels de xarxes de copolímers en bloc entrecreuant el quitosan o el carboximetil quitosan amb un polímer hidròfob de baix pes molecular com la poli (ε-

caprolactona), o bé amb un polímer hidròfil com és el poli (etilenglicol). Es tracta d'aconseguir que quan el polímer que actua com a entrecreuador es degrade, deixe grans cadenes del polímer (quitosan protronat o carboximetil quitosan) que són solubles en aigua.

El quitosan és un polímer d'origen natural que presenta bones propietats com a biomaterial (és biocompatible, biodegradable i té propietats mecàniques que s'assemblen a les dels teixits biològics). S'ha utilitzat en moltes aplicacions dins de l'enginyeria de teixits, atès que proporciona un bon entorn per a les cèl·lules i té un mecanisme de biodegradació que dóna subproductes que són metabolitzats per l'organisme sense presentar citotoxicitat. A pesar de les bones propietats del quitosan, el polímer presenta cinètiques de biodegradació lentes en condicions enzimàtiques quan conté lisozima i encara més lentes en condicions hidrolítiques.

Les propietats fisicoquímiques del quitosan depenen en gran mesura del grau de desacetilació, DD. A fi d'analitzar aquestes propietats, s'ha dut a terme la síntesi de quitosan amb un DD que variava entre el 85% i el 45%.

S'ha comprovat que l'absorció d'aigua augmenta ràpidament a mesura que el grau de desacetilació disminueix. Això sembla que contradiu el fet que l'absorció d'aigua de la quitina (DD baixos) és molt menor que no la de quitosan. Per a entendre aquest comportament s'ha analitzat la dependència del grau d'unflament de la xarxa amb els paràmetres que determina la teoria de Flory Rhener: paràmetre d'interacció aigua-polímer, les propietats elàstiques de la xarxa i la densitat d'entrecreuament en funció del contingut en aigua de la mostra. Es va comprovar que la inestabilitat dels cristalls durant el procés d'unflament augmenta en disminuir el grau de desacetilació. D'aquesta manera, es va explicar l'augment del contingut en aigua per a valors baixos de DD per la

disminució de cristal·linitat i, per tant, de densitat d'entrecreuament de la xarxa.

L'estabilitat tèrmica del quitosan en funció del DD ha sigut analitzada per termogravimetria. S'ha mesurat la degradació tèrmica del polímer en funció de la temperatura per a diverses velocitats de calfament. S'han aplicat diversos mètodes per obtenir l'energia d'activació. Encara que pareix que l'energia d'activació augmenta quan el DD disminueix, no hi ha una tendència clara. S'ha comprovat que es tracta d'un sistema complex en què l'energia d'activació depèn del grau de conversió. S'ha proposat un model amb dues etapes de degradació associades a les unitats acetilades i desacetilades de la cadena polimèrica.

Com a tècnica de preparació de membranes poroses s'ha utilitzat l'electrofilatura, ja que permet obtenir membranes primes i manipulables amb grandàries de fibra de l'ordre de micres. Les membranes obtingudes han sigut tractades amb etanol i entrecreuades amb glutaraldehid. S'ha analitzat la influència dels processos d'electrofilatura i entrecreuament amb l'estabilitat tèrmica del quitosan. S'ha utilitzat un mètode no isoconversional, el model de Kissinger, per calcular l'energia d'activació, E_a, de la degradació tèrmica del polímer sotmès a cadascun dels processos. S'ha comprovat que els valors d'E_a augmenten després de cada procés respecte de la del quitosan de partida.

S'han sintetitzat hidrogels de quitosan i carboximetil quitosan entrecreuats covalentment amb cadenes curtes de poli(ε-caprolactona) i poli(etilenglicol). Ha calgut funcionalitzar la PCL amb grups terminals aldehid perquè es poguera produir la reacció d'entrecreuament químic. La formació de les xarxes s'ha confirmat per mitjà d'assajos de solubilitat amb bons solvents per a cada polímer. En tots els casos s'han obtingut hidrogels

que absorbeixen una gran quantitat d'aigua, compresa en valors que oscil·len entre el 90 i el 5.000%. L'anàlisi de l'estabilitat tèrmica per termogravimetria ha revelat les interaccions entre els components de la xarxa; a més a més, s'ha utilitzat per determinar la proporció de cada polímer en la xarxa. Els assajos de calorimetria junt amb l'anàlisi de cristal·linitat de les xarxes per difracció de raigs X (DRX) revelen que les xarxes formades per components hidrofílic-hidrofòbic, (CHT-PCL i CmCHT-PCL) presenten separació de fases (més evident en el cas de CHT-PCL). No obstant això, no s'observa separació de fases en les xarxes formades per components hidrofílics (CmCHT-PEG).

Els estudis de les cinètiques de biodegradació tant hidrolítica com enzimàtica revelen l'obtenció de tres sistemes que es poden classificar com a hidrogels estables (per als hidrogels formats per CmCHT-PEG), hidrogels semidegradables (per al sistema CHT-PCL) i, finalment, hidrogels degradables amb cinètiques de degradació de l'ordre de dies (per al sistema CmCHT-PCL). S'han preparat estructures poroses per mitjà de l'unflament en aigua i la posterior congelació i liofilització. S'ha comprovat que la morfologia dels porus depèn de la composició. Les grandàries dels porus i la interconnexió d'aquests són adequades per a albergar cèl·lules.

Finalment s'ha dut a terme estudis biològics dels hidrogels porosos de CmCHT-PCL. Es van utilitzar fibroblastos per analitzar la citotoxicitat i optimitzar el procés de sembra. Posteriorment es van realitzar cultius amb cèl·lules mesenquimals del teixit adipós de porc (MSCs). Els resultats han revelat que aquestes xarxes poden ser utilitzades com a sistemes d'alliberament de cèl·lules en l'organisme amb temps de degradació de l'ordre d'una setmana.

Glossary

1H-NMR	Proton Nuclear Magnetic Resonance
A	Pre-exponential factor
Ac_2O	Acetic anhydride
aPCL	Dialdehyde end-capped poly(ε -caprolactone)
ATR-FTIR	Attenuated Total Reflectance-Fourier Transform Infrared Spectroscopy
a_w	Water activity
$CDCl_3$	Deuterated chloroform
CG	Collagen
$CHCl_3$	Chloroform
CHT	Chitosan
CmCHT	Carboxymethyl chitosan
$(COCl)_2$	Oxalyl chloride
CP/MAS 13C-NMR	Solid-state Cross-Polarization Magic Angle Spinning Carbon13- Nuclear Magnetic Resonance
CS	Chondroitin sulfate
D_2O	Deuterium oxide
DAPI	4′,6-Diamidino-2-Phenylindole
DC	Conversion degree of carboxymethyl chitosan
DCl	Deuterium chloride

DCM	Dichloromethane
DD	Deacetylation degree
DMEM	Dulbecco's Modified Eagle's Medium
DMSO	Dimethylsulfoxide
DS	Substitution degree
DSC	Differential Scanning Calorimetry
DTG	Derivative Thermogravimetric
E	Elastic modulus
EA	Elemental Analysis
E_a	Activation energy
ECH	Epichlorohydrin
ECM	Extracellular matrix
EWC	Equilibrium water content
EWC´	Equilibrium water content referred to the hydrophilic component weight
FBS	Fetal bovine serum
FDA	Food and Drug Administration
FGF-2	Fibroblast growth factor-2
FTIR	Fourier Transform Infrared Spectroscopy
G´	Shear storage modulus
G´´	Shear loss modulud
GA	Glutaraldehyde
Glc	D-glucosamine

GlcNAc	N-acetyl-D glucosamine
GP	Genipin
GPC	Gel Permeation Chromatography
h	Water weight content
HA	Hyaluronic acid
HCl	Chloridric acid
HCOOH	Formic acid
HFIP	1,1,1,3,3,3-Hexafluoro-2-Propanol
HPLC	High Performance Liquid Chromatography
i	Isothermal stage
IPN	Fully- Interpenetrating Polymer Networks
$MgSO_4$	Magnesium sulfate
Mn	Number average molecular weight
MSCs	Mesenchymal Stem Cells
Mw	Weight average molecular weight
n	Reaction order
Na_2CO_3	Sodium carbonate
$NaBH_3CN$	Sodium cyanoborohydride
NaOH	Sodium hydroxide
NMP	N-methyl pyrrolidine
OFW	Ozawa-Flynn-Wall
P/S	Penicillin/Streptomycin

PBS	Phosphate Buffered Saline
PCL	Poly(ε-caprolactone)
PCL-diol	Poly(ε-caprolactone) diol
PĐ	Polidispersity index
PEA	Poly(ethyl acrylate)
PEG	Poly(ethylene glycol)
PEGDE	Poly(ethylene glycol) diglicidyl ether
PHEA	Poly(hydroxyethylacrylate)
PLA	Poly(lactic acid)
PLGA	Poly(lactic-co-glycolic acid)
PTFE	Poly(tetrafluor ethylene)
R	Gas constant
RH	Relative humidity
RW	Weight loss residue
SEC	Size Exclusion Chromatography
SEM	Scanning Electron Microscopy
semi-IPN	Semi-Interpenetrating Polymer Networks
t	Time
TEA	Triethylamine
TFA	Trifluoracetic Acid
Tg	Glass Transition Temperature
TGA	Thermogravimetric Analysis

TMI	N,N,N-trimethyl chitosan iodide
TMS	Tetramethylsilane
Tp	Absolute temperature at the maximum weight loss rate
TPP	Tripolyphosphate
UV	Ultraviolet-visible spectroscopy
W	Weight
WC	Water Content
X or X'	Mass fraction
XRD	X-ray diffraction
α	Conversion degree of kinetic model
β	Heating rate
δ	Solubility parameter
ΔH_f	Heat of fusion
v	Molar volume
ρ^2	Correlation coefficient
ϕ	Volume fraction of water
χ	Flory interaction parameter

Table of contents

Chapter 1. Introduction

1.1 Overview on Tissue Engineering

Loss or damage of tissue or organs due to ageing, trauma or injury is an important field in health research. Alternative therapies such as organ and tissue transplants are sometimes used, but are not the ideal solution, due to the limited number of organ and tissue donors. In recent years considerable advances have been made in Tissue Engineering, (TE) [1], which is a multidisciplinary science that includes material science, biochemistry, cell biology, engineering and medicine (Figure 1.1). The aim of TE is to develop biological substitutes with adequate properties to repair or replace damaged tissues or organs [2].

Human tissue is formed of many different components and the cells exist on a solid support known as the extracellular matrix (ECM). The design and production of scaffolds[3, 4] that mimic the ECM [5] is an important area of research in the Tissue Engineering field. The scaffold must provide a suitable environment, which must be cell-friendly (non cytotoxic) and be able to promote cell attachment, good nutrient diffusion, the right morphology, mechanical strength and modulate degradation route. These conditions mean that scaffolds should be made from biomaterials [2, 4] characterized by their biocompatibility, non-citotoxicty and biodegradability.

The architecture [6] of the scaffolds plays an important role. The scaffolds should have an adequate pore size and good interconnectivity to facilitate nutrient transport and cell migration and provide good mechanical stability. A variety of techniques have been used to produce controllable porous structures such as electrospinning [7-10], particle leaching [9, 11], freeze–drying and freeze-gelation [9, 12, 13], and 3D printing templates [9, 14].

Biomaterials can be divided into natural or synthetic materials. Natural materials include polymers obtained from natural resources, such as collagen, CG [14], hyaluronic acid, HA [15], chitosan, CHT [16], chondroitin sulfate, CS. These are biodegradable materials that provide the right biological environment and enhance cell response, although their mechanical properties are not as good as the synthetic materials.

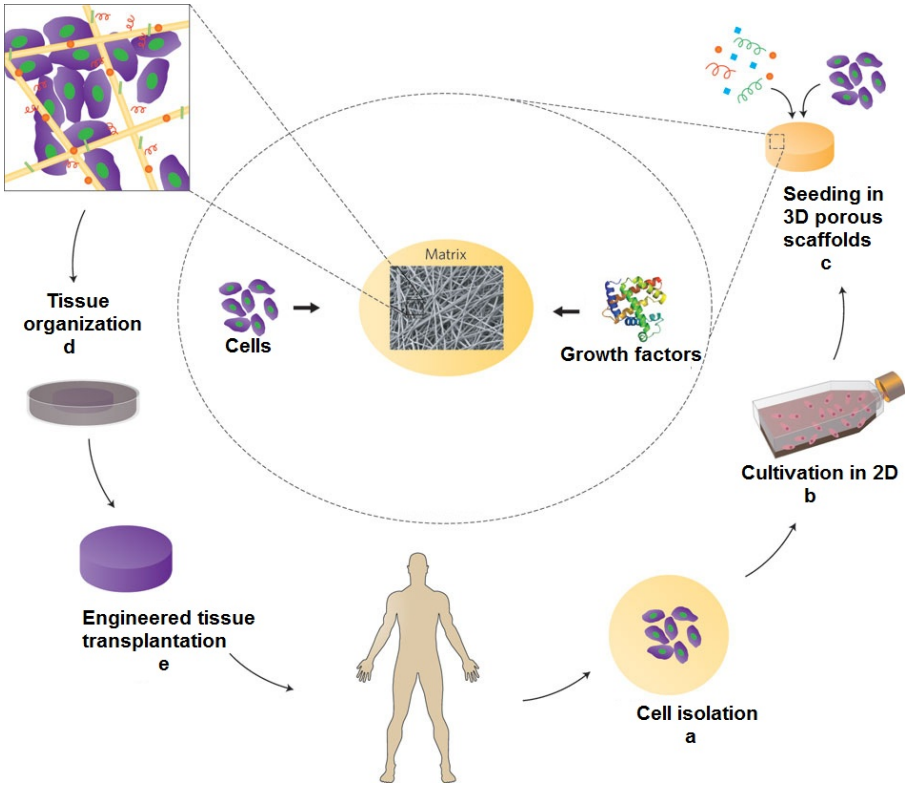

Figure 1.1. General Scheme about the concept of the Tissue Engineering. a) Cell isolation from patient, b)" in vitro" on two-dimensional surfaces for efficient expansion, c) the cells are seeded in porous scaffolds together with growth factors, d) bioreactors to provide optimal conditions for cell organization into a functioning tissue and finally e) the scaffold is transplanted on the defect to restore function. Reproduced from [5].

Synthetic materials are formed of synthetic polymers such as poly (ethyl acrylate) PEA, poly(2-hydroxyethyl acrylate) PHEA, poly(ε-caprolactone) PCL [15], poly(lactic acid) PLA, poly(lactic-co-glycolic acid) PLGA [16], poly(ethylene glycol) PEG [17] and some of them have been approved for specific clinical applications by the Food and Drug Administration, FDA. These polymers are useful in TE field and can be tailored for specific applications. They can be produced under controllable conditions with reproducible mechanical and physico-chemical properties. Scaffolds can be divided into biodegradable and biostable or permanent scaffolds.

With permanent or biostable scaffolds, the material contributes to permanent regeneration, as in load-bearing applications, bone therapy regeneration [18-20], cartilage and in drug delivery systems [21].

Biodegradable scaffolds degrade as the neotissue is regenerated. This type of scaffolds are used in cartilage [22-27], bone [25, 26, 28-30], neural [31, 32] and heart [33] regeneration.

In some applications of regenerative therapies such us, the tissue epithelial regeneration in cornea [34], oral mucosa [35] and skin [36] there is needed that the support is rapidly degraded and it is re-absorbed, while the new tissue is regenerated. In this case the biostable scaffolds could induce an inflammatory response and foreign body reaction, being the biodegradable scaffolds the best candidates to obtain the scaffolds with tunable degradation route.

In this thesis, polymer networks with good degradation properties have been developed. The networks are based on water-soluble chitosan scaffolds cross-linked with other polymers with reactive terminal groups. The physical and chemical properties and biodegradation rate of the chitosan networks obtained were modulated as a function of cross-linking

density. The biodegradation mechanism of these networks is governed by the cleavage of the cross-linking agent chains, while the water-soluble chitosan is solubilized in the media. It is of paramount importance that the product degradation does not cause cytotoxicity.

1.2 Chitosan

Chitosan and water-soluble chitosan are the proposed natural polymer candidates. Chitosan is known to have good biomaterial properties and is non-cytotoxic [37, 38]. Several chitosan applications have been put into practice in biomedical devices such as: drug delivery systems, bone therapy, cartilage replacement, as well as drug-release devices in the field of ophthalmology and the regeneration of oral mucosa and skin.

In studies on the chitosan biodegradation route and its derivatives no trace of cytoxicity was found in the degradation products [39]. Because of its easy processability, the chitosan is a good candidate for use in tissue regeneration as 3D polymeric supports, electrospinning membranes [10, 40], hydrogels [41], patches [42], nanocomposites and nanoparticles [43-45].

One of the drawbacks of chitosan is its limited solubility, since it can only dissolve in certain organic solvents and in aqueous media at acidic pH [46]. However, in spite of this, it can carry out a large number of chemical reactions, as it possesses reactive functional groups in its polymeric structure, such as the hydroxyl and amino groups. Many studies in the literature have focused on chitosan functionalization reactions and cross-linking [47-50]. In functionalization reactions, the chitosan chain can be modified to obtain new functional groups in which N,O-substitution reactions such as N-acetylation [51-53], N,O-carboxymethylation [54, 55] and N-quaternization [56, 57] raise the polymer's solubility.

One of the best known chitosan cross-linking reaction strategies is that between the polymer's amine and aldehyde groups [58], especially chitosan–glutaraldehyde, (GA) cross-linking [59-61]. A wide variety of cross-linking agents have been used to obtain chitosan networks, such as genipin, (GP) [62-64], tripolyphosphate, (TPP) [64, 65] and epichlorohydrin, (ECH) [66], among others [67, 68].

The cross-linking strategies with other polymers have been tried to obtain hybrid materials whose properties can be modified to suit a given tissue engineering application. Chitosan can combine with hydrophobic and hydrophilic polymers as a result of interesting hydrophilic/hydrophilic [69, 70] networks or hydrophilic/hydrophobic networks [71, 72].

1.2.1 Chemical structure and resource

Chitin is a homopolymer composed of β(1→4) linked N-acetyl-D glucosamine (GlcNAc) units (Figure 1.2) and is the second most abundant polysaccharide next to cellulose, obtained from natural sources like crustacean, insect exoskeletons and the cell walls of fungi.

Chitosan is an amino polysaccharide copolymer formed by β(1→4) linked of N-acetyl-D glucosamine (GlcNAc) and D-Glucosamine (Glc) units. It is obtained from N-deacetylation of chitin by alkaline treatment.

The presence of hydroxyl, acetamide and amine reactive groups in chitin and chitosan polymer chains makes chitin and chitosan promising candidates for producing chemical reactions to change physical, chemical and biological properties such as: degradation, solubility, crystallinity, cell attachment, DNA interaction and scaffold fabrication, among others.

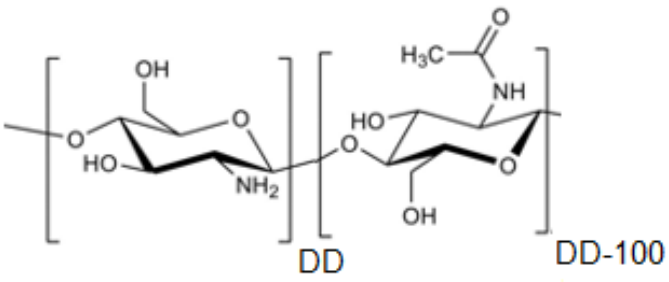

Figure 1.2. Chitin and chitosan structure, where DD is the N-deacetylated units and DD-100 is the N-Acetylated units. Reproduced from [73].

1.2.2 Deacetylation degree

The N-deacetylation degree (DD) is the relationship between amine ($-NH_2$) groups with respect to the total amount of N-acetyl ($-NHCOCH_3$) and amine ($-NH_2$) groups. Chitosan and chitin are essentially the same polymer with different degrees of deacetylation (DD). When DD is around 50% or more, the polymer is called chitosan and when the DD is less than 50% the polymer is referred to as chitin [46], but these limits are arbitrary [74].

DD is one of the most important polymer parameters, followed by molecular weight (Mw). The physical and chemical properties can be altered, and consequently the specific applications of chitin and chitosan, by adjusting DD and Mw. Because of its importance, several techniques have been used to analyze DD content, such us: Fourier Transform Infrared Spectroscopy (FTIR), Ultraviolet-visible spectroscopy (UV), titration, circular dichroism, elemental analysis (EA), but the most efficient method is proton Nuclear Magnetic Resonance (1H-NMR) Spectroscopy because of its precision, robustness and reproducibility [75].

1.2.3 Molecular weight

The molecular weight (Mw) of chitosan is divided into three categories in the literature: low molecular weight, medium molecular weight and high

molecular weight. Chitosan with high molecular weight leads to greater entanglement between the polymer chains, providing stronger complexes. In contrast, when the chitosan is low molecular weight the complex is weaker. The entanglements between polymer chains are due to strong inter-chain associations via H-bonding.

Several authors have analyzed the molecular weight using High Performance Liquid Chromatography, HPLC and Light Scattering techniques. One of the simplest and rapid methods for determining molecular weight is by viscosimetry. Although, this is not an absolute method it requires the determination of constants.

The Gel Permeation Chromatography, GPC technique is the most powerful technique for characterizing polymer molecular weight. However, it is a relative method and needs molecular weight standards for calibration to obtain the relation between elution volume and molecular weight.

The molecular weight of the chitosan is calculated by applying the Mark-Houwink [76] equation:

$$[\eta] = K.M^{\alpha} = 1.81x10^{-3}\,M^{0.93} \quad (1.1)$$

Where α and K are constants determined with a solution of the 0.1 M acetic acid and 0.2 M sodium chloride solutions.

1.2.4 Solubility

Chitosan is soluble in acid media and some organic solvents such as acetic acid formic, acid propanoic, acid malenic among others [77]. The presence of amine groups in the chemical structure means that chitosan's solubility (Figure 1.3) depends on the pH media. The amine group in chitosan has a pKa of 6.5, so at pH< 6.5, the amine group (NH_2) is protonated ($-NH3^+$) and the chitosan chains are water-soluble. At pH> 6.5 the amine groups are not protonated and chitosan is not water-soluble [65, 78].

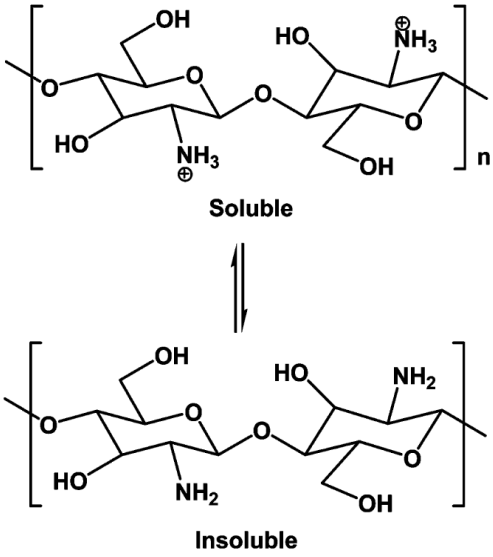

Figure 1.3. Chemical equilibrium of soluble and insoluble chitosan.

Due to chitosan's insolubility, some modification reactions can be carried out, such as introducing hydrophilic groups into the chitosan chain to improve its solubility. Shashiwa studied the solubility of the *N*-chitosan derivatives at various pHs [79]. Carboxymethyl chitosan is easily soluble in water and quaternization reactions have also been studied to increase its solubility.

1.2.5 Crystallinity

Chitin and chitosan are semi-crystalline polymers formed by crystalline and amorphous regions. The crystalline structure in the polymer depends on the chain arrangement; this is given by the inter or intra-molecular hydrogen bonds between the polymer chains.

Chitin presents three different crystalline structures, which are defined in relation to the packing of the polymer chains. The anti-parallel arrangement is called α-chitin, parallel arrangement, β-chitin and mixed

arrangement (α and β), δ-chitin. The crystalline structure depends on the chitin sources [73, 80], where the most stable and abundant is β-chitin. Nevertheless, chitosan's crystallinity is also affected by the starting chitin.

In a study of the crystalline structure of chitosan, Samuel *et al*., reported [81] that it has two crystalline forms, I and II; form I has orthorhombic crystals with cell dimensions a) 7.76 Å, b) 10.91 Å, and c) 10.3 Å. In X-ray diffraction (XRD) was observed a strong reflection for chitosan at $2\Theta \approx 11°$. In form II was observed an orthorhombic crystal with cell dimensions a) 4.4 Å, b) 10.0 Å, and c) 10.3 Å and the X-ray diffractometer showed a reflection around $2\theta = 20°$ and $2\theta = 10°$. Several authors have demonstrated that chitosan can constantly transform between form I and form II [82, 83]. Chitosan´s crystallinity depends on the packing of the polymer chains and some factors can contribute to changes in the chitosan crystallinity and some examples are described. Cross-linked chitosan presented a lower crystallinity when it was cross-linked because cross-linking disturbs the arrangement between polymer chains [84]. The deacetylation degree of the chitosan is an important factor to consider in the crystallinity behavior. In previous studies the chitosan´s film with different DD showed typical reflections peaks to (020) appears at $2\theta = 20^{o}$ and (010) appears at $2\theta = 10^{o}$. The films with the highest DDs presented the most intense peaks around $2\theta = 20\text{-}21^{o}$, and the films with lower DDs showed the most intense peaks around $2\theta = 9\text{-}10^{o}$ [85]. The crystallinity was also dependent of the water content in hydrated or immersed chitosan films, showing that the water had an important role in the chitosan´s crystal structure [84, 85].

1.3 Chemical modification of chitosan

As mentioned above, one of the drawbacks of chitosan is its poor solubility in aqueous media requiring acidic pH. The property of being water-soluble is especially important for certain tissue engineering applications.

Chitosan is a molecule amenable to chemical modifications. The linear polymer has three reactive groups in its structure; in (C-2) it has the amino group (NH_2) on each deacetylated unit, the primary (C-3) and secondary (C-6) hydroxyl groups (OH). These reactive groups mean that chitosan can react with different chemical groups to improve its solubility and consequently to alter its physico-chemical and biological properties.

Specific O-substitution reactions [86, 87] in the chitosan polymer are via-hydroxyl interactions obtaining products with ester and ether groups. The amine reactions are the most important due to their higher reactivity than the hydroxyl groups [88]. Specific N-substitutions reactions [89] of partial deacetylated chitosan have been studied. The Michael addition is an important reaction mechanism of chitosan to obtain water-soluble derivatives [90]. It involves the addition of the electrophilic groups carbon–carbon double bond, also called Michael acceptors, conjugated with a carbonyl group like α,β-unsaturated carbonyl alkyl, acrylate [91] or acrylamide compounds, with nucleophilic groups, also called Michael donor, like amino and thiol groups. They are largely utilized due to their higher nucleophilicity and selectivity at physiological pH and temperature [92, 93].

The other important mechanism reaction is the formation of Schiff base intermediate [94]. It involves the amine group of chitosan with aldehyde or ketones to form imines, (Figure 1.4). Several N-substitution reactions have been studied, such as N-acylation [95], N-alkylation and N-

acrylation [53, 95-97], where the chitosan nucleophilic amino group can react with acyl, alkyl and acryl groups respectively via Schiff base formation.

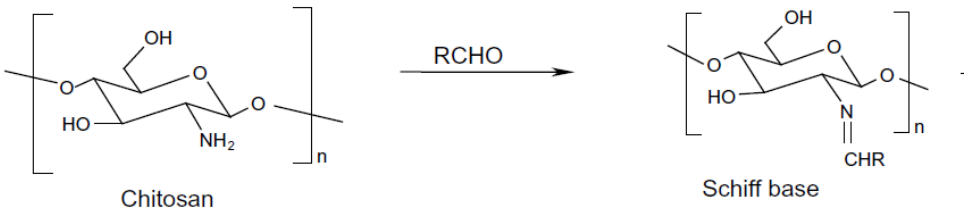

Figure 1.4. The Schiff base formation mechanism. Reproduced from [98].

1.3.1 N-alkylation chitosan reaction

N-alkylation of chitosan can be done in two ways; the first is direct N-alkylation using a halogen displacement reaction [99]. N-alkylation is performed between the amino and alkyl halide groups under heterogeneous conditions [100]. This reaction involves high temperature, high sodium hydroxide concentration, resulting in a low substitution degree and molecular weight degradation (Figure 1.5).

The other N-alkylation method is by the reductive amination reaction (Figure 1.6). This reaction is carried out between the amino groups and aldehyde or ketone groups, via Schiff base intermediates.

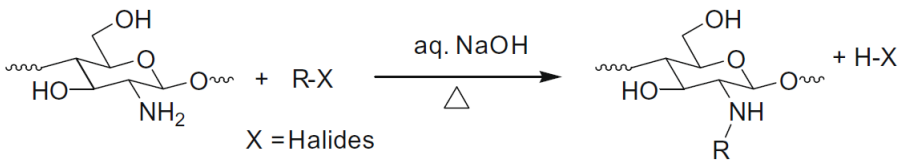

Figure 1.5. N-substitution of chitosan by halogen displacement reaction. Reproduced from [99].

This reaction is performed in acid conditions followed by the reduction of the Schiff base intermediate with sodium cyanoborohydride or sodium borohydride. Sodium cyanoborohydride is a reducing agent, especially reducing imines in mild conditions, known as Borch reductive amination [101].

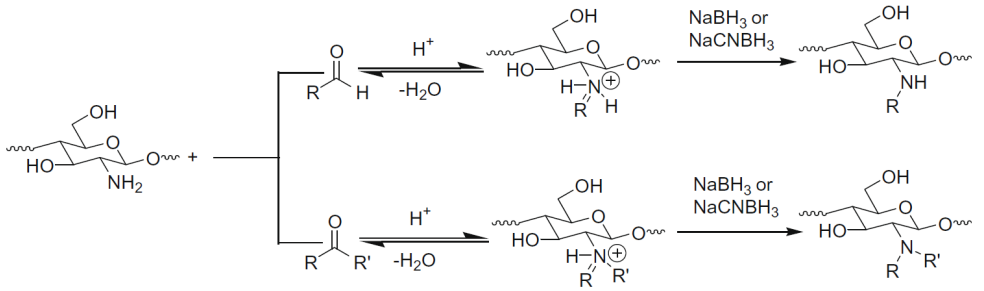

Figure 1.6. Synthesis of N-substitution chitosan derivatives by reduction, where R and R´=methyl alkyl, aryl groups. Copied from [99].

1.3.2 N-quaternization of Chitosan

One of the chitosan reactions is the N-quaternization of the amine group. The most common reaction can be achieved with methyl iodide in alkaline media with N-methyl pyrrolidine (NMP), to obtain N,N,N-trimethyl chitosan iodide (TMI), (Figure 1.7) [102]. The synthesis and characterization of different quaternized CHT derivatives have been described in a recent series of studies [99]. The quaternization of chitosan shows more solubility than chitosan in a broad pH range. The positive charge is associated with the Substitution degree (DS) of CHT derivatives, which affects the positive charge density. Chitosan quaternization derivatives presents good mucoadhesive properties as a function of the quaternization degree [98]. Quaternizated chitosan presents different antibacterial activity according to the DS of the quaternary ammonium [103].

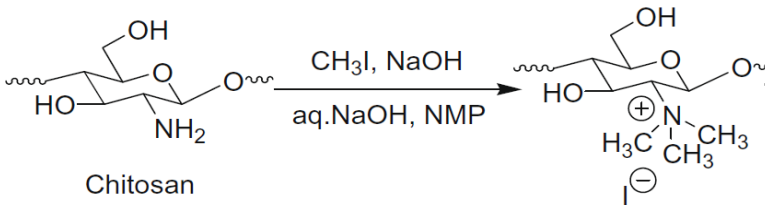

Figure 1.7. N-quaternization reaction with methyl iodide (CH_3I), in alkaline media with N-methyl pyrrolidine, (NMP) as a catalyst. Reproduced by [99].

1.3.3 N-acetylation

N-acetylation of chitosan is a widely studied reaction due to the importance of improving the solubility of the polymer. Several reaction conditions have been studied to obtain chitosan with different DDs. Water-soluble chitosan around 50% DD have been obtained by N-acetylation [79] of chitosan with high DD.

Acetylation of chitosan in homogenous conditions is possible using the acid acetic–water-methanol-pyridine system [104, 105]. Another system used is acid acetic-methanol-acetic anhydride to obtain water-soluble chitosan derivatives [106]. The degree of N-acetylation increases with increasing molar ratio of acetic anhydride, Ac_2O with respect to the Glc units when the reactions are carried out at room temperature.

1.3.4 N-carboxymethylation

Carboxymethyl chitosan is a water-soluble chitosan derivative [95, 107] widely used for its good biocompatibility [108]. Carboxymethyl chitosan is soluble in a wider range of pH than chitosan.

Two mechanism reactions can be carried out in order to obtain water-soluble carboxymethyl chitosan derivatives:

I)-Reductive alkylation. The reductive alkylation of chitosan to obtain

water-soluble carboxymethyl chitosan is carried out with glyoxylic acid to form a Schiff base intermediate (Figure 1.8), and the sodium cyanoborohidrure is employed to reduce the amine group [107, 109].

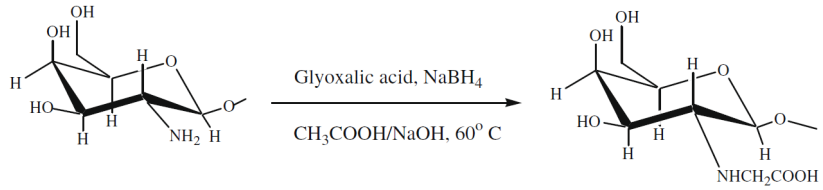

Figure 1.8. N-carboxymethyl chitosan obtained from the reaction with glyoxylic acid and reductive amination with sodium borohydride, ($NaBH_4$). Reproduced from [110].

In carboxymethylation conditions the amine group of chitosan is activated due to its affinity to react with the aldehyde group. In these conditions it is also possible to obtain a di-substituted carboxymethyl group in the amine group to form a mono or di-substituted carboxymethyl chitosan, although this depends on the reaction conditions, according to Muzarelli [111], who studied the N-carboxymethylation of chitosan as a function of molecular weights and different ratios of amino/glyoxylic acid.

II)- Direct alkylation. The direct alkylation of chitosan to obtain water-soluble carboxymethyl chitosan is carried out with monochloroacetic acid [107, 108]. Depending on the reaction conditions, it is possible to obtain N-carboxymethyl chitosan, O-carboxymethyl chitosan or a mixture N, O-carboxymethyl chitosan. When the alkaline medium in the reaction is around pH 8-8.5, the N-carboxymethylation is activated, but it is necessary to constantly dissolve the chitosan, since it precipitates in alkaline media. The final product is a mono or di-substitute N-carboxymethyl chitosan. When the concentration of alkaline media is around 50%, all the reactive groups in the chitosan structure are activated and follow the reactive order:

OH-6>OH-3> NH_2. In these reaction conditions a major O-carboxymethyl chitosan product is obtained (Figure 1.9).

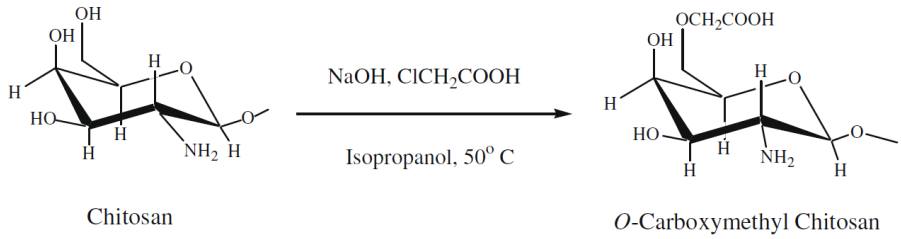

Figure 1.9. O-carboxymethyl chitosan obtained from direct alkylation with monochloroacetic acid, (ClCH2COOH) in alkaline medium, (NaOH). Reproduced from [110].

1.4 Chitosan hydrogels

There are several possible definitions of a hydrogel, but the most common definition used is "A hydrogel is a cross-linked polymer network capable of hosting large quantities of water without becoming dissolved" [112]. In the literature it is possible to find several classifications; based on their polymer nature, hydrogels can be classified into natural or synthetic hydrogels. Hydrogels formed by synthetic polymers have the advantage of having tunable mechanical properties. They involve a wide range of chemical modifications, obtaining low batch-to-batch variations.

The hydrogels formed by natural polymers help to mimic natural ECM and have good cell-adhesion. However, the drawback of natural hydrogels is that they present relatively poor mechanical properties and high batch-to-batch variations. Hydrogels combining synthetic and natural polymers is a good way to combine the main advantages of both materials.

Robust cross-linking to obtain the hydrogel is essential to prevent it dissolving in aqueous media. A variety of physical and chemical cross-linking mechanisms have been used to synthesize hydrogels. The cross-linking density of the hydrogel dictates the physico-chemical properties of

the hydrogel. The interactions can be classified as follows:

(a) Physical bond

Polymer networks with physical bonds are formed by reversible bonding and the interaction can be ionic, hydrogen bonds, Van der Waals, hydrophobic interactions or entanglement between the polymer chains [113]. These networks have better adsorption properties, weaker mechanical properties and are susceptible to pH-sensitive swellings. The most common mechanism to obtain chitosan polymer networks with physical interaction is by using a cross-linking agent such as tripolyphosphate [65, 114] in which the interactions depend on the pH medium. Physical interactions of chitosan with other polymers require a polyanionic polymer [115, 116] like alginate or collagen. J. Berger *et al.*, show a table with some polyelectrolyte complexes with chitosan [113].

(b) Chemical bond

Polymer chains bond chemically with other polymeric chains or cross-linking agents by covalent or irreversible links [98]. These networks are characterized by good absorption and mechanical properties. The covalent bonds in the networks can be activated in two ways: by using an external cross-linking agent and between polymers with reactive groups. In the case of chitosan, they can be cross-linked by cross-linking agents like glutaraldehyde [117], genipin [63, 118], epichlorohydrin [119] or with other polymers with specific reactive groups able to crosslink directly or by the use of initiators and catalysts [120].

Chitosan's most common cross-linking reaction is with aldehyde groups, which is an N-alkylation of the amine group and is performed in mild conditions. It is not necessary to use external activated agents.

Different polymers can be cross-linked to obtain polymer networks with suitably tailored properties for a given tissue application. The networks can be classified into homopolymer networks formed by cross-linking between monomer units of the same polymer. Heteropolymer networks are formed by cross-linking monomer units of one polymer with monomer units of another polymer, also called a copolymer network or block-copolymer network. Block-copolymer networks are formed by cross-linking between macromolecule polymers with other monomer units of a different polymer (Figure 1.10).

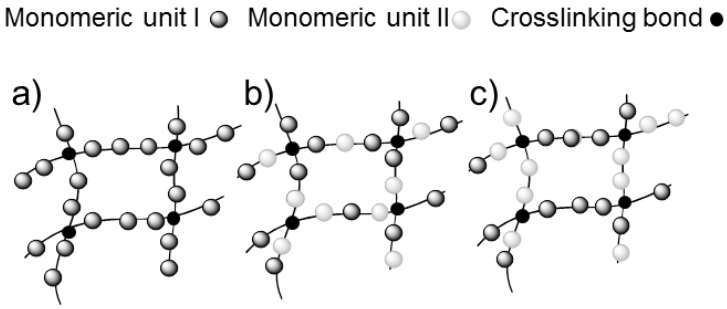

Figure 1.10. Polymeric structures where a) is a homopolymer, b) is a copolymer network and c) is a block-copolymer network.

Fully-Interpenetrating polymer networks, IPN, are formed by two cross-linked networks. Semi-Interpenetrating polymer networks, Semi-IPN, are formed by an entangled polymer in a cross-linked polymer.

Hydrogels can be synthesized with required properties according to their chemical structure, composition, the nature of the starting materials, polymer chain linking density, hydrophobicity and hydrophilicity for a particular biomedical application [121].

Studies have been carried out on strategies for seeking materials with tunable properties to obtain hydrogels by block-copolymer networks. The block-copolymer networks of poly(ethyl acrylate), PEA, and its copolymers

with 2-hydroxyethyl acrylate, P(EA-co-HEA) [122-124], the methacrylate-endcapped caprolactone, poly(CLMA-co-HEA) [125] and poly (L-lactide) and 2-hydroxyethyl acrylate, (HEA), p(mLA-co-HEA) are synthesized by UV polymerization from synthetic polymers. Wettability, mechanical properties, protein adhesion and cell attachment have been modulated as a function of the material's composition. The block-copolymer networks are synthesized by covalent attachment. The polymers are previously functionalized with ended reactive groups. For example, the block-copolymer networks formed by cross-linking with poly(ε-caprolactone), (PCL) with poly(ethylene glycol), (PEG) or poly(L-lactide) acid, (PLLA) and poly(ethylene glycol), PEG [126, 127] and poly(L-lactide)-co-(glycolic), (PLGA) with poly(ethylene glycol), PEG.

Chitosan networks have been obtained by covalent cross-linking with other polymers. For example, chitosan cross-linked with hyaluronic acid [128]. Chitosan cross-linked with collagen [61] or with polyurethane to repair skin defects [36]. These covalent cross-linking have been obtained by Michael addition reaction or base Schiff formation as previously described [129].

1.5 Chitosan biodegradation

Polymer biodegradation is one of the most important properties in Tissue Engineering applications. The biomaterial should degrade and be resorbed at a rate that matches the regeneration of new tissue. Degradation is a mechanism that involves a cleavage of the polymer chains to form by-products: oligomers and/or monomers that can be absorbed or excreted by the body.

The distinct biodegradation types can be classified into via backbone chain

breakage, via enzymatic, via hydrolytic, and microbial degradation, or a combination of these methods.

The degradation rate is attributed to several factors, such as: the nature of the chemical bond, the pH media, and the polymer´s properties: crystallinity, molecular weight and hydrophylicity/hydrophobicity.

Kinetic degradation of chitosan is directly related to its deacetylation degree (DD) and the molecular weight (Mw) of the polymer. CHT is a polymer formed by β(1→4) O-glycosidic bonds and the degradation mechanism must involve the cleavage of these specific bonds. A variety of pathways have been used to degrade chitosan, such us ultraviolet and gamma radiation [130], acid hydrolysis, oxidative degradation with hydrogen peroxide via powerful oxidizing species to attack the β(1→4) O-glycosidic linkages of the chitosan [131] and also in enzymatic and hydrolytic conditions.

Chitosan can be degraded enzymatically by chitinases, chitosanases [132] and α-glucosidases [133], in which lysozyme is the most frequently used. The mechanism of the degradation is activated because lysozyme contains a hexameric-binding site that can bind to hexasacharide units, where almost three or four of these units should be acetylated. For these reasons, the degradation kinetics of chitosan depends on its DD. Lysozyme exists in some human body fluids and tissues with concentrations from 4 to 13 mg/L in serum and 450 to 1230 mg/L in tears [134, 135].

A variety of "*in vitro*" studies can be found in the literature on tests of the optimal enzymatic activity. However the chitosan present a lower degradation rate in hydrolytic and enzymatic conditions [135-137] being a disadvantage for some TE applications.

Chapter 2. Hypothesis, Objectives and Outline

2.1 Hypothesis

Cell transplant for soft tissues regeneration requires supporting materials able to absorb large amounts of water. Hydrogels allow good permeability to water-soluble substances, nutrients, oxygen and growth factors. Furthermore, the material also should present good cell adhesion and degradation kinetics adequate to each application, with the timing of neo-tissue formation like corneal therapy or skin regeneration. In some of these applications quite fast degradation kinetic is necessary.

Chitosan is a biomaterial with good properties for soft tissue regeneration. Nevertheless, its degradation is quite slow in enzymatic media and nearly null in purely hydrolytic conditions.

Thus, we hypothesize that the degradation kinetics can be modulated by using low molecular weight biodegradable polyester/polyether as cross-linker of water-soluble chitosan. In this way the hydrolytic or enzymatic degradation of the cross-linker will deliver the polysaccharide chains that will be dissolved. Besides by introducing hydrophobic polyester blocks into the supporting material, an increase cell-material interaction is expected. And introducing the hydrophilic polyether blocks a highly swellable supporting material is expected.

2.2 Objectives

The main objective of this thesis is to obtain supporting materials with tunable degradation rate for cell transplant. The supporting materials consist of block-copolymer networks being one of the components a water-soluble modified chitosan. Their physical properties and degradation kinetics in different media, including cell culture are also studied.

The specific objectives carried out are:

- To contribute to the understanding of the influence of deacetylation degree on the water sorption and physical properties of chitosan.

- To synthesize dialdehyde end-capped poly(ε-caprolactone) to be use as cross-linker (aPCL).

- To obtain block-copolymer networks consisting of a hydrophilic and water-soluble polymer (protonated chitosan (P-CHT) or carboxymethyl chitosan, (CmCHT)) and a hydrophobic polymer, (PCL) which degrades by hydrolysis.

- To prepare hydrogels with very high equilibrium water content consisting of combinations of two hydrophilic components: carboxymethyl chitosan (CmCHT) and poly(ethylene glycol), (PEG).

- To control the degradation kinetics of the obtained polymeric networks.

2.3 Outline

This thesis is divided into nine chapters. After the Introduction, Hypothesis and Objectives, Chapter 3 describes the main properties of chitosan in relation to its degree of deacetylation (DD) and some approaches are suggested for determining the influence of DD on the capacity for water sorption. We also clarify its influence on thermal degradation and on the preparation of electrospun chitosan membranes.

Chapters 4, 5 and 6 concentrate on copolymer networks based on chitosan and carboxymethyl chitosan. Our goal here is to control the degradation rate by using low molecular weight biodegradable polyester/polyether as the cross-linker of water-soluble chitosan. Chapter 4 deals with the preparation the chitosan-poly(ε-caprolactone) copolymer networks. We study the hydrolytic and enzymatic degradation of protonated water-soluble chitosan. In Chapter 5 deals with the preparation the water-soluble carboxymethyl chitosan-poly(ε-caprolactone) block-copolymer network to obtain very fast degradation and propose this material as candidate for a cell culture study. In Chapter 6 we describe the highly swellable hydrogels of carboxymethyl chitosan and poly(ethylene glycol).

Finally in Chapter 7 we recapitulate the major findings of the thesis. The Bibliography is included in Chapter 8 and the publications related to the thesis are listed in Chapter 9.

Chapter 3. Physico-chemical characterization of chitosan

3.1 Determining the influence of N-acetylation on water sorption in chitosan films.

3.1.1 Abstract*

Water absorption in chitosan rapidly increases when the deacetylation degree decreases between 85 and 45%. This seems to contradict the fact that water absorption in chitin is much lower than that of chitosan. The aim of this chapter is to understand this feature by measuring the main parameters affecting equilibrium water content. Since swelling capacity depends on the water-polymer interaction, the Flory Huggins interaction parameter was evaluated, finding small or null dependence on the deacetylation degree. Other factor influencing elastic energy is chain stiffness related to the elastic modulus that was measured as a function of deacetylation degree. Besides, crystalline structure was measured by X-ray diffraction patterns as a characteristic of cross-linking density. These observations led us to conclude that the instability of crystals during the swelling process increases with decreasing deacetylation degree, explaining the high equilibrium water content of low deacetylation chitosans.

*The results presented in this chapter have been published in:
M. A. Gámiz-González, A. E. Piskin, C. Pandis, C. Chatzimanolis-Moustakasb, A. Kyritsisb, B. Marí. J. L. Gómez Ribelles, A. Vidaurre. Determining the influence of N-acetylation on water sorption in chitosan films. Carbohydrate Polymers. 133,110–116 (2015).

3.1.2 Introduction

Chitin is the second most abundant natural polysaccharide next to cellulose. It is obtained from natural resources like insects, marine invertebrates and fungi. The N-deacetylation degree is the relationship between amine ($-NH_2$) groups with respect to the total amount of N-acetyl ($-NHCOCH_3$) and amine ($-NH_2$) groups in the polymer. Chitin is a fully acetylated polymer and is called chitosan when the deacetylation degree (DD) is between 50-90%, but these limits are arbitrary [74].

Chitosan is thus a copolymer formed by glucosamine and N-acetyl glucosamine units linked by O-glycosidic bonds β(1→4) and is a biocompatible, biodegradable and non-toxic hydrogel [138]. Due to its natural origin and physical properties, it is one of the hydrogels proposed for many applications in the field of tissue engineering, regenerative medicine, pharmaceutics, in particular drug delivery, and the cosmetic industry [139].

The physico-chemical properties of chitosan vary widely and depend on factors such as the natural source from which the polymer is obtained, or the chemical process yielding N-acetylation or/and N-deacetylation to obtain the desired DD value [140]. The N-deacetylation degree (DD) is one of the most important determinants of chitosan behavior concerning physico-chemical properties such as reactivity [79], crystallinity [81], swelling degree and mechanical properties [141, 142]. Chitosan exhibits a highly hydrophilic behavior [143] due to the presence of hydroxyl and amino groups. The complete removal of the water molecules upon drying, even at temperatures above 100 °C, is very difficult [144].

In this chapter chitosan with varying DD was prepared in mild conditions by acetylation reaction [97] of high DD medical grade chitosan with acetic

anhydride. It was found that the equilibrium water content increases when DD decreases. Water absorption in chitosan rapidly increases when the deacetylation degree decreases between 85 and 45%. This seems to contradict the fact that water absorption in chitin is much lower than that of chitosan.

The main purpose of the first part of this chapter is to get a better understanding of this behavior, so important in tissue engineering applications. To the best of our knowledge this chapter is the first experimental study determining the main parameters of the equilibrium water content of chitosan with varying DD in a homologous series of samples.

3.1.3 Materials and methods

3.1.3.1 Materials

Chitosan, medical grade polymer, was purchased from Novamatrix (Protasan UP B 80/20) with 80-89% deacetylation degree, according to the supplier's information, and apparent viscosity of 20-199 mPa.s. Acid acetic, acetic anhydride, deuterium oxide (D_2O) and deuterium chloride (DCl), analytical grade, were purchased from Sigma-Aldrich and used without further purification. Sodium iodide and sodium hydroxide pellets were purchased from Scharlau and used as received.

3.1.3.2 N-acetylation reaction

Chitosan was dissolved in acid acetic 2% (w/w) under stirring for three hours, after which methanol was added and the solution was left to stir overnight. Different quantities of acetic anhydride were mixed with methanol and were added to the chitosan solution [97]. The reaction was

stirred overnight and then NaOH 1M was added to neutralize the chitosan solution. All synthesis steps were carried out at room temperature.
The chitosan samples were washed several times with water until neutral pH was obtained. Chitosan was freeze-dried to obtain a white powder with different deacetylation degrees.

3.1.3.3 1H-NMR Spectroscopy

The deacetylation degree (DD) was determined by nuclear magnetic resonance of proton spectroscopy (1H-NMR) using a Varian Unity Plus 300 [75, 145]. Five milligrams of the synthesized chitosan powder were added to NMR tubes containing 1 mL of 2% (v/v) deuterium chloride solution in deuterated water. The chitosan solutions were heated to 70 °C for 2-3 hours, carrying out the experiment at this temperature. The deacetylation degree of the samples was calculated by the equation (Lavertu *et al.*, 2003):

$$DD(\%) = \left(\frac{H1D}{H1D + {HAc}/{3}}\right)100 \tag{3.1}$$

Where H1D is the signal area corresponding to the proton from C1 of glucosamine unit and HAc is the signal area corresponding to the proton from methyl group of N-acetyl-glucosamine unit.

3.1.3.4 Gel Permeation Chromatography

Molecular weight distribution of chitosan films with different DD were analyzed using a Gel Permeation Chromatographer, GPC, at 35 ºC using a Waters Breeze GPC system with a 1525 Binary HPLC pump (Waters Corporation, Milford, MA) equipped with a 2414 refractive index detector and four serial columns of water (Ultrahydrogel 7.8 mm ID x 30 cm). The samples were dissolved in a buffer solution of CH_3COOH

0.5M/CH_3COONa 0.2M, pH=4.5 that was also used as mobile phase at a flow rate of 0.5 ml/min and 20µl injection volume. The calibration curve was prepared by using monodisperse PEG poly(ethylene glycol) standards (Showa denko).

3.1.3.5 Preparation of chitosan films

Chitosan films were formed from a 2% (w/v) solution by a solvent casting method [77]. Chitosan solutions with different DD were prepared in an aqueous solution of acetic acid 2% (v/v). When the chitosan solution was totally dissolved, it was filtered through a nylon cloth to remove any insoluble fractions and put in a teflon mold until the solvent was completely evaporated. After drying, the films were neutralized in 25mL (NaOH) sodium hydroxide 1M aqueous solution in order to deprotonate the amine groups of chitosan chains. Finally, the films obtained were washed several times with distilled water until neutral pH.

3.1.3.6 Equilibrium water content

Chitosan films (N=5 replicates for each DD) were dried in vacuum desiccators at 50 °C and weighed (W_0). They were then immersed in deionized water at room temperature until equilibrium (72 hours). The swollen films were taken out of the liquid water and their surfaces were wiped with filter paper to remove excess water and then weighed, W_s.

The equilibrium water content for each sample was calculated from the following equation:

$$EWC(\%) = \frac{W_s - W_0}{W_0}\ 100 \qquad (3.2)$$

3.1.3.7 Water vapor absorption isotherms

Water vapor absorption experiments were performed by the gravimetric technique at 25 °C using a VTI-SA+ (TA Instruments) vapor absorption analyzer for water activities up to 0.95. The water weight content, h, is defined as:

$$h = \frac{m_{Water}}{m_{dry\ polymer}} \tag{3.3}$$

The volume fraction of water was calculated from the following relation:

$$\phi = \frac{h}{h + {\rho_w}/{\rho_{dry}}} \tag{3.4}$$

Where ρ_{dry} and ρ_{w} are polymer and water density respectively.

The density of the polymer samples (ρ_{dry}) was determined using the Density Kit mounted to a Mettler Toledo (AX 205) balance. The measurements for density determination were preformed based on Archimides' principle by weighting the dried samples in air and when immersed in an auxiliary liquid of known density. N-octane (purchased from Sigma-Aldrich) was used as the auxiliary liquid because chitosan does not dissolve or swell in it.

3.1.3.8 Crystallinity

X-ray diffraction spectra of the chitosan films were obtained on a Rigaku Ultima IV X-ray diffractometer in the Bragg-Bentano configuration using the Kα radiation of a Cu anode. The dry samples were scanned from 2θ=5-70° at a speed of 2°/min. Diffraction patterns were deconvoluted, using "PDXL" Integrated X-Ray powder diffraction software, to three non symmetrical Gaussian peaks. Relative crystallinity was determined as the ratio to the integrated crystalline intensity to the total intensity for

comparative purposes [73]. Diffraction spectra were measured for wet samples from 2θ=5-35º at a speed of 2º/min. Wet samples were immersed in deionized water until they were placed in the diffractometer chamber.

3.1.3.9 Mechanical testing

Dynamical mechanical analysis of the CHT films was carried out by a tensile test in a Perkin Elmer DMA 8000 device. Five samples (N=5) of each chitosan film were cut into long narrow strips with a cross section of approximately 5 mm in width. Measurements were performed on samples of 6 mm free length, at room temperature, 1 Hz, and at different levels of relative humidity in both swollen and dry states. The samples were equilibrated in sealed desiccators containing over saturated salt solutions of NaCl, NaI and pure water, to obtain relative humidities of 36%, 75% and 100%, respectively. The samples were then mounted in the device and a flow of air with the same %RH was allowed to circulate through the measuring chamber. This humid air was obtained by allowing air to bubble in three consecutive recipients containing the corresponding over saturated salt solutions (NaCl, NaI and water). The measurements were also performed on dry samples and on samples previously immersed in liquid water. These samples were maintained immersed in deionized water, placed in a teflon reservoir, while the measurements took place. In all cases the samples were allowed to equilibrate before the data were recorded.

3.1.3.10 Statistical analysis

The data were analyzed by ANOVA using an SPSS computer program (SPSS Statistic 16.0), while means were compared by the Tukey-*b* test with the level of significance set at $P<0.05$.

3.1.4 Results and discussion

Chitosan with different deacetylation degrees (DD) ranging from values of 72 to 45% were obtained from CHT-Or with DD=85%, as determined by 1H-NMR spectroscopy, following Eq (3.1). GPC measurements indicated (Figure 3.1b) an increase in molecular weight with decreasing deacetylation, that suggest the formation of aggregates of higher molecular weight [146]. The samples are given a number after the CHT to indicate their DD, for example, CHT-45 means DD=45%.

3.1.4.1 Equilibrium water content. Water absorption from the liquid.

Figure 3.1 shows that the equilibrium water content (EWC) increases when the deacetylation degree decreases. The EWC for CHT-Or is around 242 ± 13% whereas it is 540 ± 50% for CHT-45. This result is in good agreement with the literature [147].

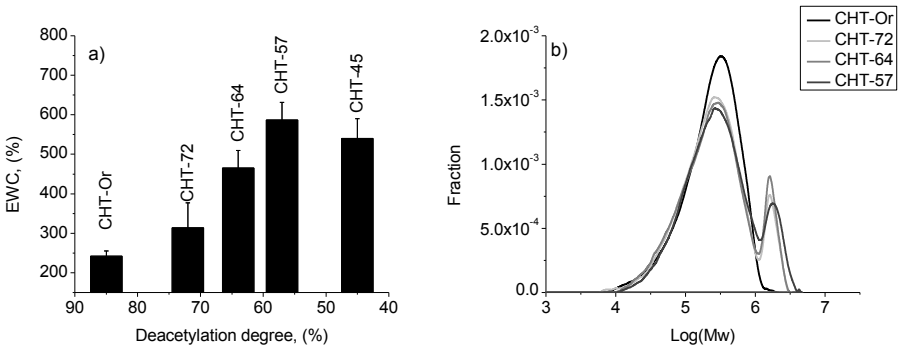

Figure 3.1.a) Equilibrium water content EWC of chitosan with different deacetylation degrees after 72 hours immersed in deionizer water at room temperature. b) Molecular weight distribution of chitosan with varying deacetylation degrees.

Statistical analysis showed that there is no significant difference in EWC between samples with lower DDs (CHT-64, CHT-57 and CHT-45).

Chitosan is water-soluble at acidic pH but, as can be seen in Figure 3.1, at pH7, non-protonated chitosan is able to absorb really large amounts of

water but it is not water-soluble. This can be explained by the formation of a network structure in which crystalline entities and physical entanglements play the role of physical crosslinks even when chitosan was not chemically cross-linked. Thus, swelling behavior must be analyzed in terms of the swelling theory of polymer networks. The Flory-Rehner equation is obtained by minimizing the free energy of the swollen network, which is the sum of the free energy of mixing (determined by Flory interaction parameter between the polymer segments and the solvent) and the elastic free energy depending on the length and stiffness of the polymer chains between cross-links. The Flory-Rehner equation [148, 149] gives the relationship between the swelling capacity of a polymer network when immersed in a liquid solvent and the number of effective polymer chains between crosslinks per unit volume of polymer, n_c/V

$$ln(\emptyset) + (1 - \emptyset) + \chi(1 - \emptyset)^2 + v_{sol}\frac{n_c}{V}(1 - \emptyset)^{\frac{1}{3}} = 0 \quad (3.5)$$

where ϕ is the volume fraction of water in the swollen network, v_{sol} is the molar volume of the solvent and χ is the Flory interaction parameter between polymer and solvent and n_c/V will be determined by the number of crystalline structures or chain entanglements.

From Eq (3.5) one can infer that the increase in water content when DD decreases, as shown in Figure 3.1, can only be explained by (i) a decrease of χ and /or (ii) a decrease of chain stiffness and/or (iii) a decrease of crystallinity when DD falls to between 85 and 50%.

3.1.4.2 Water absorption from the vapor phase: Flory Huggins parameter

In order to verify the influence of the polymer-water interaction, the absorption isotherms were analyzed by measuring the water content of

chitosan films equilibrated in a vapor atmosphere at different relative humidities, i.e. with varying water activity, a_w. Figure 3.2 shows the water content measured on a dry basis, h, as a function of water activity. These isotherms belong to Class II in the Brunauer classification [150]. The above sigmoidal shape is typical of hydrogels, while the departure from linear behavior for higher water activities is explained in terms of the clustering of water molecules [151].

The water-polymer interaction parameter was calculated from the Flory-Huggins theory [152], by the equation:

$$lna_w = ln\phi + (1-\phi) + \chi(1-\phi)^2 \tag{3.6}$$

Where, a_w is the water activity, and ϕ and χ have been previously described.

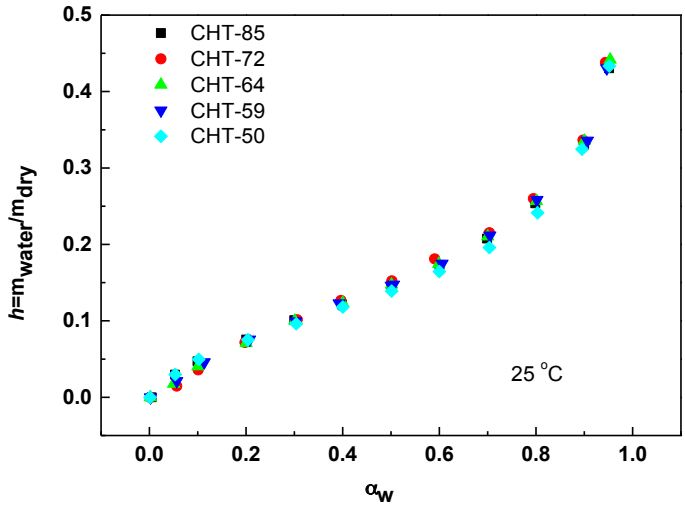

Figure 3.2. Water content in the films with different DD to different water activity.

It should be emphasized the great difference between the amount of water adsorbed from the vapor phase with that from liquid water. The water

uptake obtained from measurements of water vapor absorption is about 45% on dry basis, for the highest water activity, that is α_w=0.95. In contrary, when immersed in liquid water the water content varies between 250-600%. Similar high values have been reported previously [153] for chitosan films. The above behavior is typical for hydrogels and could be explained by taking into consideration that the amount of water absorbed in the form of bulk water is much higher than that forming a homogeneous mixed phase with the hydrogel [154]. The former depends more on the elasticity of the network, whereas the latter depends more on the number of absorption sites in the polymer chains. Furthermore the significant network expansion of chitosan when immersed in liquid water could also be followed by the disentanglement of micelles formed by hydrophilic groups (hydroxyl and amino groups), creating in that way new absorption sites and additional space for lodging of liquid water [155]. Consequently, the equilibrium water content is appreciably higher when compared with absorption from water vapor.

The apparent interaction parameter χ was calculated from the data obtained from the water vapor absorption isotherms using Eq (3.5) and Eq (3.6). As water absorption isotherms are practically independent of DD, the interaction parameter is also independent of DD. Figure 3.3 shows the Flory Huggins interaction parameters calculated between $0.3< a_w <1$, (when water activity was lower than 0.3, samples were not able to reach equilibrium during the experimental time). The χ values increase with water activity, reaching a value around 0.7 for all samples at the highest relative humidity level. It is worth highlighting here that the affinity of chitosan to water molecules does not significantly depend on DD.

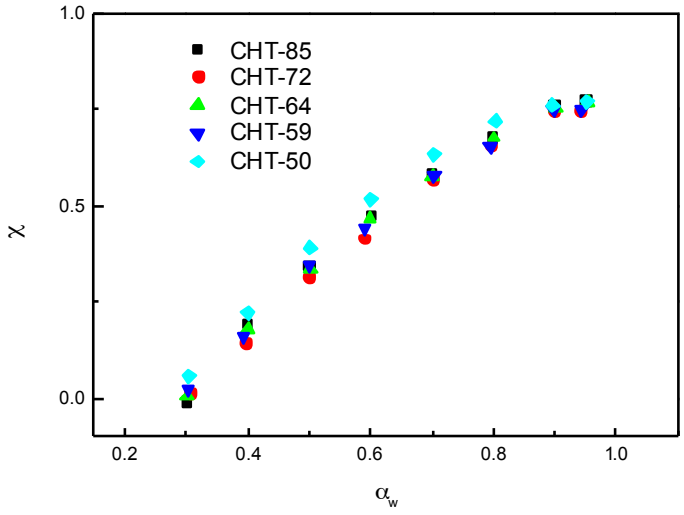

Figure 3.3. Flory Huggins interaction parameter of chitosan films as a function of water activity in the vapor phase.

This result is in agreement with what could be obtained from group contribution calculations. This method can be estimated from solubility parameters of solvent, δs, and polymer, δp, [156]:

$$\chi_{ps} = 0.34 + \frac{v_s}{RT}(\delta_P - \delta_S)^2 \quad (3.7)$$

For the different deacetylation degrees, the solubility parameter of the polymer can be calculated from that of chitin and chitosan by:

$$\delta_p = \delta_{chitin}\left(1 - \frac{DD}{100}\right) + \delta_{chitosan}\frac{DD}{100} \quad (3.8)$$

The solubility parameter values of chitin and 100% deacetylated chitosan are not significantly different. The average of the values determined by different group contribution methods was δ_{chitin}=41.15 J ^{½} cm$^{-3/2}$ while $\delta_{chitosan}$=43.06 J ^{½} cm$^{-3/2}$ [157].

The interaction parameter of 0.55 for CHT-Or and 0.58 for CHT-59 was obtained by applying Eqs. (3.7) and (3.8).

3.1.4.3 Mechanical testing

The mechanical tests on the different chitosan films were analyzed in order to determine the effect of chain stiffness on the swelling capacity of the polymer. The experiments were carried out at room temperature under five different conditions: in a dry state in a vapor atmosphere, at three different relative humidities, and immersed in liquid water.

As could be expected, the elastic modulus shown in Figure 3.4 falls as water content of the sample rises, both in a vapor atmosphere and immersed in liquid water, and the elastic modulus also increases with DD when the samples are measured in a vapor atmosphere. This indicates that the stiffness of the polymer chain increases with the presence of amine groups in the backbone of the polymer. However, when the samples are immersed in water, their elastic modulus seems to depend on water content, whatever the DD. The straight line in Figure 3.4 for water content above 200% is intended to be a guide only.

It is accepted [158] that the differences in the conformational mobility of the chitosan chains with DD can be affected by the highly packed chains due to inter-chain interactions, mainly by hydrogen bonding; and these interactions are favored when DD is reduced. Nevertheless, the results shown in Figure 3.4 seem to indicate that, as the polymer is immersed in water, the rearrangements of the chains are quite similar for all DDs, so that chain stiffness could not be the determinant parameter for water content.

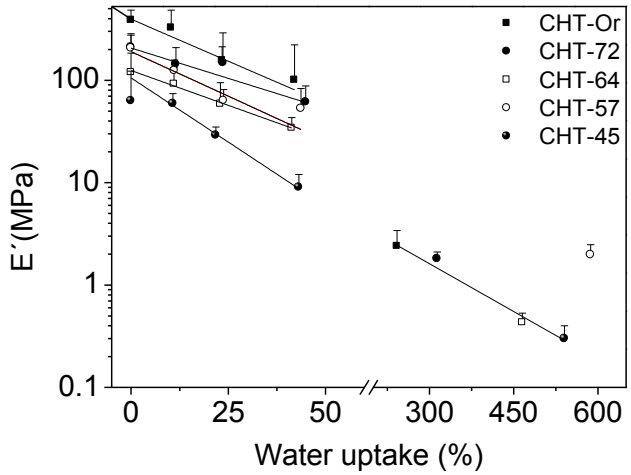

Figure 3.4. Elastic modulus of chitosan films at room temperature with different deacetylation degrees in a dry state, different relative humidity conditions, and immersed in water. Lines are only intended as guides.

The dependence of chain stiffness with DD for lower water contents could produce a change in the absorption kinetics, since the higher chain stiffness in the more deacetylated samples could slow down the absorption rate in the first stages of the absorption process, while equilibrium final states could be unaffected. This hypothesis was nevertheless not checked, as being outside the scope of this work.

3.1.4.4 Crystallinity

If the large increase in gel swelling capacity with decreasing deacetylation cannot be ascribed either to the polymer-water interaction or to chain stiffness, the parameter that determines this behavior can only be the density of the physical cross-links (crystals).

In order to verify this hypothesis, the X ray diffraction spectra were measured. Figure 3.5 shows the diffractograms of samples in a dry state. Diffraction peaks were deconvoluted using three non symmetrical Gaussian peaks showing a typical spectrum of the chitosan polymer with

two strong reflections at 2θ =9-10º for (020) reflections and at 2θ=20-21º for (110) and (120) reflections [140]. The wide peak, located about 38º, with crystallite size lower than 9 Å is ascribed to the amorphous [84]. The films with the highest DDs present the most sharp and intense peaks around 2θ=20-21º, whereas the films with lower DDs show the most intense peaks around 2θ=9-10º. Relative crystallinity, calculated by dividing the area of the crystalline peaks by the total area under the curve, increases as DD decreases, ranging from 79% ± 2% for CHT-Or to 92.6% ± 0.6% for CHT-45 [82]. This change in crystallinity is attributed to the incorporation of different amounts of acetyl groups in the polymer, consequently reorganizing the chitosan's crystalline structure.

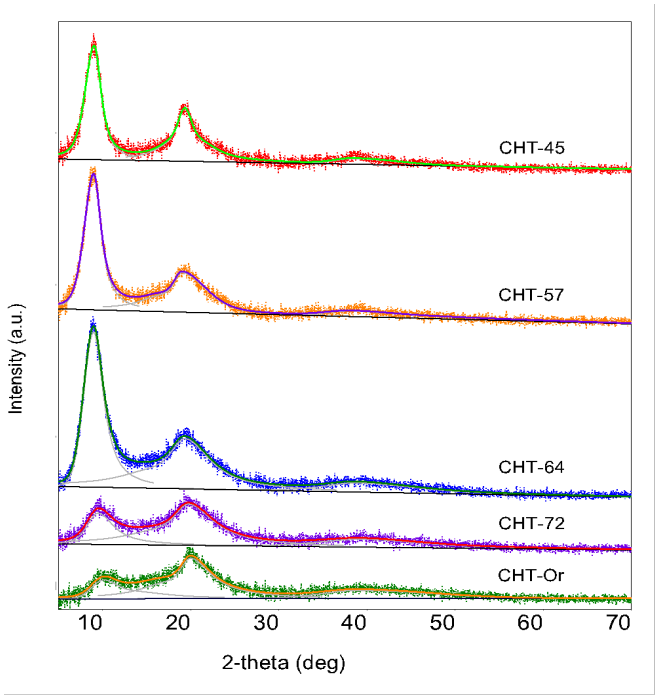

Figure 3.5. Diffractograms of chitosan films with different DDs measured in a dry state. The experimental spectra, the Gaussians for each peak(grey), and the model obtained by gaussians superposition are shown in the plot.

Water also plays an important role in the formation of chitosan's crystal structure, as the peak observed at 10º is generally attributed to the integration of water molecules in the crystal lattice [159]. More specifically, this peak is associated with the linkage between acetylated glucosamine (GlcNAc) groups of neighboring chains, facilitating the incorporation of water molecules into such a network and forming a hydrated crystal [160]. Therefore, while it is logical to see the lower intensity in the XRD diffractograms in the samples with higher DDs, meaning fewer acetylated glucosamine units, on the other hand, it is worth noting that the intensity of that peak reaches the maximum intensity for the sample with 64 % DD, implying that the large amount of glycosamine groups may cause steric hindrance to the formation of this hydrated crystal structure.

In order to verify the relationship between crystalline structure and water absorption capacity, the X-ray diffraction spectra of samples with different water contents were measured. The experimental procedure was as follows: swollen samples in water were placed in the diffractometer and spectra were collected while the samples were losing water. The diffractogram of the hydrated sample was obtained by the difference between the measured diffractogram and the background, which includes the water signal. Figure 3.6 shows an example of the diffractogram of a swollen sample, the background, and the difference between both signals. A new scan was measured every 3 minutes until no further changes were observed.

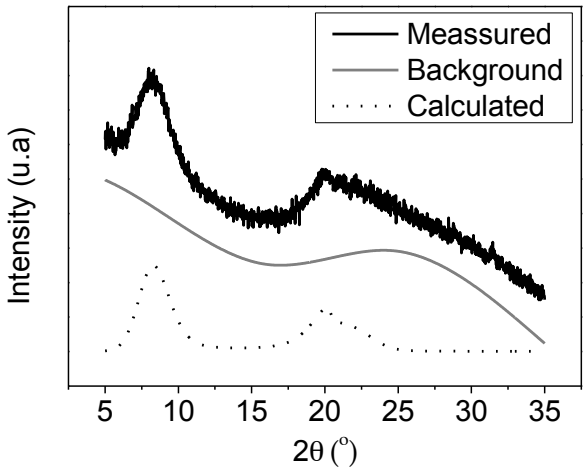

Figure 3.6. Diffractograms of a swollen sample, background and the difference between both signals, considered as the diffractogram of the hydrated sample.

Figure 3.7 shows the calculated diffractograms for CHT-Or and CHT-64 as a function of time. It can be observed that significant changes in the crystalline structure occur during the drying process. In all cases the dry samples (T5) show more intense peaks than the corresponding swollen samples (T0).

The most deacetylated sample, CHT-Or, shows comparatively fewer changes with water content than the most acetylated ones. For the CHT-Or sample, small changes were observed in the $2\theta=10^{o}$ peak, whereas an increase in the intensity of the $2\theta=20^{o}$ peak is observed throughout the drying process. In contrast, significant changes were observed in the rest of the samples; e.g. Figure 3.7b shows the results for CHT-64. It can be observed that the crystalline peak around $2\theta=9\text{-}10^{o}$ does not appear in the swollen state and the $2\theta=20^{o}$ peak presents a very low intensity.

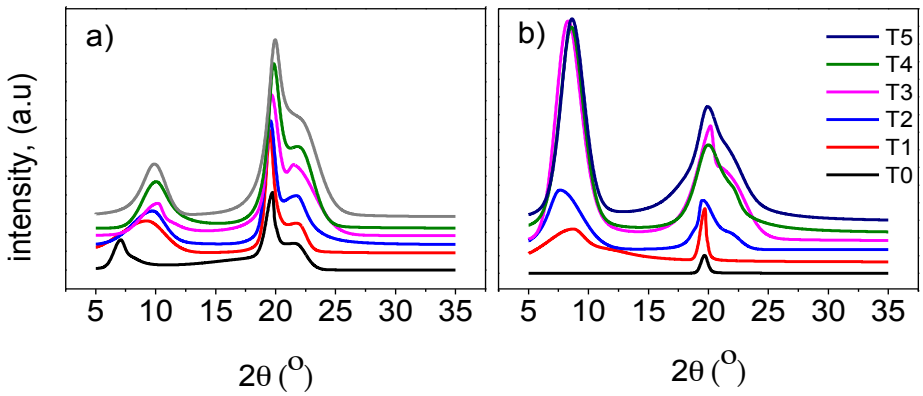

Figure 3.7. Calculated diffractograms of a) CHT-Or and b) CHT-64 taken every 3 minutes (T0=0 min, T1=3 min and so on) starting from swollen films until dry at room temperature.

These results suggest that water dissolves part of the crystals and that this effect is more pronounced in samples with lower DD. Both crystalline peaks increase in intensity as the film loses water. This behavior was also observed by [80], who stated that the β-chitin shows a reversible crystalline structure when water molecules disappear from inside the sample. To sum up, the DRX results show that the samples with higher DDs present a more stable crystalline structure, which acts as a cross-linker, hindering the expansion of the network. On the other, the samples with the lowest DDs, which are more crystalline in the dry state, become less crystalline in the swollen state due to the dissolution of a part of their crystals.

3.1.5 Conclusions

In this chapter we analyzed the physical origin of the increase of chitosan's equilibrium water content with decreasing degrees of deacetylation. Three different physical properties were studied: the interaction water-polymer parameter χ, the elasticity of the polymer chain, and the crystalline structure.The results show that the low dependence of the polymer-water

interaction parameter on the deacetylation degree cannot explain the differences in equilibrium water content. The mechanical test indicates some differences in polymer chain stiffness when the samples contain small amounts of water (from the vapor atmosphere), but no differences when they are immersed in water. The differences in chain stiffness with deacetylation degree cannot therefore explain the evolution of the water absorption behavior either. However, the DRX diffractograms show significant differences in the crystalline structure of the dry and swollen samples. In the dry state those with lowest DD are more crystalline than CHT-Or. However, when the samples are immersed in water the tendency changes and those with the highest DD are the most crystalline.

In conclusion, this study of the crystalline structure of swollen samples finds that equilibrium water content increases as DD decreases, due to the crystalline regions which act as physical cross-linkers and are partially dissolved by water. This effect is more pronounced in the samples with lower DD.

3.2 Kinetic study of thermal degradation of chitosan as a function of deacetylation degree

3.2.1 Abstract*

Thermal degradation of chitosan at different deacetylation degree (DD) was analyzed by dynamic thermogravimetric analysis at different heating rates in a nitrogen atmosphere in the temperature range between 300 and 1073 K. The present study focused on the temperature range between 500 and 800 K, above water evaporation. Chitosan samples at various DD were obtained by mild condition reactions with different quantities of acetic anhydride. DD, calculated by 1H-NMR spectroscopy, ranged between 85% for the original sample and 50%. Thermal degradation showed a main degradation stage for the samples with the highest DD content and a second stage that appeared as a shoulder in the derivative curves at high temperatures for the samples with the lowest DD. The Kissinger and isoconversional Ozawa-Flynn-Wall models were employed to evaluate the activation energies corresponding to the two thermal degradation processes. Different kinetic models were tested with a non-linear least squares fitting routine using the values of the activation energy obtained by the isoconversional method and searching for the rest of the model parameters. The best fitting of the experimental data was obtained for Sestack-Berggren model.

*The results presented in this chapter are in preparation to be published as scientific article:

M. A. Gámiz-González, D. M. Correia, S. Lanceros-Mendez, V. Sencadas, J. L. Gómez Ribelles and A. Vidaurre.

Kinetic study of thermal degradation of chitosan as a function of deacetylation degree.

3.2.2 Introduction

The thermal stability of chitin is higher than that of chitosan. In both cases the degradation occurs by the cleavage of glycosidic linkages (C-O-C) [161]. Thermal degradation of chitosan occurs in two stages. The first stage corresponds to the degradation of the less thermally stable components and the second stage is due to degradation of acetyl groups.

Many different methods have been proposed for the calculation of the activation energy (E_a) of the thermal decomposition of chitosan and its derivatives. Isothermal and dynamic conditions, in air or a nitrogen atmosphere, as well as different DDs, make it very difficult to compare the different results. Different kinetic models, $f(\alpha)$, have been proposed in the literature, although very often a first order reaction, $f(\alpha) = (1 - \alpha)$, is assumed. Isoconversional or model free methods have also been used to process TGA data and obtain the activation energy without an explicit model from experimental thermal degradation data.

Among the more prominent methods in this category are the Friedman method [162], Kissinger [163] and Ozawa-Flynn-Wall [164] allowing the determination of the activation energy from dynamic experimental data measured at different heating rates [165].

Wanjun *et al.*, [161] studied the thermal degradation of chitin (DD=7.5%) and chitosan (DD=85%) by using TGA and DSC in a nitrogen atmosphere. By applying the Friedman method they studied the dependence of the activation energy with the degree of conversion and found no variation in the case of chitin, whereas activation energy increased with the degree of conversion in the case of chitosan. This suggests different degradation mechanisms for acetylated side chains that increase the thermal stability of the linked main chain parts. De Britto and Campana-Filho [166]

performed dynamic and isothermal experiments for chitosan with DD=88% and reported that the activation energy was E_a=149.6 kJ/mol and E_a=138.5 kJ/mol applying the Ozawa-Flynn-Wall and Kissinger method, respectively. E_a=153 kJ/mol was obtained in isothermal conditions. They also found that the kinetic model that best fitted the experimental data was the catalytic Sestak-Berggren model.

In this work we analyzed the influence of DD on the thermal degradation of chitosan. In the first step the activation energy was calculated by the Kissinger and Ozawa-Flynn-Wall methods. The TGA data was later processed using model-fitting methods such as the first and second order reactions and the Sestack-Berggreen model. We also considered computational methods that minimized the differences between the function and the experimental data.

Kinetic models

The kinetics of the thermal degradation process can be evaluated from the thermogravimetric data, considering that the degradation rate depends only on two variables, temperature, T and conversion degree, α [167]:

$$\frac{d\alpha(t)}{dt} = k(T)f[\alpha(t)] \tag{3.9}$$

The degree of conversion is defined by:

$$\alpha = \frac{w_0 - w_{(t)}}{w_0 - w_\infty} \tag{3.10}$$

w_0, $w_{(t)}$, and w_∞, being the weights of the sample before degradation, at a given time t and after complete degradation, respectively. The value of α reflects the progress of the overall transformation that can involve multiple steps, each of which has its specific extent of conversion and $f(\alpha)$ is the kinetic reaction model.

The temperature dependence of the degradation rate is usually parametrized through the Arrhenius equation:

$$k(T) = A\ exp\left(\frac{-E_a}{R\ T}\right) \tag{3.11}$$

where A is the pre-exponential factor, E_a is the activation energy, R is the gas constant (8.314 $J.mol^{-1}.K^{-1}$).

For constant heating rate, $\beta = \frac{dT}{dt}$, Eq (3.9) can be rearranged as:

$$\beta \frac{d\alpha}{dT} = A\ exp\left(\frac{-E_a}{R\ T}\right)\ f(\alpha) \tag{3.12}$$

Different approaches have been proposed to calculate the kinetic parameters, A and E_a, without any reaction model assumption. Once the activation energy has been obtained, it is possible to find the kinetic model that best fits the experimental data [168].

a) Isoconversional Ozawa-Flynn-Wall method

The isoconversional method of Ozawa-Flynn-Wall (OFW) [164, 169], which uses the Doyle approximation [170], is a method which assumes that the conversion function $f(\alpha)$ does not depend on the heating program. In this model the activation energy is a function of the degree of conversion and can be obtained from the slope of the linear relationship between $\ln(\beta)$ and 1/T given by the Eq:

$$ln(\beta) = const - 1.052\frac{E_a}{RT} \tag{3.13}$$

This method makes it possible to determine the activation energy without previous knowledge of the kinetic model. If the calculated values of E_a were the same for all the values of α, the existence of a single step reaction could be concluded. On the other hand, a change of E_a with the degree of

conversion would be an indication of a complex reaction mechanism that invalidates the separation of the variables involved in the OFW analysis [166, 167].

b) Kissinger's method

The Kissinger method [163] is used to determine the activation energy from plots of the logarithm of the heating rate versus inverse of temperature at the maximum reaction rate, in constant heating rate experiments. The activation energy is obtained from the slope of the straight line according to the Eq:

$$ln\left(\frac{\beta}{T_p^2}\right) = \frac{ln\,(AE_a)}{T} + ln\left[n(1-\alpha_p)^n\right] - \frac{E_a}{RT_p} \tag{3.14}$$

where T_p and α_p are the absolute temperature and the degree of conversion at the maximum weight loss rate. As in the OFW method, in the Kissinger method the activation energy can be determined without a precise knowledge of the reaction mechanism. However, it should be taken into account that the activation energy obtained by this method is only reliable if $f(\alpha_m)$ is independent of the heating rate β [171].

c) Reaction models

The most common equation model for decelerating-type processes is a reaction-order model:

$$f(\alpha) = (1-\alpha)^n \tag{3.15}$$

where n is the reaction order.

Sestak-Berggren [172] includes the consideration of different mechanisms in the empirical model depending on three parameters m, n, and p:

$$f(\alpha) = \alpha^m(1-\alpha)^n - [ln(1-\alpha)]^p \tag{3.16}$$

This is normally used in its reduced form (p=0), which represents an example of the autocatalytic model.

d) Computational method

Numerical calculation allows fitting non-isothermal degradation thermograms to empirical models using non-linear least squares search routines. In this work, the modeling of a TGA heating ramp was performed by substituting the heating ramp by a series of successive 0.5 ºC temperature steps, followed by isothermal periods Δt_i, to obtain the average experimental heating rate. After each isothermal stage i, at temperature T_i, with the conversion degree αi, a sudden change of temperature to T_{i+1} was considered to maintain the conversion degree unchanged, $\alpha_{i+1,0}=\alpha_i$. The conversion degree at the end of the i+1 isothermal was determined by an iterative procedure. The rate of change of the conversion degree was calculated using Eq (3.9), and the conversion degree at the end of the i+1 isothermal was determined as a first approximation by integration of Eq (3.9) to obtain the value $\alpha_{i+1,1}$. The mean value of $\alpha_{i+1,1}$ and $\alpha_{i+1,0}$ was used to recalculate $d\alpha/dt$ and with this derivative a new value of the conversion degree at the end of the step was calculated. A convergence of the value of α_{i+1} was obtained after three iteration cycles. This procedure can determine the thermogram for a given kinetic model correponding to Eq (3.9) with given values of the model parameters. The thermograms predicted in case of superposition of more than one degradation mode are also readily obtained. A least squares routine obtains the model parameters for the best fit to the experimental thermogram. Nevertheless, due to the strong correlation between activation energy and the pre-exponential parameters in the kinetic models, the activation energy for fitting was fixed with the value obtained

by the methods described above. The rest of the model parameters were determined by simultaneous fitting of the conversion degree and the weight derivative thermograms at a heating rate of 20 K/min.

3.2.3 Materials and methods

3.2.3.1 Materials

Chitosan medical grade polymer was purchased from Novamatrix (PROTASAN UP 80/20) with DDs between 80-89% and apparent viscosity 20-199 mPa.s. Acetic acid (99%), Sodium hydroxide, acetic anhydride, deuterium oxide (99%) and deuterium chloride (99%) were purchased from Sigma-Aldrich.

3.2.3.2 N-acetylation of chitosan

N-acetylation of chitosan medical grade was carried out with the same reaction conditions as previously described in section *3.1.3.2*. Chitosan medical grade was dissolved in 20 mL acid acetic 2% (w/w) by stirring for three hours, then 15 mL of methanol were added, and the solution was stirred overnight. Different quantities of acetic anhydride were mixed with methanol and added to the chitosan solution [97]. The reaction was stirred overnight and then NaOH 1M was added until neutral pH. The entire process was carried out at room temperature. Finally the N-acetylated chitosan was freeze-dried to obtain a white powder.

3.2.3.3 1H-NMR Spectroscopy

The DD of the chitosan samples was evaluated by proton nuclear magnetic resonance (1H-NMR), explained in section *3.1.3.3*. The spectra were recorded between 0-10 ppm in a Varian Unity plus 300 at 70ºC. Chitosan powder (5 mg /mL) at different DDs was dissolved in a deuterated aqueous

acid (D_2O/DCl) [97]. The chitosan solutions were dissolved by stirring at 70 °C for 1h. The DD was calculated by the integrals of the peak of proton H1 of deacetylated monomer (H1D) and the peak of the three protons of acetyl group (HAc) following the Eq (3.1).

3.2.3.4 Thermogravimetric Analysis (TGA)

Thermogravimetric measurements were performed using a TA-Instrument Model SDT-Q600 system. TGA tests were carried out in alumina crucibles in which weight samples of between 5 and 10 mg were heated from 303 K to 1073 K at different heating rates ranging from 10 K/min to 40 K/min. TGA experiments were performed under a nitrogen atmosphere (flow 20mL/min).

3.2.4 Results and discussion

3.2.4.1 Deacetylation degree

The DD of chitosan powder obtained from the N–acetylation reaction was calculated using the 1H-NMR spectroscopy by applying Eq (3.1), being 85% for the original chitosan and 72%, 64%, 59% and 50% for the N-acetylated chitosan. Samples were identified according to their DD: CHT-72, CHT-64, CHT-59 and CHT-50 except the original chitosan CHT-Or.

3.2.4.2 Thermogravimetric Analysis

The thermal degradation of CHT-Or and N-acetylated samples, CHT-72, CHT-64, CHT-59 and CHT-50, were analyzed in detail with dynamical TGA experiments at different heating rates ranging from 10 K/min to 40 K/min.

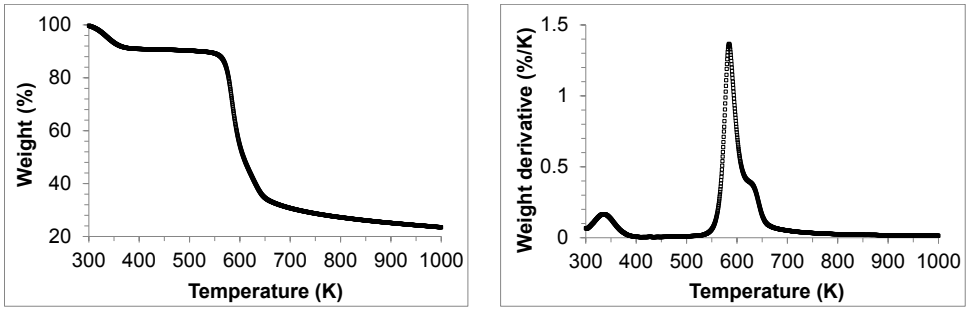

Figure 3.8. Weight loss and weight loss derivative for the CHT-50 sample at a heating rate of 20 K/min.

Figure 3.8 shows, by way of example, the weight and weight derivative for the CHT-50 sample at a heating rate of 20 K/min. Four phenomena can be observed: between room temperature and 400 K the weight loss is due to the evaporation of the absorbed water, between 500 and 800 K two overlapped peaks in the weight derivative are due to the degradation of the polymer chains as explained below, then a slow and continuous weight decrease follows until the end of the thermogram at 1000 K. To isolate the two central processes a baseline was drawn between 500 and 800 K in the weight derivative curve. The integration of the weight derivative peak in this region allows the conversion degree to be calculated, which is thus equal to 0 at 500 K and equal to 1 at 800 K, as shown in Figure 3.9. We excluded in this work the weight loss, below 500 K, corresponding to the water loss.

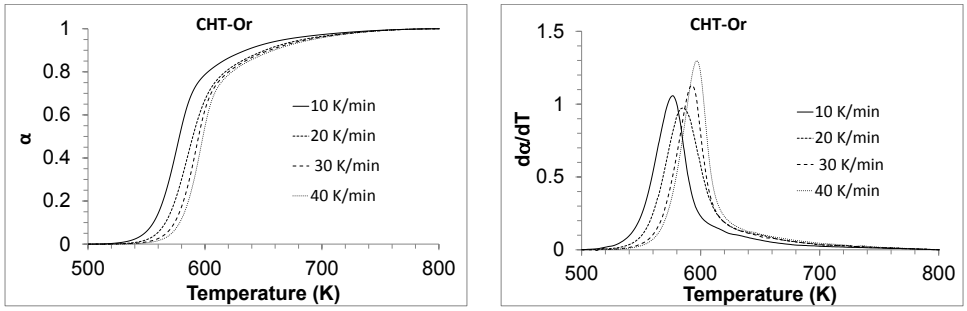

Figure 3.9. Conversion degree (left) and its derivative (right) of original chitosan (CHT-Or) at different heating rates.

Figure 3.9 (left) shows the experimental conversion curves for the thermal degradation of CHT-Or, at different heating rates, between 500 and 800 K. It can be observed that when the heating rate (β) increases, the curves shift towards higher temperatures. This effect is better observed in the derivative curves, Figure 3.9 (right), where the maximum of the derivative of the conversion degree appears at: 576 K, 583 K, 591 K and 596 K for heating rates: 10 K/min, 20 K/min, 30 K /min and 40 K/min, respectively. Figure 3.10. shows the conversion degree (left) and its derivative (right) for chitosan and its acetylated derivatives, at a heating rate of 10 K/min. Whereas the main peak remained at a temperature around 570 K for all samples, a second phenomenon (appearing as a shoulder on the high temperature side of the main peak between 600 and 650 K) increased in intensity as DD decreased.

According to Guinesi & Cavalheiro, and Nam *et al.*, [173, 174], the first degradation stage, around 550-600 K, is attributed to the depolymerization of chitosan D-Glucosamine (Glc) units, while the second decomposition temperature can be ascribed to the degradation of N-acetyl-D glucosamine (GlcNAc).

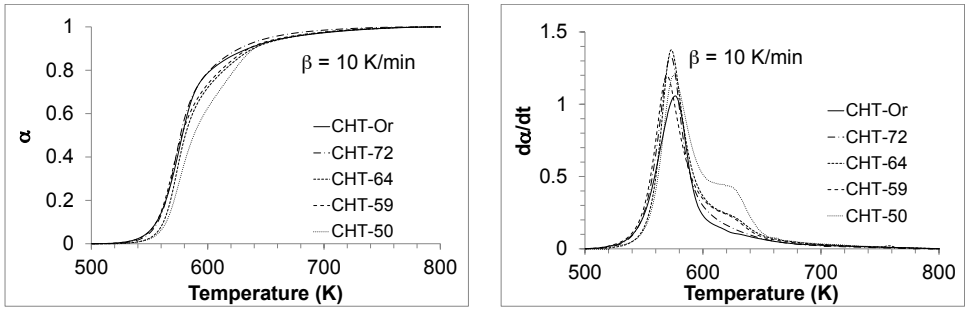

Figure 3.10. Conversion degree (left) and its derivative (right) of chitosan (CHT-Or) with different DD at 10 K/min.

At temperatures above 750 K a slow weight loss was observed due to residual decomposition reactions produced in inert conditions. All the polymer samples presented a residual mass of around 30-40%, regardless of DD, although this was not taken into consideration, as we had set the conversion degree equal to 1 at 800 K for all samples.

3.2.4.3 Determination of activation energy (E_a)

The activation energy (E_a) values were calculated following the Kissinger method [175] from the slope of the line determined by plotting $\ln(\beta / T^2p)$ against 1/Tp, according to Eq (3.14). Figure 3.11 (left) shows the plots corresponding to the first degradation peak.

The obtained activation energy as a function of DD is represented in Figure 3.11 (right). Although the activation energy seems to decrease with DD there is no clear tendency. The results show a greater activation energy corresponding to the second peak at higher temperatures. This method has some limitations, as has been pointed out in the study presented by the International Confederation for Thermal Analysis and Calorimetry (ITAC), [167]. A strict linear relationship is only accomplished for a first order kinetic model. Another important limitation of this method is that it can only be adequately applied to single-step

kinetics. In the case of multi-step kinetics, as in our case, it would be necessary to use an isoconversional method to better estimate the activation energy.

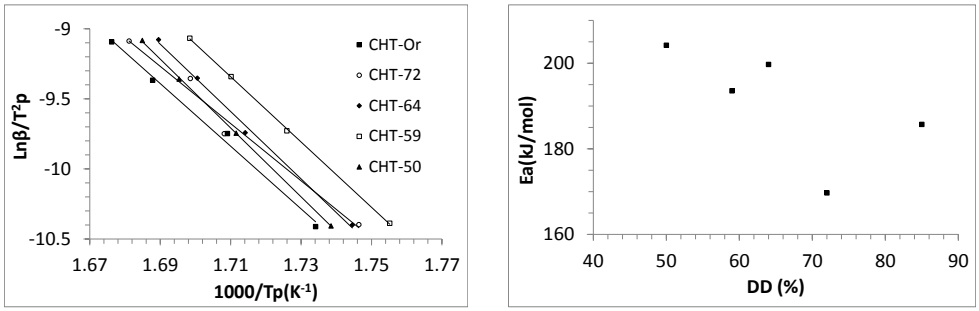

Figure 3.11. Kissinger plot of Ln (β) /T2p versus 1000/Tp for the chitosan and its N-acetylated derivatives (left); E_a values obtained from the slope of the straight lines (right).

To apply the isoconversional OFW method to the thermal degradation of chitosan scanned at different heating rates, the extensions of conversion α=0 and α=1 were taken at 500 K and 800K, respectively (see Figure 3.9 and 3.10). Thus the curves of ln (β) versus 1000/T were plotted for experimental data in the range $0.05 < \alpha < 0.95$ (see Figure 3.12 for CHT-Or and Figure 3.13 for CHT-59; the rest of the samples presented similar representations). In the case of CHT-Or, Figure 3.12, it can be observed that, in general, the experimental points were quite well aligned, with the correlation coefficient ρ^2 ranging between 0.94 and 0.9994. For the CHT-59 (see Figure 3.13) again, experimental points were well aligned except for the higher conversion degree α=0.95 with a ρ^2 as low as 0.53.

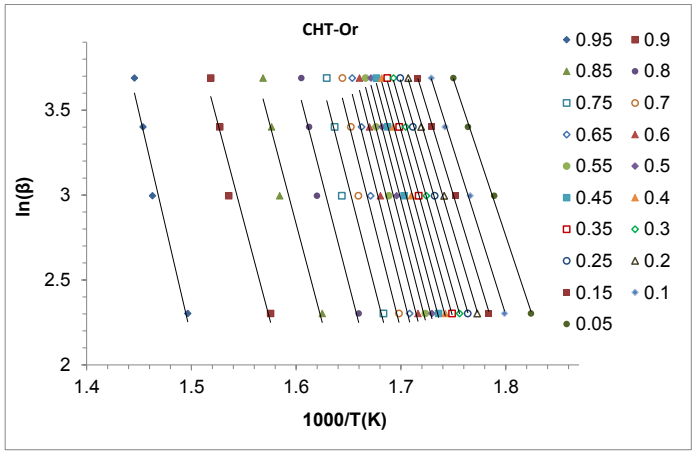

Figure 3.12. Representation of the ln (β) as a function of the inverse of temperature (1000/T) calculated for different values of the degree of conversion, α for CHT-Or sample. The linear plot is also represented for each α value.

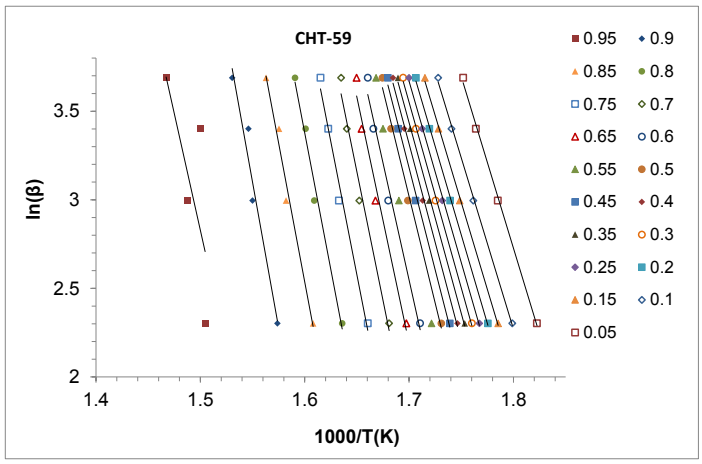

Figure 3.13. Representation of the ln (β) as a function of the inverse of temperature (1000/T) calculated for different values of the degree of conversion, α for the CHT-59 sample. The linear plot is also represented for each α value.

The activation energy as a function of the degree of conversion was determined by applying Eq (3.13) to the slope of these straight lines. The results of the activation energy for each sample as a function of the degree of conversion in the range $0.05< \alpha <0.90$ are represented in Figure 3.14.

In the region 0.15< α <0.7 the activation energy values ranged between 150 and 250 kJ/mol with no clear dependence on DD. In all cases small changes with the degree of conversion were observed with a net increase, around 50 kJ/mol, for all samples. In the region corresponding to higher degrees of conversion, 0.7< α < 0.95, the values of E_a differ for each chitosan derivative. Whereas CHT-Or and CHT-72 showed a decrease in activation energy, the rest of the samples showed an increase.

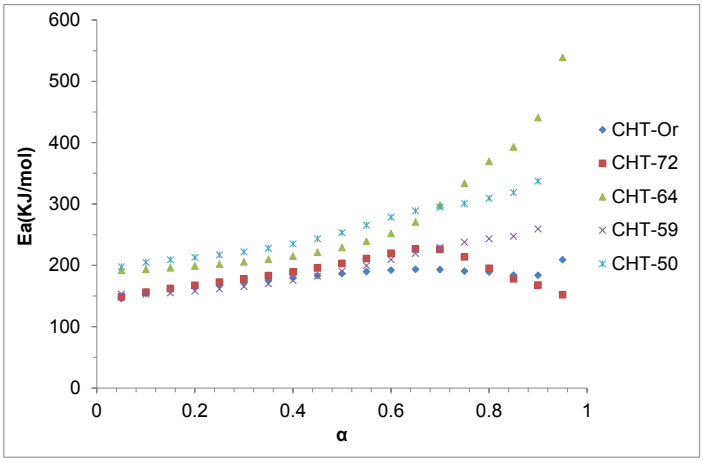

Figure 3.14. Activation energy, E_a, as a function of the conversion degree, α, for all samples.

This was particularly pronounced in the CHT-64 sample. The results of the average E_a for different conversion degree regions are shown in Table 3.1. In all cases the average E_a is higher for the interval corresponding to higher values of the degree of conversion. The same dependence of activation energy with the degree of conversion had previously been found [161] by applying the Friedman method for chitosan at DD=85%. In our results this dependence was most noticeable when DD was lowest, CHT-64 being the sample with the highest variation. It is worth noting that Wanjun et al. found no dependence of E_a on α for chitin, although, as they

explain, the presence of randomly acetylated side-chains confers stability on the polymer.

Table 3.1. Activation energy as obtained from the Kissinger method and the average obtained from the OFW method. The average has been calculated for different conversion degree regions: all values (0.1< α <0.95), low conversion degree (0.1< α <0.6) and high conversion degree (0.6< α <0.95); error is calculated as the standard deviation.

	E_a (kJ/mol)	E_a (kJ/mol) OFW		
	Kissinger	**0.1< α <0.95**	**0.1< α <0.6**	**0.6< α <0.95**
CHT-Or	186	179 ± 15	173 ± 14	192 ± 8
CHT-72	170	187 ± 24	182 ± 21	194 ± 27
CHT-64	200	274 ± 96	213 ± 18	378 ± 84
CHT-59	194	195 ±36	173 ± 18	239 ± 13
CHT-50	204	257 ± 42	231 ± 24	308 ± 16

3.2.4.4 Kinetic model

Once the values of the activation energy have been obtained from isoconversional model-free models, it is possible to test the prediction of the different kinetic models. The shape of the conversion degree and its temperature derivative were reproduced for the thermograms obtained at a heating rate of 20 K/min. Two overlapped degradation processes were considered. In the first fitting the activation energies were kept constant with the values obtained from the OFW method, while the remaining parameters were determined by the least squares search routine. In the case of CHT-Or, in which the high temperature degradation peak is small, first order kinetic model (Eq (3.9), (3.11) and (3.15)) predicted a quite asymmetric peak in dα/dT qualitatively different from the experimental curves and it was discarded. With second order kinetics the peak obtained was broader than the experimental for any value of the pre-exponential factor A, which the only adjustable parameter in this case if E_a is kept constant in the search routine (Figure 3.15).

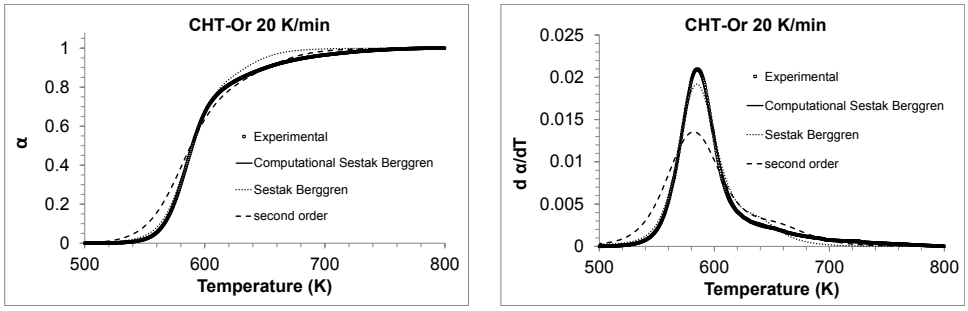

Figure 3.15. Experimental and fitted data for conversion degree (left) and its derivative (right) for CHT-Or at 20 K/min. The fitted computational Sestak Berggren curve is superimposed on the experimental data. Fitting parameters are shown in Table 3.2.

Better results were obtained when the Sestak-Berggren model (Eqs (3.9), (3.11) and (3.16)) was applied using the activation energies obtained by the OFW method. In this case the experimental curve is reproduced quite accurately. However, much better results were obtained if the computational method was applied, assuming a Sestak Berggren reaction model and searching for the activation energy and pre-exponential factor.

Table 3.2. Pre-exponential factor and activation energy used to reproduce the model curves presented at Figure 3.15 for fitting of the experimental data of CHT-Or at 20 K/min.

CHT-Or 20 k/min	**First stage**		**Second stage**	
	A_1 (s^{-1})	**E_{a1} (kJ/mol)**	**A_2 (s^{-1})**	**E_{a2} (kJ/mol)**
Second order	6.10^{13}	170	7.10^{13}	190
Sestak-Berggren (n=2, m=0.4)	1.10^{14}	170	1.10^{14}	190
Computational Sestak-Berggren (n=2, m=0.4)	7.10^{15}	190	3.10^{6}	100

The optimized values of A and E_a are shown in Table 3.2. The fit of the experimental results is then very good, but the values of the pre-exponential factors for both degradation processes seem unrealistic. The value of the activation energy of 190 kJ/mol is required to get a narrow

peak in dα/dT.

The same procedure was followed for the CHT-50 sample. In this case it was interesting to check whether the different models were able to reproduce the high temperature degradation stage that appeared as a shoulder in the derivative curve.

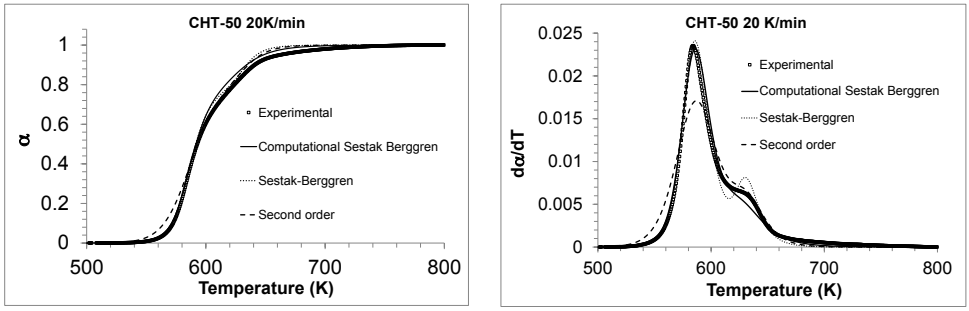

Figure 3.16. Experimental and fitted data for conversion degree (left) and its derivative (right) for CHT-50 at 20 K/min. Fit parameters are shown in Table 3.3.

Figure 3.16 show the results of the different fitting methods compared with the experimental data. It can be seen that in this case the Sestak-Berggren model predicts a sharper separation of the two degradation processes in the dα/dT. Second order kinetics still draws a broader main peak, and perhaps because of this the overlapping region of the two processes is more similar to the experimental thermogram. If all the parameters are considered free in the search routine, then the fit is excellent, both with the Sestak-Berggren and second order models. Figure 3.17 shows the contribution of each individual peak.

Table 3.3 shows the parameters obtained for each fitting method to the CHT-50 sample thermogram. As happened with CHT-Or, the fit with the Sestak-Berggren model, allowing all parameters to change freely, yields a very good fit, but the parameter values are unrealistic.

Table 3.3. Pre-exponential factor and activation energy used to reproduce the model curves presented at Figure 3.16 for fitting of the experimental data of CHT-50 at 20 K/min.

CHT-50 20 k/min	First peak		Second peak	
	A_1 (s^{-1})	E_{a1} (kJ/mol)	A_2 (s^{-1})	E_{a2} (kJ/mol)
Second order	$1.85\ 10^{19}$	230	2.10^{24}	310
Sestak-Berggren (n=2, m=0.4)	$3.6\ 10^{19}$	230	3.10^{24}	310
Computational Sestak-Berggren (n=2, m=0.4)	$1.5\ 10^{30}$	350	4.10^{18}	238

In this case, in addition to the high activation energy and pre-exponential parameter of the low-temperature degradation, the activation energy of the high temperature process obtained from the fitting is lower than that of the low-temperature peak, unlike the results of the OFW method, which was as expected. Nevertheless, the activation energies obtained with the direct Sestak-Berggren fitting are more realistic.

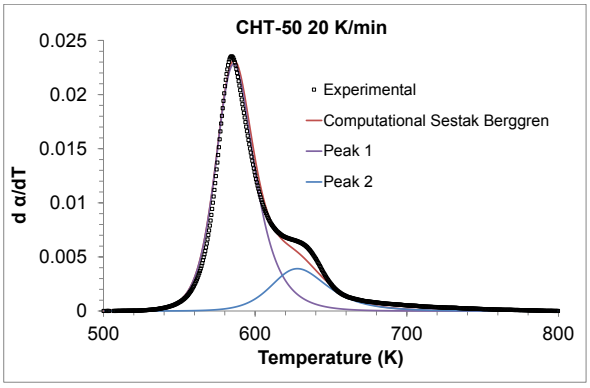

Figure 3.17. Experimental and fitted data of the derivative of the conversional degree for CHT-50 at 20 K/min, considering two peaks. The fitted curve is superimposed to the experimental data. The contribution of each peak is also shown.

In principle, it could be thought that the width of the dα/dT peak in a degradation process should be directly related to the activation energy of the process, since a higher value of E_a determines a faster increase of the

degradation rate with increasing temperature and thus a narrower dα/dT peak. Nevertheless, the relationship between E_a and the width of the peak is not straightforward and is extremely dependent on the kinetic model used in fitting. Thus, the suitability of a kinetic model to describe the chitosan degradation process can be assessed only after determining E_a by a method independent of the model, such as OFW. This analysis shows first or second order kinetic models are not realistic and the Sestak-Berggren Equation including one more parameter should be preferred.

3.2.5 Conclusions

The thermal stability of chitosan of varying DD was analyzed in dynamic experiments with heating rates ranging from 10 to 40 K/min. Whereas the main peak remained at approximately the same temperature for all samples, a second degradation process appears as a shoulder in the high temperature side of the main peak, increasing in intensity as the DD of the sample decreased.

The activation energy values were obtained by applying "free model" methods such as Ozawa-Flynn-Wall and Kissinger. The results showed that the E_a followed a similar tendency for the different samples. Two clear degradation stages could be established with their corresponding values for activation energy and the pre-exponential factor. In all cases the activation energy of the high temperature stage was higher than that corresponding to lower temperatures.

The kinetic parameters were used to check different kinetic models. In all cases two stages were assumed. First and second order models were tested, as well as the Sestak Bergreen model. The second order model, even if it was able to reproduce quite accurately the experimental curves, to do so needs unrealistic values of the model parameters. The Sestak Bergreen

model was able to fit the experimental thermograms with an activation energy that was in good agreement with the OFW method. However, the E_a corresponding to the second stage was not well reproduced at any case.

3.3 Effect of neutralization and cross-linking on the thermal degradation of chitosan electrospun membranes

3.3.1 Abstract*

Thermal degradation of as electrospun chitosan membranes and membranes subsequently treated with ethanol and cross-linked with glutaraldehyde (GA) have been studied by thermogravimetry (TGA) coupled with an infrared spectrometer (FTIR). The influence of the electrospinning process and cross-linking in the chitosan thermal stability was evaluated. Up to three degradation steps were observed in the TGA curves of electrospun membranes corresponding to water dehydration reaction at temperatures below 100 ºC, loss of side groups formed between the amine groups of chitosan and trifluoroacetic acid between 150 – 270 ºC and chitosan thermal degradation that starts around 250 ºC and goes up to 400 ºC. The Kissinger model was employed to evaluate the activation energies of the electrospun membranes during isothermal experiments and revealed that thermal degradation activation energy increases for the samples processed by electrospinning and subsequent neutralization and cross-linking treatments with respect to the neat chitosan powder.

*The results presented in this chapter have been published in:
D. M. Correia, M. A. Gámiz- González, G. Botelho, A. Vidaurre, J. L. Gomez Ribelles, S. Lanceros-Mendez and V. Sencadas.
Effect of neutralization and cross-linking on the thermal degradation of chitosan electrospun membranes. Journal of Thermal Analysis and Calorimetry 123,130–117 (2014).

3.3.2 Introduction

Chitosan can be used in a variety of physical shapes, including beads, films, sponges, tubes, powders and fibers since it is quite soluble under acidic aqueous solutions [1]. Electrospinning is a versatile production method to produce porous fibers membranes with diameters ranging from few micrometers to several nanometers [8, 176]. This process uses a high voltage source to inject charge of a certain polarity into a polymer solution or melt, which is then accelerated, in the form of a thin jet, and when the applied electric field is strong enough to overcome the surface tension of solution the jet is drawn into a fiber that is collected on a surface of a grounded target [176-179].

Chitosan was successfully electrospun into fibers from dissolution of the polymer in trifluoracetic acid (TFA) [180, 181] a co-solvent system of TFA with dichloromethane (DCM) [182], and it was reported that the last solvent improve fiber spinability. Further, Ohkawa *et al.*, [180] refers that the success of the chitosan dissolution in TFA was probably a result of the formation of salts between TFA and amino groups along the chitosan chain leading to a smaller interaction between chitosan molecules, which results in a more stable solution to perform electrospinning. However, the resulting chitosan membranes lose their fibrous structure when in contact with a neutral or weak basic aqueous media, due to the dissolution of the trifluoracetate salts that are formed when chitosan is dissolved in TFA [183]. In order to remove those salts a neutralization process was applied in which the polymer mats were immersed in a sodium hydroxide (NaOH) or sodium carbonate (Na_2CO_3) aqueous solution [183], while other authors use absolute ethanol as neutralizing agent of chitosan [182, 184, 185].

Greiner and coworkers [181] reported that nanofibers of water-soluble polymers obtained by electrospinning decompose more rapidly in contact

with water. In order to improve polymer stability to aqueous environments, a cross-linking process is required. This can be achieved by chemical methods that exploit chemical agents to modify chitosan groups.

Chitosan cross-linking can be achieved by glutaraldehyde (GA), genipin or diisocyanates that leads to intermolecular bridges forming crosslinks between the polymer structure [60], reducing crystalline degree present in the electrospun chitosan fibers with a small decrease in the average fiber diameter [184, 186].

TGA has been used to investigate the kinetics of the chitosan thermal degradation. It has been reported that the degradation of chitosan occurs in two separate steps, where the first step corresponds to dehydration and the second one to chitosan weight loss [161]. The first step is described as a result of the strong affinity of polysaccharides with water, as they can be easily hydrated [187]. Taboada *et al.* [188] refers that the water loss occurs in the temperature range between 25-140 ºC, where the chitosan presents a mass loss between 4 and 7%, and a strong polymer weight loss occurs between 190-410 ºC via the cleavage of glycosidic linkages. Hong *et al.*,[189], found that the activation energy (E_a) of chitosan thermal degradation process change with the degree of conversion during the thermal degradation process and three weight loss steps were proposed: the first corresponds to the volatilization of low molecular materials with E_a between 0-140 kJ mol^{-1}, the second with a E_a between 140-160 kJ mol^{-1} caused by thermal degradation of chitosan main chains, and in the last step an increase of E_a with increasing degree of decomposition during thermal degradation of residual carbon was observed.

In a previous work, neutralized and cross-linked electrospun chitosan membranes were prepared. It was found that the deacetylation degree does

not suffer changes during the processing and a small decrease of the mean fiber diameter was observed [184].

This chapter reports the influence of the processing technique, neutralization and cross-linking with GA on chitosan thermal degradation properties. Thermal degradation kinetics was analyzed and discussed using the Kissinger's mathematical model in order to characterize the thermal behavior and degradation kinetics of chitosan electrospun membranes.

3.3.3 Materials and methods

Chitosan medical grade polymer was purchased from Novamatrix (Protasan UP B 80/20) with 80-89% deacetylation degree and apparent viscosity of 20-199 mPa.s [190]. Dichloromethane (DCM, 99%) and trifluoracetic acid (TFA, 99%, ReagentPlus) were purchased from Sigma-Aldrich. All materials were used as received from the provider.

Electrospun membranes were processed according to the method explained elsewhere [184]. Briefly, Protasan powder was dissolved in a TFA/DCM solution (70:30% v/v) volume ratio for a 7% (weight / total solvent volume) of polymer. The solution was prepared under a constant and vigorous magnetic stirring (JPSelecta, Agimatic-E) at room temperature until complete dissolution of chitosan. The polymer solution was placed in a commercial plastic syringe fitted with a steel needle with an inner diameter of 0.5 mm, a distance between the metallic tip and the grounded collector of 150 mm and an applied voltage of 25 kV with a PS/FC30P04 power source from Glassman was applied. A syringe pump fed the polymer solution into the tip at a rate of 1 mL h^{-1}. As-spun chitosan fiber mats were neutralized in a vapor chamber (JPSelecta Vacuo-Temp), at low pressure with ethanol (99%, Merck) for 72 h at 40 ºC. After this process the samples were desiccated at 80 ºC, for another 72 hours to remove the ethanol

excess. Cross-linking of as-spun and neutralized membranes was performed in a vapor chamber (JPSelecta Vacuo-Temp), at low pressure. 10 mL of glutaraldehyde (GA, 50% water, Panreac) was placed at the bottom of the chamber and vaporized at 25 ºC, for 24 h.

Fluor quantification present in the chitosan sample and the compositional changes that occur during neutralization and cross-linking were characterized by microanalysis in an Energy Dispersive X-ray (Oxford Instrument X-Max detector) attached to scanning electron microscope JSM - 6300 from JEOL. Samples were previously coated with carbon in vacuum and spectra were taken at 5 kV of acceleration voltage and silicon was employed as standard.

Simultaneous thermogravimetry coupled with Fourier transform infrared spectrometer (TGA-FTIR) was performed on a thermal analyzer (TGA, SDTQ600 TA instruments) and a FTIR (Spectrum one). For TGA analyses, the samples were heated to 40-800 ºC, at different heating rates (between 5 and 40 ºC.min^{-1}) under a nitrogen flow rate of 25 mL.min^{-1}. The transfer line used to connect TGA and FTIR had an internal diameter of 1.5 mm, and the temperature was maintained at 523 K. The FTIR spectra were collected at 8 cm^{-1} resolution.

3.3.4 Results and discussion

3.3.4.1 Electrospun membrane morphology

Chitosan was electrospun into a flat grounded collector, and the obtained fibers shown a smooth, bead free, continuous and random oriented (Figure 3.18) [184]. It was observed that samples treated with ethanol and cross-

linked with GA retain their integrity with cylindrical fibers, similar to the as-spun fibers (Figure 3.18b).

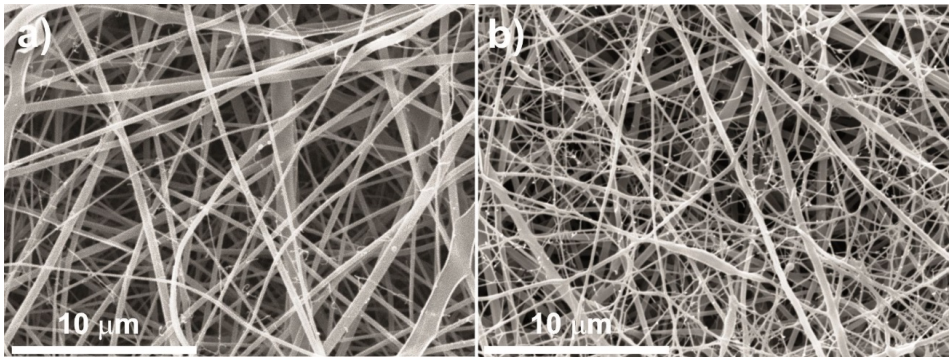

Figure 3.18. Electrospun chitosan membrane prepared from a 7% (w/v) polymer solution, travelling distance of 15 cm, needle inner diameter of 0.5 mm, flow rate of 1 mL.h^{-1} and a applied voltage of 25 kV: a) as-spun fibers and b) neutralized with ethanol followed by GA cross-linking.

Finally, it was observed that neutralization and cross-linking does not had significant influence on average fiber diameter and distribution (Figure 3.18), but a fiber shrinkage around 10% was observed after neutralization with ethanol [184].

3.3.4.2 Effect of the electrospinning process and chemical treatments on thermal degradation

In the present work, the influence of the processing technique and the subsequent neutralization and cross-linking on thermal degradation of chitosan was studied by thermogravimetric analysis (TGA) under dynamic conditions.

For pristine chitosan powder two main steps were observed (Figure 3.19): the first step, that takes place below 100 ºC, corresponds to the dehydration process due to water evaporation that was absorbed in the sample, with a weight loss of approximately 8%. The second thermal step occurred between 250-375 ºC with a weight loss around 45 % and is

related to polymer decomposition and release of volatile products (Figure 3.19), [191].

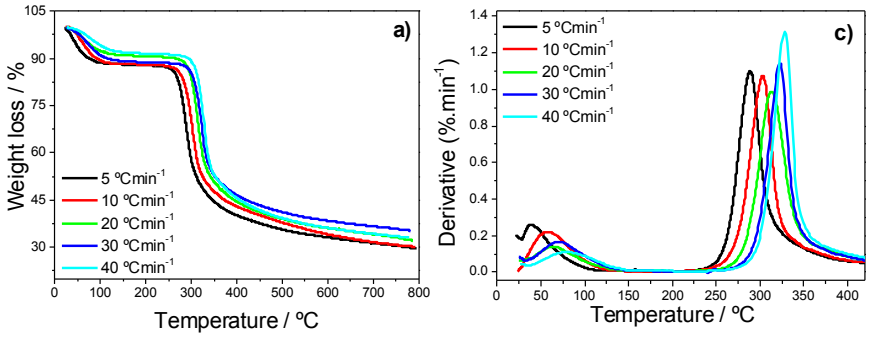

Figure 3.19. TGA (a) and DTG (b) thermograms of pristine chitosan for different heating rates (5, 10, 20, 30 and 40 °C min⁻¹).

Figure 3.20 shows the effect of the electrospinning process, neutralization and cross-linking treatments on chitosan thermal stability. The electrospun membranes showed three major degradation steps. The first, at low temperatures, below 100 ºC, is associated to dehydration and is quite similar to the one observed for the as-received material (Figure 3.19 and 3.20) between 150-270 ºC and 270-400 ºC, respectively (Figure 3.20 a). In the derivative (DTG) curves three peaks can be observed, corresponding to the thermal decomposition of chitosan fibers (Figure 3.20 b).

The second degradation process shown by the derivative peak presents a maximum around 240 ºC, which is absent in the pristine chitosan powder (Figure 3.19), and can be ascribed to the loss during heating scan of side groups formed by the association of TFA and the amine groups of chitosan. Films of chitosan formed by solvent casting from a solution of pristine chitosan in TFA were prepared and submitted to TGA analysis showing similar thermograms to those of electrospun mats (Figure 3.20), what indicates that the new degradation peak is not the result of a special

orientation or organization of chitosan chains due to electrospinning process.

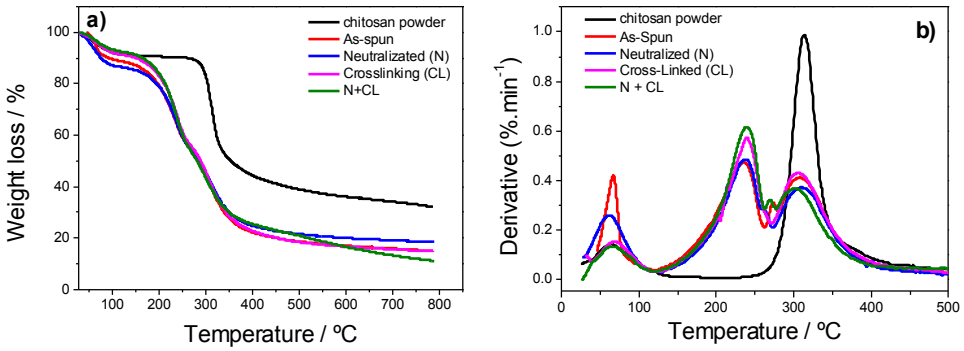

Figure 3.20. TGA (a) and DTG (b) thermograms of the pristine chitosan and as-spun membranes.

To prove the origin of this relaxation peak, films of chitosan were analyzed by TGA at different heating rates in the range between 200 and 300 ºC and then to elemental analysis to detect the presence of fluoride in the sample. The results shown in Figure 3.21 reveals that fluoride is still present in the original film (a similar pattern was shown by electrospun mats, results not shown), but when the sample is taken to temperatures in the range of the second stage degradation peak, the fluoride peak decreases (Figure 3.21a and 3.21b). The salts produced by the interaction of TFA and amine groups of chitosan during the dissolution and electrospinning process persists in the as-spun mats, and favor polymer dissolution under aqueous environments. Sample cross-linking with GA renders the electrospun mats insoluble in water but TFA-amine salts persists in the fiber membranes. Further, chitosan films neutralized with ethanol showed the presence of fluoride in the sample, and for the samples treated with NaOH is absent of fluoride as it can be observed in Figure 3.21d.

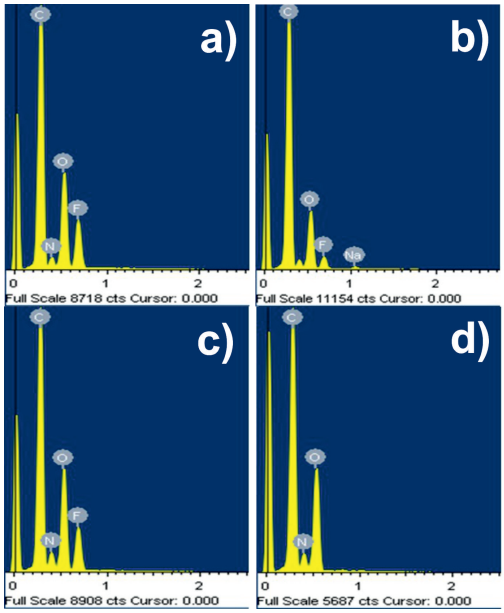

Figure 3.21. Elemental analysis of: a) pristine chitosan dissolved in TFA/DCM before thermal annealing, and b) after annealing at 300 º C; c) pristine chitosan dissolved in TFA/DCM and subsequent neutralization with ethanol and d) neutralized with NaOH.

TGA is a sensitive technique to detect the presence of these side groups within samples. In order to ensure that the second degradation stage was due to the presence of trifluoracetate salts, chitosan samples were neutralized with NaOH. TGA of these samples shown a similar trend to the one obtained for the pristine chitosan powder, i.e., without any TFA residues (Figure 3.22), which is in accordance to the elemental analysis results obtained for the samples neutralized with NaOH (Figure 3.21d).

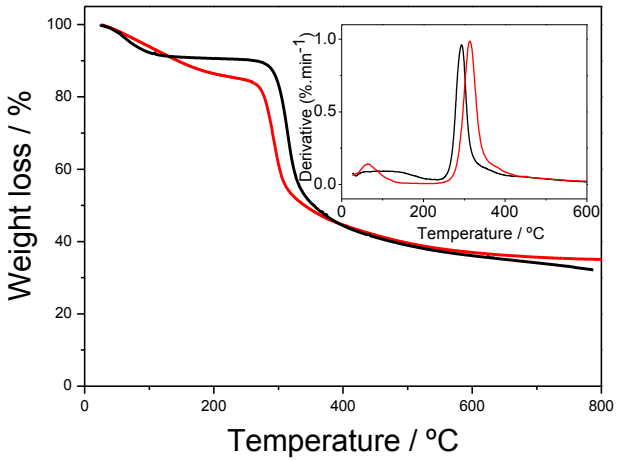

Figure 3.22 Thermogravimetric data obtained for pristine chitosan and for the electrospun membrane neutralized with NaOH.

Comparing the onset temperatures of as-received chitosan and electrospun membranes, it is possible to observe that the electrospinning process decrease their thermal stability and this is related to the release of TFA compounds produced during the polymer dissolution and posterior electrospinning process. Further, the amount of absorbed water found for all the prepared samples is quite similar between them, revealing that processing techniques does not had influence in sample hydration (Table 3.4).

Table 3.4. Parameters obtained from de TGA curves of pristine chitosan and chitosan membranes.

Membranes	Water absorption (%)	Residue at 400 °C (%)	Residue at 600 °C (%)
Pristine chitosan	9	45	36
As-spun	9	22	17
Neutralizated (N)	13	25	20
Cross-linking (CL)	8	23	17
Neutralization + Cross-linking (N+CL)	7	25	17

Moreover, sample neutralized with ethanol showed a higher amount of water absorbed which may be due to the strong capacity of ethanol to establish linkages by hydrogen bonds with water (Table 3.4).

3.3.4.3 FTIR analysis of gas products

During chitosan thermal degradation, the released gases were analyzed by FTIR spectroscopy using the experimental conditions described above. It was observed that electrospun membranes release more gaseous products than as-received chitosan, leading to conclude that the chitosan dissolution in a TFA/DCM solution provide less thermal stability to the electrospun membranes, which is in accordance to the observed in Figure 3.19 and 3.20. From the obtained results, three major absorption bands were perceived: at 3735 cm^{-1} represents the water dehydration that occurs in the first step (Figure 3.19 and 3.20) [192]; the absorption bands at 1660 cm^{-1} and 1560 cm^{-1} are assigned to the C=O in the amide group (amide I band) and NH bending vibration in the amide group, respectively [193]. At 300 ºC (Figure 3.23), the peaks at 1660 cm^{-1} and 1560 cm^{-1} became broader, which indicate changes that occurs to chitosan during thermal degradation due to the formation of unsaturated structures. The absorption band at 1380 cm^{-1} was assigned to the CH_3 of chitosan amide group [193]. Furthermore, Zeng *et al.*, [191] propose a chitosan pyrolysis mechanism and formation of volatile compounds such as pyrazines, pyridines, pyrroles and furans that are generated from the polymer thermal degradation. Compounds like pyrazine are the most important products among the volatiles that were identified. A strong absorption band was observed at 1150 cm^{-1} for the electrospun samples heated until 300 ºC (Figure 3.23), corresponding to the C – F stretching band due to the $–NH_3^+CF_3COO^-$ salts previously formed during polymer dissolution in a TFA/DCM

mixture, and proves the existence of such residues, probably located in the side groups of the electrospun polymeric chains [194, 195]. The absorption band at 1150 cm^{-1} was also observed for the chitosan samples submitted to ethanol neutralization and cross-linking with GA.

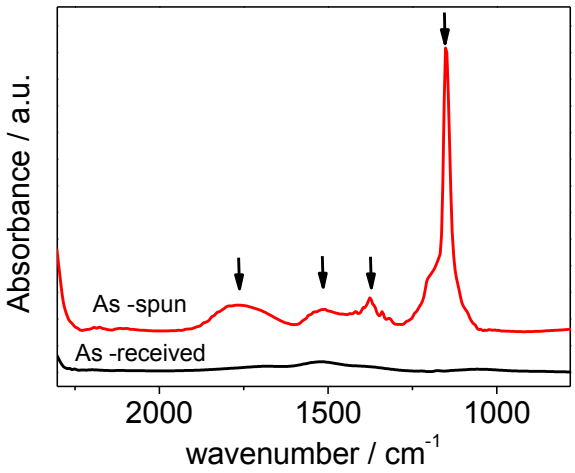

Figure 3.23. FTIR spectra of as-received and as-spun chitosan membranes along degradation from TG analysis, obtained at 300 ºC.

3.3.4.4 Thermal degradation kinetics

Polymer thermal stability can be characterized by the kinetic parameters of the thermal degradation [196]. Kissinger developed a mathematical model which is used to determine the activation energy from plots of the logarithm of the heating rate vs reciprocal temperature at the maximum reaction rate, in constant heating rate experiments [175, 197].

In the Kissinger method the activation energy (E_a) can be obtained without a precise knowledge of the reaction mechanism, according to the following equation [175]:

$$ln\left(\frac{\beta}{T_p^2}\right) = \frac{ln\,(AE_a)}{T} + ln\left[n(1-\alpha_p)^n\right] - \frac{E_a}{RT_p} \qquad (3.18)$$

where T_p and α_p are the absolute temperature and the conversion at the maximum weight loss rate, respectively.

In the present work, the degradation kinetics was evaluated by the method proposed by Kissinger (Eq 3.18), in which the E_a for the water evaporation reaction (first step), degradation of TFA salts present in the membrane (second step) and chitosan thermal degradation (third step) can be calculated by plotting $\ln \beta/T_p^2$ vs $1000/T_p$. Figure 3.24 shows that the fitting straight lines were nearly parallel, which implies that this method was suitable to apply to the chitosan polymer membranes.

According to the Kissinger's mathematical model for the degradation kinetics, the slope of straight lines is proportional to the E_a, and the obtained results for the different thermal degradation steps are reported in Table 3.5. All linear fittings were obtained with $R > 0.97$.

The values obtained for water evaporation E_a (first step) are higher after the electrospinning process and decrease after cross-linking with GA in vapor phase, which probably is related to the water affinity of TFA salts formed during polymer dissolution in a TFA/DCM solvent mixture and to the strong capacity of ethanol establish linkages by hydrogen bonds with water.

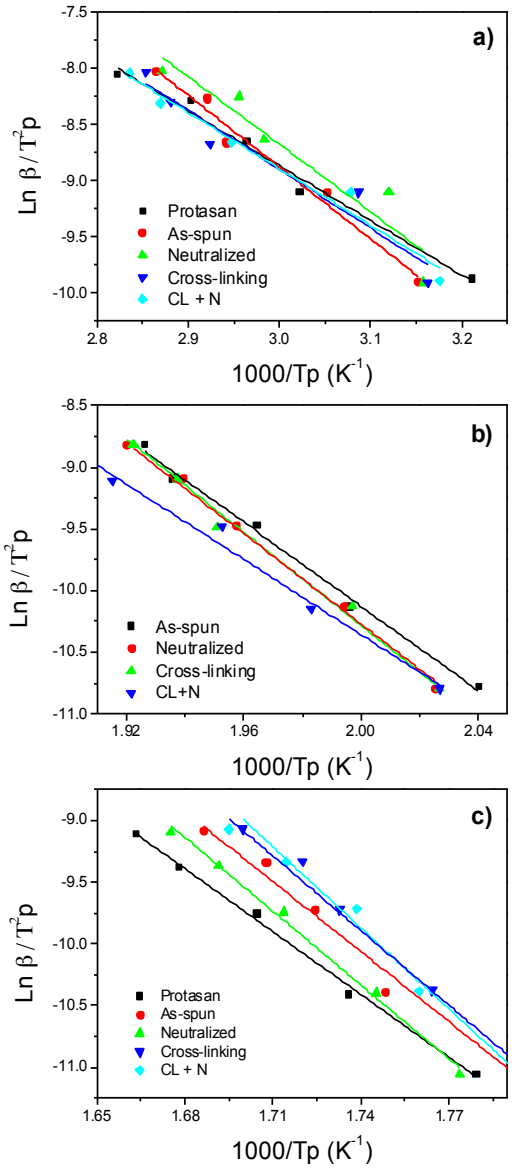

Figure 3.24. Kissinger plot of $\ln \beta / T_p^2$ *versus 1000/Tp for the as-received and chitosan membranes: a) water dehydration, b) second step degradation process and c) third step degradation process.*

Moreover, the difference between the activation energy for pristine chitosan and electrospun fibers with and without neutralization is around

10-13 kJ.mol^{-1}, which is comparable to the energy of the hydrogen bond [198], which confirms the interaction between the TFA salts and water and ethanol. Further, for the samples submitted to neutralization and cross-linking the activation energy for the dehydration process decreases to a value similar to the one found for pristine chitosan. For the second degradation process, related to the TFA salts produce by the interaction between the TFA/DCM solvents and the polymer, the E_a is higher for the sample submitted to ethanol neutralization process when compare to the as-spun mats and decreases for the cross-linked samples. Moreover, activation energy for the chitosan thermal degradation (third step) is around 142 kJmol^{-1} and increases with the subsequent neutralization and cross-linking (Table 3.5).

Table 3.5 - Values of E_a obtained by Kissinger mathematical model.

Samples	E_a (kJ.mol-1)		
	First step	Second step	Third step
Pristine chitosan	41	-	142
As-spun	53	142	157
Neutralizated (N)	50	157	165
Cross-linking (CL)	43	152	177
Neutralization+ Cross-linking (N+CL)	42	141	167

It has reported that chitosan E_a follows in the range between 140- 160 kJ.mol^{-1} caused by thermal degradation of chitosan main chains [188, 189]. Thermal degradation process of chitosan may be a random degradation of polymer chains and it was reported that the degradation starts from the scission of the C-O-C bond at a weak point [161]. Electrospinning and cross-linking has a strong influence on the amount of the amorphous phase present in the chitosan fiber mats [184].

The reaction of the chitosan with GA vapor induces a reorganization of the polymeric chains, and intra and intermolecular hydrogen bonds of chitosan network would break apart [186]. Cross-linking induces discontinuities along the polymer chains, which hinder crystal formation leading to a more amorphous polymer mats. Also, leads to formation of a new C=N bonds of imine group, decreasing the primary amine bond when the chitosan fibers which as higher bond strength when compared to C-O, C-H, C-C and O-H present in polymer chain, which implies that a greater energy is needed to supply in order to start its thermal degradation process [199]. This can explain the increase of the activation energy observed for the cross-linked samples (Table 3.5).

3.3.5 Conclusions

The influence of electrospinning processing and the subsequent neutralization and cross-linking on the thermal degradation of chitosan was studied by TGA. It was observed that chitosan shows up to three degradation steps: the first step was attributed to a dehydration process associated to evaporation of water absorbed below 100 ºC and the second to chitosan degradation and release of volatile products that occurs between 250 – 375 ºC. A third step, which is absent in the original chitosan powder appears between 150 – 270 ºC in electrospun chitosan fibers and chitosan films dissolved in TFA/DCM. FTIR spectra revealed the presence of $NH_3^+CF_3COO^-$ salts produced by the interaction of TFA and amine groups of chitosan during the dissolution and persists after the electrospinning process, favoring polymer dissolution in aqueous environments.

After neutralization with ethanol in a vapor chamber $NH_3^+CF_3COO^-$ salts still can be found in the polymer fibers, which decrease material thermal

stability. Thermal degradation activation energy of chitosan fiber mats (third step) was slightly higher for the samples treated with ethanol and with GA, when compared to the values found for the chitosan powder.

Chapter 4. Biodegradable chitosan-poly(ε-caprolactone) copolymer networks

4.1. Abstract*

Chitosan-PCL block-copolymer networks were synthesized using different amounts of dialdehyde end-capped poly(ε-caprolactone) as cross-linking agent. The cross-linking reaction was performed by dissolving both components in the common solvent 1,1,1,3,3,3-Hexafluoro-2-Propanol, (HFIP). The formation of the network was confirmed by solubility tests in good solvents of both components. The resulting composition was determined by thermogravimetric analysis. The hydrophilic/hydrophobic networks behave as hydrogels; water sorption at pH7 is around 70% that of pure chitosan for a network containing 36% PCL blocks. The PCL domains were not able to crystallize, except for the CHT-64 sample as shown by Differential Scanning Calorimetry and X-ray diffraction. Degradation in hydrolytic and enzymatic media was characterized. Enzymtic degradation of these networks is quite fast, thus, the network with 36% PCL presented a remaining weight of 22% of their initial mass after 28 days of degradation in lipase. Nevertheless in purely hydrolytic degradation medium, the remaining weight was 86 ± 3% for the same time and the same composition.

*The results presented in this chapter are in preparation to be published as scientific article:
M. A. Gámiz-González , A. Vidaurre and J. L. Gómez Ribelles.
Biodegradable chitosan-poly(ε-caprolactone) copolymer networks.

4.2 Introduction

Hydrogels are cross-linked networks than can absorb large amounts of water without dissolving. The cross-linking of these networks can be irreversible (chemical cross-linking) [200] or reversible (physical cross-linking) [113]. Due to their soft nature, hydrogels have been proposed as good candidates for regenerating soft tissue in cases such as wound dressing, drug delivery systems or corneal ulcers [201]. Their hydrophilicity facilitates the diffusion of nutrients and disposable molecules and also enables the access of water molecules to the hydrolysable bonds, favoring biodegradation. There are some tissue engineering applications that require a short biodegradation time that matches the rate of formation of new regenerated tissue [202]. On the other hand, hydrophobic materials have demonstrated good cellular adhesion, favoring proliferation and differentiation. Hydrogels that contain both hydrophilic and hydrophobic domains have thus been proposed for tissue engineering applications.

Poly(ε-caprolactone), (PCL) is a synthetic polyester widely used in biomedical applications [204]. PCL is a semicrystalline and hydrophobic polymer with good mechanical properties [205] that can be hydrolytically and enzymatically degraded by lipase through the hydrolysis of the ester bond [206].

Several strategies have been proposed to cross-link chitosan and obtain stable hydrogels. Cross-linking is usually achieved by the reaction between amine from the chitosan and aldehyde groups by Schiff base formation with glutaraldehyde [207, 208]. Chitosan hydrogels have been synthesized by combination with hydrophobic polymers in order to control their water uptake, mechanical behavior and crystallinity [69]. However, these chitosan networks have the drawback of a low degradation rate in both enzymatic and hydrolytic conditions.

This chapter focuses on cross-linking CHT by low molecular weight dialdehyde end-capped poly(ε-caprolactone) aPCL. The covalent cross-linking was tested by immersing the samples in good solvents of both polymers. "In vitro" (enzymatic and hydrolytic) degradation profiles of the block-copolymer networks were analyzed and the results confirmed an adequate degradation rate, making them suitable for soft tissue engineering applications.

4.3 Materials and methods

4.3.1 Materials

Medical grade Chitosan was purchased from Novamatrix (Protasan UP B 80/20) with 80-89% DD and apparent viscosity of 20-199 mPa s, according to the supplier's information. Poly(ε-caprolactone) diol with a molecular weight (Mn) of 2000 (Da), 1,1,1,3,3,3-hexafluoro-2-propanol, HFIP, chloroform, $CHCl_3$, dimethylsulfoxide anhydrous, DMSO, oxalyl chloride $(COCl)_2$, hydrochloric acid, HCl, Sodium hydroxide, NaOH, anhydrous dichloromethane, DCM, triethylamine, TEA, sodium cianoborohydride, $NaBH_3CN$, and magnesium sulfate, $MgSO_4$, all analytical grade, were purchased from Sigma–Aldrich.

4.3.2 Methods

4.3.2.1 Synthesis of dialdehyde end-capped poly(ε-caprolactone)

The dialdehyde end-capped poly(ε-caprolactone), (aPCL) was prepared via Swern oxidation Groth *et al.*, conditions from poly(ε-caprolactone) diol, (PCL-diol). Anhydrous DCM was used like solvent due to the high toxicity that present the carbon tetrachloride, CCl_4. All reaction vessels and

reagents were manipulated in an inert atmosphere.

Oxalyl chloride (0.85 mL; 10 mmol) was mixed in anhydrous DCM (50 mL). The solution was cooled to -47 °C. DMSO (1.5 mL; 0.625 mmol), was mixed with DCM, and slowly added to the oxalyl chloride/DCM solution. PCL-diol (5g; 2.5 mmol) previously dissolved in DCM (16 mL) was added to the cooled solution drop by drop. The mixture was stirred during 3 hours at -47 °C. The catalytic amount of TEA (5.2 ml; 9.3 mmol) was then added and allowed to reach room temperature. The resulting product was diluted in DCM and extracted with HCl 1M and a supersaturated NaOH solution. The extracts were dried with $MgSO_4$. The resulting solution was rotaevaporated and the final product was dissolved in chloroform and reprecipitated with cool diethyl ether and then dried in a vacuum. The substitution degree of the product was determined as 40 ± 18% by 1H-NMR spectroscopy.

4.3.2.2 Preparation of chitosan-PCL block-copolymer networks

CHT and aPCL were dissolved in HFIP in glass vials and stirred overnight at 46 ºC. The aPCL solution was added drop by drop to the CHT solution in 80:20, 65:35 and 50:50% (w/w) CHT:aPCL ratios. Cross-linking reaction started instantly, so the hydrogel was carefully removed from the glass vial and placed in a poly(tetrafluor ethylene), (PTFE) mold. After solvent evaporation, the samples were reduced with $NaBH_3CN$ 1% (w/v) solution to obtain the (C-N) bond between aPCL aldehyde end groups and CHT amine groups. The block-copolymer networks obtained were washed several times with acetone (a good solvent of PCL) to remove the non-bonded aPCL, then the samples were dried for 48h in a vacuum at 50 °C and the xerogel was obtained. In order to determine the possibility of obtaining a porous structure, the samples were swollen in water and

frozen at -20 °C for 48h and then lyophilized. The mass percentage of CHT in the samples was calculated by thermogravimetric analysis (TGA) and the samples were labeled as CHT followed by a number that indicates the mass fraction per cent of CHT in the sample: CHT-64, CHT-82 and CHT-79.

4.3.2.3 Fourier Transform Infrared Spectroscopy (FTIR)

FTIR spectra of the samples were recorded on a Thermo Nicolet Nexus FTIR with OMNUC software using the Smart Diffuse Reflectance method. The networks were analyzed as a powder and the reference was dried KBr. The spectra were obtained by continuously accumulating 32 scans in the 500-4000 cm^{-1} range at 4 cm^{-1} resolution at room temperature.

4.3.2.4 Thermogravimetric Analysis (TGA)

Thermogravimetric measurements were performed using a TA-Instrument Model SDT-Q600 system. TGA tests were carried out in alumina crucibles in which weight samples of between 5 and 10 mg were heated from 30 °C to 800 °C at a heating rate of 10 °C /min. TGA experiments were performed using a nitrogen atmosphere (flow 20 mL/min).

As it will be shown below, thermal degradation of chitosan starts at lower temperatures than PCL. The main peak, in the weight derivative plot, DTG, of pure chitosan appears before the degradation onset of PCL. Thus, CHT mass fraction in the copolymer networks, X_{CHT}, was determined from the area of this first peak calculated on the basis of Gaussian fit deconvolution of the DTG curves. X_{CHT} in the copolymer networks was calculated by comparing the mass loss corresponding to this peak with that obtained for pure CHT. DTG peaks were adjusted to Gaussian curves by the Origin Pro 8.5 program. Copolymer network samples will be named

CHT-XX, XX being the weigh % of chitosan.

On the other hand, at 600 ºC the thermal degradation of pure aPCL is completed with a small residue around 4% while the residue of pure chitosan is around 30%. Thus the weight residue at 600 ºC, RW_{600} in the networks could be ascribed to chitosan and weight fraction of chitosan in the copolymer network could be calculated from it. We will consider the residue excluding water evaporation:

$$RW = \frac{RW_{600}}{RW_{180}} \tag{4.1}$$

RW_{180} being the residue measured at 180 ºC. Thus, the chitosan mass fraction would be:

$$X'_{CHT} = \frac{RW_{Network} - RW_{aPCL}}{RW_{CHT} - RW_{aPCL}} \tag{4.2}$$

Where RW_{CHT}, RW_{PCL} and $RW_{network}$ are the residue of CHT, PCL and the networks calculated by applying the Eq (4.1). As we will discuss below X'_{CHT} values are unrelistically high showing that PCL degradation products are saved inside chitosan residue.

4.3.2.5 Equilibrium water content and solubility

Lyophilized samples (N=5 replicates) ranging between 9-10 mg were immersed in 3 mL of deionized water until equilibrium was reached (72 hours). The weight of the samples was measured gravimetrically after careful elimination of the surface water by filter paper. The equilibrium water content (EWC) was determined by Eq (4.3):

$$EWC = \frac{m - m_o}{m_o}\ 100 \tag{4.3}$$

where m_o refers to the initial weight in dry state and m refers to the sample weight after 72 h of immersion. The weight was measured on a balance (Mettler Toledo) with a sensitivity of 0.01 mg.

The solubility of the copolymer networks was tested in two good solvents of the polymers, acetone and acetic acid solution, in order to determine the efficiency of the covalent cross-linking. After washing in acetone, the samples (N= 5 replicates) were immersed for 24 hours in 3 mL of 1% (v/v) acetic acid solution. The swollen capacity was calculated by applying Eq (4.3), in which the m now refers to the sample weight after 24 hours of immersion in acetic acid solution.

4.3.2.6 Differential Scanning Calorimetry (DSC)

Differential scanning calorimetry (DSC) was performed on a Pyris DSC8000 (TA Instruments) calibrated with indium and zinc standards in a nitrogen atmosphere. The dry samples (4-10 mg in weight) were equilibrated at 30 ºC in the DSC chamber. They were then cooled from 30 to -87 ºC at a cooling rate of -20 ºC /min, equilibrated and heated from -87 to 90 ºC at a heating rate of 20 ºC /min, equilibrated at 90°C and cooled and heated again under the same conditions.

4.3.2.7 X-ray diffraction (XRD)

X-ray diffraction spectra of the CHT-PCL co-polymer networks were obtained on a Rigaku Ultima IV X-ray diffractometer in the Bragg-Bentano configuration using the K_α radiation of a Cu anode. The network samples were scanned from 2θ=5-70º at a speed of 2º/min.

4.3.2.8 Degradation studies

Degradation studies of the CHT-PCL networks were carried out in

hydrolytic and enzymatic media (lipase). Cylindrical samples 5 mm in diameter and 0.17 ± 0.04 mm of thickness (N=5 replicates at each degradation time) were used. The CHT-PCL samples were previously protonated with acetic acid 1% (v/v) in order to improve chitosan solubility. Hydrolytic degradation was performed by immersing samples in a PBS solution (pH=7.4 and 0.02% (w/v) of sodium azide to avoid bacterial proliferation) for 28 days. The enzymatic degradation media was prepared by adding 1mg/ml of lipase to PBS (pH=7.4 with 0.02% (w/v) of sodium azide). During the degradation experiments the temperature was held at 37 °C and the degradation medium was changed twice per week in enzymatic conditions. The degraded samples were extracted from the medium at predefined degradation intervals and washed in water. The equilibrium water content was calculated by applying Eq (4.3). Samples were lyophilized and the percentage of the remaining weight after degradation was determined by comparison of the weight of the dry sample before degradation (m_o) with the weight of the dry sample after degradation (m_d) by Eq (4.4):

$$Remaining\ Weight\ (\%) = \frac{m_d}{m_o} 100 \qquad (4.4)$$

4.3.2.9 Statistics

The data was analyzed by ANOVA using the SPSS Statistic 16.0 computer program, while means were compared by the Tukey-*b* test with the level of significance set at $P<0.05$. The results were presented as the mean ± standard deviation.

4.4 Results and discussion

4.4.1 Synthesis

Cross-linking of chitosan with dialdehydes is a well known procedure to obtain insoluble chitosan [207, 208]. In this work a dialdehyde cross-linker is obtained by Swern oxidation of the hydroxyl terminal groups of commercial poly(ε-caprolactone) diol. The cross-linker, aPCL, is thus a hydrophobous, water unsoluble solid. Cross-linking reaction could be performed by dissolving both polymers in HFIP, which is a common solvent for aPCL and CHT. The covalent cross-linking is expected to take place between the chitosan amine groups and the aPCL terminal aldehyde groups (Figure 4.1), as happens with other dialdehydes.

Once the xerogel was formed, the imines were chemically reduced to the amine group with $NaBH_3CN$ solution at 1% (w/v), (Figure 4.1). The uncross-linked polymer chains were eliminated by washing the samples several times with acetone. The remaining weight after reduction and washing was followed gravimetrically (Table 4.1). The global yield of the block-copolymer network formation was around 97 ± 1%. CHT film (CHT-F) was also obtained by casting from a 2% (w/v) HFIP solution and used as reference.

The network produced has a block-copolymer structure with randomly distributed PCL blocks (average molecular weight 2000 Da) and chitosan blocks. This copolymer network can eventually present nano-phase separation due to the high immiscibility of the two components, as has been reported in other hydrophilic/hydrophobic block-copolymer networks [208-210].

Furthermore, micro-phase separation can also appear, depending on the homogeneity of the diffusion of the cross-linker when mixed with the chitosan solution.

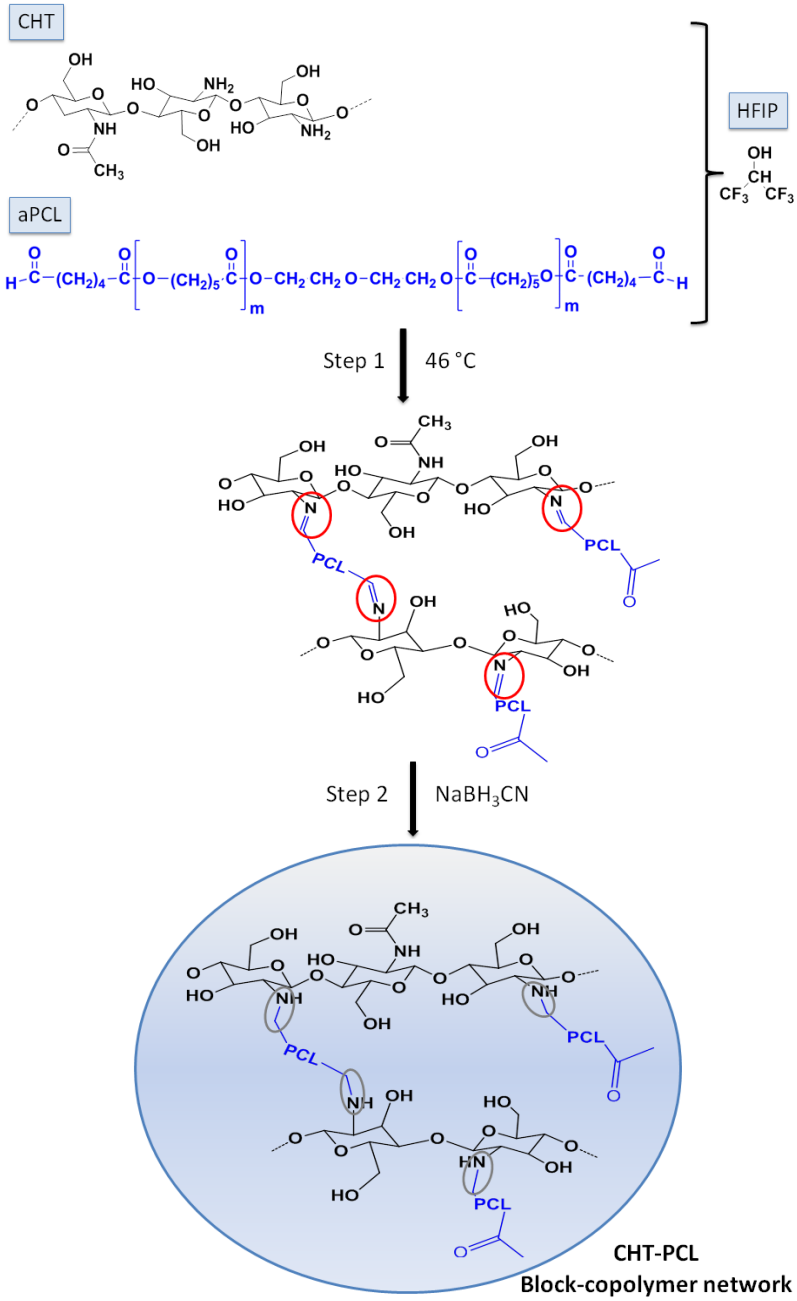

Figure 4.1. Scheme of the cross-linking reaction between chitosan (CHT, black) and poly(ε-caprolactone), (aPCL, blue). The polymers were dissolved in 1,1,1,3,3,3-Hexafluoro-2-Propanol, (HFIP) overnight at 46 °C. Spet 1: the cross-linking reaction was carried out by Schiff base formation (C=N), (red circle). Step2: Mechanism of reduction to obtain amine group (C-N), (gray circle) with Sodium cyanoborohydride (NaBH₃CN).

Complete extraction of unbonded CHT chains should be performed in an aqueous solution medium at low pH. However, the huge swelling capacity of the networks in this solvent made the swollen samples extremely fragile. For instance, the swelling capacity in 1% (v/v) acetic acid solution was 9000 ± 2000 % for CHT-64, 10000 ± 3000% for CHT-82 and 19000 ± 1000 for CHT-93, respectively, while CHT-F dissolves in this medium. Weight loss after washing in 1% (v/v) acetic acid was around 30% for CHT-64 and CHT-93 and around 50% for CHT-82. However, this is only a rough estimation of the fraction of the extraction of CHT chains, due to the difficulties experienced in its measurement, although these solubility tests do demonstrate the formation of the block-copolymer network. As it was decided not to perform the complete extraction of unreacted CHT chains, the presence of these chains interpenetrated with the copolymer network cannot be discarded.

Nevertheless, in degradation experiments the samples were washed in an acetic acid solution in order to protonate the non-reacted CHT amine groups. As a consequence, the chitosan chains resulting from the cleavage of PCL blocks became water-soluble and were released from the sample. These protonated samples are known as P-CHT-64, P-CHT-82 and P-CHT-93 hereafter, 64, 82 and 93 being the percentage weight of CHT in the network.

4.4.2 Equilibrium water content

The EWC of the CHT-PCL networks in liquid water is shown in Table 4.1. The networks are not soluble in water, since the amine groups are not protonated.

Table 4.1. Data of the cross-linking yield, mass fraction of CHT (X_{CHT}) and equilibrium water content (EWC) of the block-copolymer networks.
[a]Remaining weight of the xerogel after [a]reduction with $NaBH_3CN$, [b]after washing in acetone.

[c]Mass fraction of chitosan (X_{CHT}) calculated from [c]weight loss step II after washing with acetone and [d]after washing with acetic acid 1% (v/v).

CHT/PCL (%)	[a]Remaining weight (%)	[b]Remaining weight (%)	[c]X_{CHT}	[d]X_{CHT}	[e]EWC (%)
80/20	99 ± 0	98 ± 0	0.79 ± 0.06	0.93 ± 0.04	120 ± 20
65/35	94 ± 3	95 ± 2	0.82 ± 0.09	0.82 ± 0.11	110 ± 40
50/50	98 ± 1	98 ± 0	0.64 ± 0.03	0.64 ± 0.02	90 ± 20

The values obtained for swelling capacity for CHT-82 and CHT-93 are not significantly different ($P<0.05$) from the chitosan film (CHT-F, EWC=120%), indicating that the networks retain the same swelling capacity, except for the sample that contains the highest amount of hydrophobic component, CHT-64, which decreases by around 30% (see Table 4.1).

4.4.3 Thermogravimetryc analysis

The thermograms of pure chitosan present a thermal decomposition divided into two mass steps, or two peaks in the weight derivative (labeled Peak I and Peak II in Figure 4.2). The first, between 37 °C and 150 ºC, is attributed to the evaporation of the water contained in the sample, which is very difficult to eliminate and typically reaches 10% by weight [211]. The second degradation step was attributed to polymer degradation taking place between 200 ºC and 500 ºC. A shoulder on the high-temperature side of the main peak is ascribed to the acetylated groups of the chitosan chain [174]. Due to the high DD of the CHT used in this work, this degradation step is not resolved in a weight derivative peak. Thermal degradation of CHT in a nitrogen atmosphere presents a residue around 31 ± 1% at 800 ºC, followed by a very slow weight loss until the end of the thermogram [212]. On the other hand, aPCL presents a single degradation peak (Peak

III) between 300 ºC -500 ºC and has a low residue, in the order of 4 ± 2%, at 800 ºC (Figure 4.2).

The thermal degradation profile of the samples after reduction and washing in acetone presented a complex degradation profile in the temperature range between 190 ºC and 500 ºC (see e.g. the results of CHT-64 in Figure 4.2). Also shown is the thermogram of the protonated network (P-CHT-64). When compared with that of pure chitosan, there is less weight loss in the first step, below 150 ºC, since the samples are more hydrophobic.

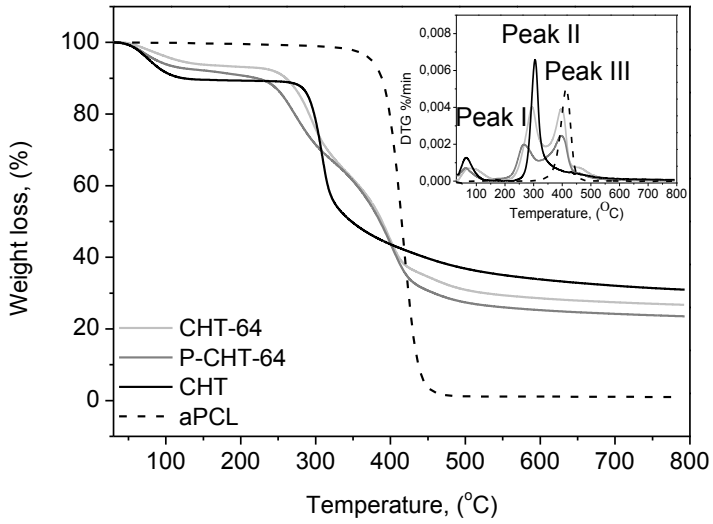

Figure 4.2. TGA and DTG (inset) curves from block-copolymer network after washing in acetone CHT-64, and after protonation in acetic acid 1% (v/v) P-CHT-64. Pure component aPCL and CHT thermograms are shown for the sake of comparison.

The residue at 600 ºC is 27.1 ± 1.2% for CHT-64, 31.8 ± 3.4% for CHT-79 and 31.8 ± 3.0% for CHT-82, smaller than that of pure CHT (34.0 ± 0.6%), but higher than expected. If the CHT fraction in the network were to be calculated from the residue at 600 ºC by applying Eqs 4.1 and 4.2, X'_{CHT}=77% would be obtained for CHT-64, X'_{CHT}=86% for CHT-82 and X'_{CHT}=93% for CHT-79. Thus one would conclude that the samples are

much richer in CHT than expected from the amount of aPCL introduced in the reaction. However, some data indicated that the composition calculated in this way is wrong.

Interestingly enough, the appearance of the residues after the TGA experiments was clearly different; whereas in pure CHT it was a stiff black film at the bottom of the sample holder, in the case of the network it was quite a rubbery material. It can be hypothesized that since PCL degradation takes place at higher temperatures than CHT, the PCL chains were embedded in CHT residue when depolymerized and even after reaching very high temperatures part of the degradation products were not able to escape from the sample and thus did not contribute to the weight loss. To test this hypothesis, the fraction of CHT was also determined from the weight loss in the first CHT degradation step, (Peak II, Figure 4.3). As the degradation of both components is superposed (see Figure 4.2), the weight fraction of CHT was determined from the Gaussian peak (Peak II) fitted to the DGT curve. The mass loss obtained from the area of Peak II for pure CHT was 44 %. The CHT mass fraction in the networks was obtained by comparing the area of Peak II in the network with that of pure CHT. The results obtained for all the samples are listed in Table 4.1 and are used to label the samples.

Furthermore, it can be observed that the degradation peaks in the networks are shifted with respect to the pure components, which is a clear indication of the interaction between the CHT and PCL blocks (see Figure 4.2). It can also be seen that the mass loss starts at lower temperatures in the networks than in the pure components, which suggests that the association between CHT chains is disturbed in the network, thus decreasing thermal stability. As stated above, the position and shape of Peak III due to the depolymerization of PCL chains is disturbed by the fact

that degradation takes place while the chains are entrapped in the CHT residue.

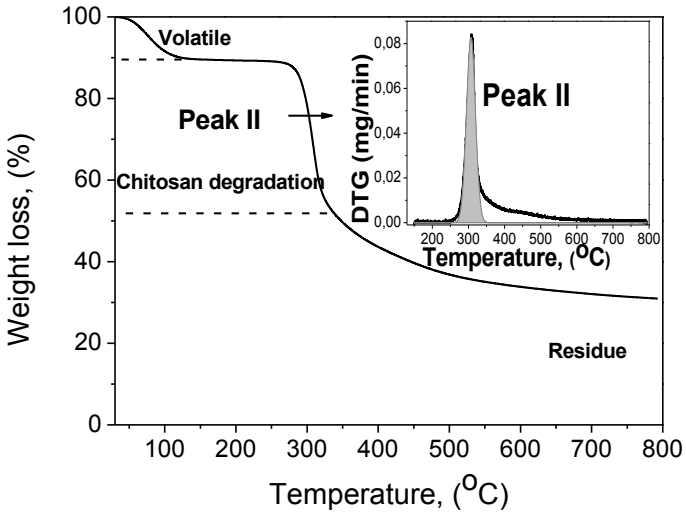

Figure 4.3. Thermogram of pristine CHT showing the thermal degradation steps. DTG curve including Gaussian fit peak for thermal degradation of CHT of Peak II between 200°C and 360°C.

4.4.4 FTIR study

The structural composition of the polymer networks was confirmed by analyzing the FTIR spectra (Figure 4.4). It shows the characteristic peaks of CHT at: 3400-3000 cm^{-1} (-OH stretch) and 2874 cm^{-1} (-CH- stretching bond). The bands at 1658 and 1589 cm^{-1} correspond to the carbonyl group (ν -C=O) from amide I and amide II (C-N stretching) [213] respectively. The intense overlapped peaks from 1200-900 cm^{-1} correspond to several bond vibrations (C-O-C, C-O, C-O-H stretching, N-H bending and OH and C=O deformation). The aPCL polymer shows a band at 1720 cm^{-1} due to the C=O of the ester group, and the characteristic band of the alkyl chains that appears at 2938-2863 cm^{-1}. As the aPCL content in the copolymer networks increased, the intensity of its characteristic peaks, at 1720 and 2938 cm^{-1} also rose.

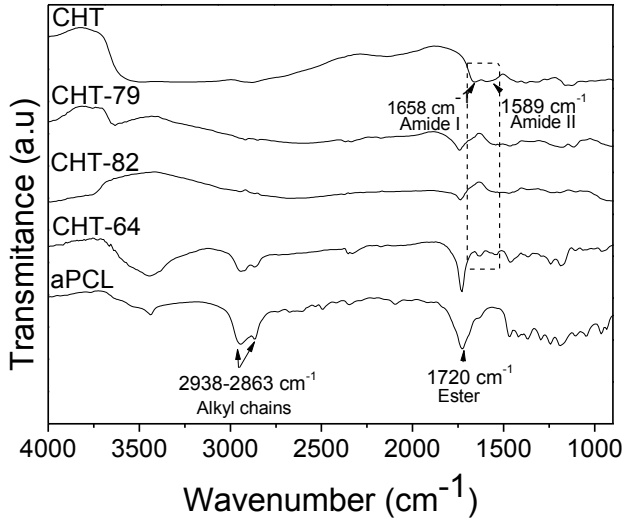

Figure 4.4. FTIR spectra from block-copolymer network samples compared with pure polymers CHT and aPCL.

In the polymer networks the peaks from amide I and amide II are shifted towards a lower wavenumber with respect to pristine CHT as a consequence of cross-linking between polymers. This effect is more pronounced in CHT-64, with a larger number of amine groups involved in cross-linking bonds.

4.4.5 Morphology of porous samples

The possibility of obtaining a porous morphology without using any external porogen is an important factor in tissue engineering applications. Porous scaffolds enable the penetration and migration of cells and the vascularization and transport of the nutrients to the cells.

After reduction and washing with acetone, the networks were swollen in water and then freeze-dried. SEM was employed to characterize the porous network morphology (Figure 4.5). Only the CHT-64 showed a porous morphology with irregular pore size and interconnectivity; the average pore size for the sample was 13.7 ± 3.6μm.

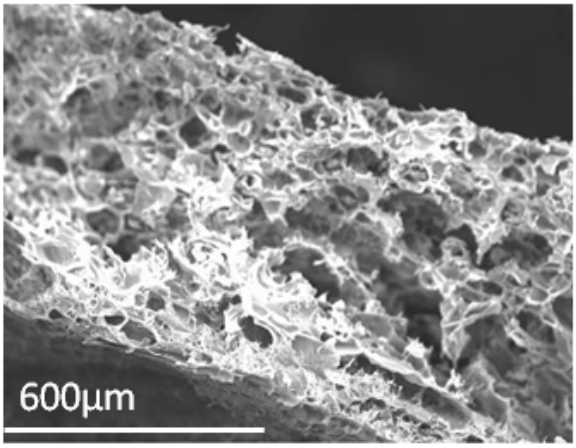

Figure 4.5. SEM images of the CHT-64 block-copolymer network.

4.4.6 XRD and DSC. Phase separation and crystallization

The XRD and DSC experiments were carried out in order to obtain information about the miscibility and the crystallization of both components in the block-copolymer network.

Figure 4.5 shows the XRD spectra recorded on pristine CHT-F film and the copolymer networks. The CHT-F diffractogram presents the double broad crystalline peaks characteristic of chitosan [82, 140] with maxima at around $2\theta \approx 11°$ and $2\theta \approx 20°$ [85]. PCL has two intensive crystalline peaks around $2\theta \approx 21°$ and $2\theta \approx 23°$ [214].

The DSC experiments confirm the XRD results. Figure 4.6 (inset) shows the DSC traces recorded in the second heating scan. PCL presents a glass transition temperature (Tg) around -60°C and melting temperature around Tm =50-60 °C [214]. In the DSC PCL thermogram a bimodal melting peak appears around Tm=46 °C and Tm=51 °C. This behavior is attributed to the presence of two crystal sizes. The DSC CHT thermogram does not show any transition in the temperature interval of the measurements [215].

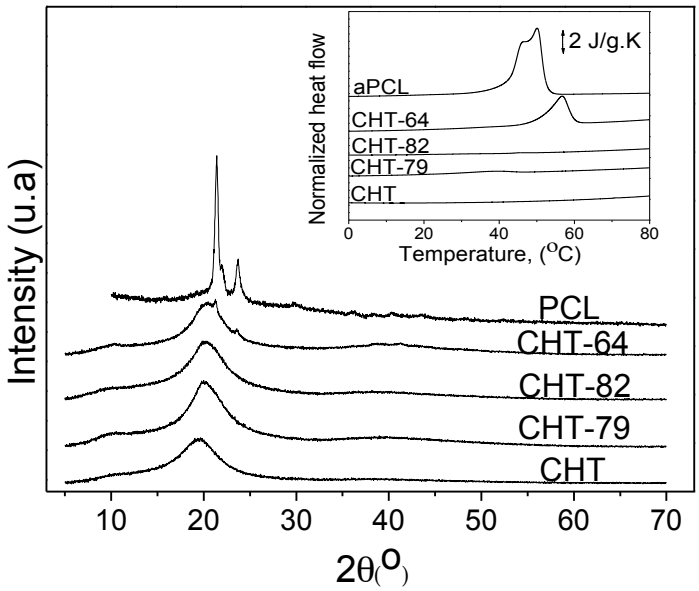

Figure 4.6. X-Ray diffractograms of CHT-PCL block-copolymer network.

Only the CHT-64 sample, with 36% of the PCL mass in the network, presents a clear melting peak at higher temperatures than in pure aPCL, Tm=57 °C, showing a unimodal fusion peak. Nevertheless, as expected from the XRD results, only small traces of melting peaks are observed in the networks with smaller amounts of PCL. In these samples PCL blocks may be dispersed in the CHT matrix without the ability to diffuse and incorporate to growing crystals, if there are any.

4.4.7 Hydrolytic and enzymatic degradation

The degradation profile of CHT-PCL samples was tested in enzymatic and hydrolytic conditions for up to 28 days. In this time period neither CHT nor PCL pure components had a significant weight loss in a purely hydrolytic medium [135]. Studies of the poly(ε-caprolactone) films showed a weight loss of 47% after 100 hours of degradation in lipase [206]. The CHT is degraded by lysozyme but is quite slow; the degradation of 80%

DD CHT had a weight loss around 10% at 28 degradation days [135].

Experiments on enzymatic degradation were performed in lipase media with protonated CHT-PCL samples. After the cleavage of PCL chains the protonated CHT chains were water-soluble and could leave the sample. The network degradation process was evaluated by measuring the remaining weight and EWC. The EWC rapidly increases when the number of effective crosslink points in the network is reduced. Results of the remaining weight and EWC of samples P-CHT-64 and P-CHT-93 are shown in Figure 4.7.

In lipase medium, cleavage of PCL chains was quite fast. As expected P-CHT-64 degraded faster than CHT-93; the remaining weights were 22.4 ± 0.5% and 51.9 ± 0.3% after 28 days of degradation, respectively (Figure 4.6a and 4.6b). Interestingly, the swelling behavior showed an initially rapid increase, with a maximum of the EWC after seven days of degradation, indicating that the cross-linking density of the network decreased. After that, the EWC became nearly constant, even if the weight of the sample decreased. This result could be explained by the proportion of the hydrophilic component in the degraded samples.

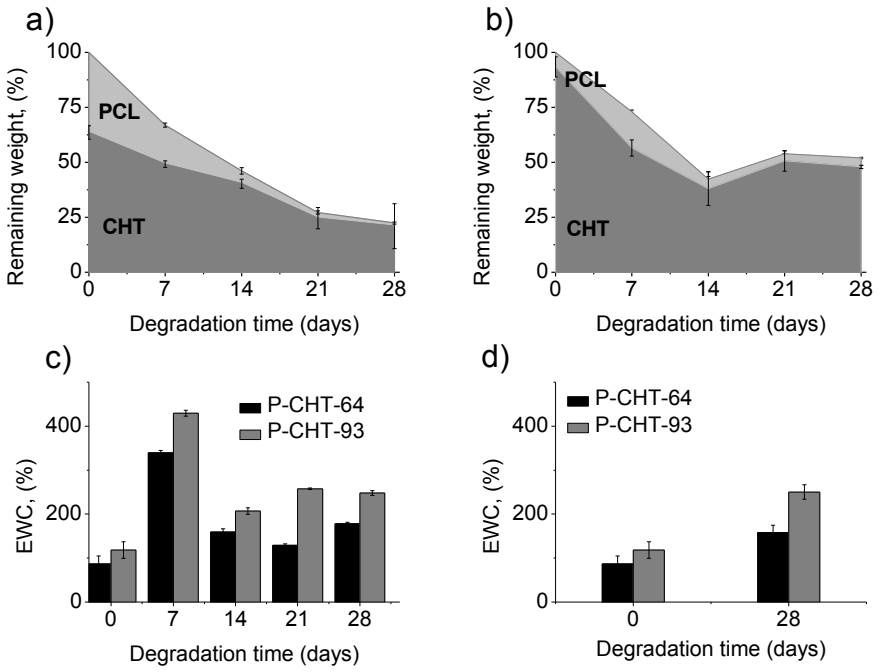

Figure 4.7. Evolution of X_{CHT} and X_{PCL} in enzymatic degradation conditions for a) P-CHT-64 and b) P-CHT-93. Water content in enzymatic c) and d) hydrolytic conditions.

To further study this point, the composition of the degraded samples was analyzed by TGA using the procedure to calculate the area of the chitosan peak (Peak II) described above for the non-degraded samples. Results are shown in Figure 4.7a for P-CHT-64 and Figure 4.7b for P-CHT-93. The X_{CHT} for P-CHT-64 increases gradually as the degradation process with lipase proceeds. This behavior, which is more pronounced in the sample that contains a higher amount of PCL (P-CHT-64) indicates that the PCL chains are degraded while the CHT chains are released and some of them are solubilized due to the previous protonation of the amine group. This degradation profile was confirmed by the TGA and DTG curves. As the degradation time progresses, the maximum temperature of Peak II and Peak III in the DTG curves became more similar to those of pure polymers

CHT and aPCL. For instance, while before degradation the sample P-CHT-64 presented a maximum Peak II at Tmax=260 °C and a maximum Peak III Tmax=381 °C, the data after 28 days of degradation showed that Tmax=308 °C to Peak II shifted to a similar temperature to pure chitosan (Tmax=306 °C).

Although the weight loss in PBS degradation after 28 days was quite modest (remaining weight around 90%), the water content of the network doubled the initial value in both samples after 28 days (see Figure 4.7d), implying that a considerable number of chains were broken. The dispersion of the PCL blocks in the CHT matrix allowed water to diffuse and produced the hydrolysis of the PCL ester groups.

4.5 Conclusions

Hydrophilic/hydrophobic block-copolymer networks of CHT were synthesized using dialdehyde end-capped PCL as cross-linking agent. The EWC of the networks was similar to that of pure CHT, except for the sample containing the highest amount of hydrophobic PCL component (CHT-64), which absorbs 70% of the water absorbed by pure CHT. The DSC and XRD experiments indicated that the PCL domains were not able to crystallize, except for the CHT-64 sample. In the networks with lower PCL content, the chain segments could not diffuse to incorporate into formed crystals, which show the good dispersion of PCL chains in the network. Degradation experiments were performed on protonated CHT networks. Enzymatic degradation of PCL chains enabled the release of water-soluble CHT chains and allowed the fast degradation of the networks. For instance, the sample with 36% PCL (CHT-64) presented a remaining weight of 22.4 ± 0.5% after 28 days of degradation in a lipase medium. The increase in the water content of P-CHT-93 degraded in

lipase and of both the P-CHT-64 and P-CHT-93 samples in PBS indicated that some chains were broken, although the network structure prevented any weight loss.

Chapter 5. Fast degrading polymer networks based on carboxymethyl chitosan

5.1 Abstract*

In this chapter macroporous membrane for mesenchymal stem cells, MSCs, transplant has been developed. The membranes support cell seeding and proliferation and completely degrade in less than one week in "in vitro" culture. The biodegradable material is a polymer network based on carboxymethyl chitosan (a water-soluble modification of chitosan) cross-linked by poly(ε-caprolactone) PCL, fragments which are susceptible to hydrolytic degradation. Synthesis was performed in solution in a common solvent for the two components of the network. The gel fraction was assessed by extraction in selective solvents. Physical characterization of networks of varying composition included water sorption capacity and the crystallinity of poly(ε-caprolactone) in the network. In this way polymer networks are synthesized that loose between 39 ± 7 and 100% of their mass when immersed in water for 28 days. The same weight loss is attained in enzymatic medium in only 4 days. Porcine bone marrow MSCs were seeded in macroporous membranes to show cell viability, and proliferation up to 7 days culture when the biomaterial is completelly dissolved in the medium.

*The results presented in this chapter are in preparation to be published as scientific article:

M. A. Gámiz-González, P. Guldris, C. M. Antolinos Turpín, J. Ródenas Rochinaa, A. Vidaurre,and J. L. Gómez Ribelles.

Fast degrading polymer networks based on carboxymethyl chitosan.

5.2 Introduction

Chitosan (CHT) is a polysaccharide [203] used in a wide variety of tissue engineering applications such as bone, cartilage, and skin regeneration [203, 216, 217]. Chitosan is not water-soluble in a basic or neutral pH aqueous medium [80]. It is susceptible to enzymatic degradation by lysozyme [218]. Ren *et al.*, [134] found that after 84 days of enzymatic degradation in lysozyme, the mass loss was only 10% for chitosan with a deacetylation degree of around 81%. Hydrolytic degradation in aqueous media is nearly zero [135]. This limits chitosan applications in tissue engineering.

Carboxymethyl chitosan (CmCHT) is a water-soluble chitosan derivative. It is suitable as a biomaterial and is widely used in different fields such as tissue engineering applications, targeted drug delivery, and gene therapy.

Chemical cross-linking of chitosan is the most common method for producing permanent polymer networks using covalent bonding between the polymer chains [200]. Genipin [62], Tripolyphosphate [64], and particularly dialdehyde cross-linkers such as glutaraldehyde [208, 219, 220], have been used as cross-linking agents. The chitosan networks have applications as supporting biomaterials in regenerative medicine therapies [4, 221], and for transplanting stem cells to organisms.

In this chapter, we used a new cross-linker based in a medium molecular weight poly(ε-caprolactone), (PCL) chain. PCL is susceptible to hydrolysis although the hydrolytic degradation of bulk PCL is quite slow due to its hydrophobicity and high crystallinity. PCL has been used in the production of scaffolds for tissue engineering applications, mainly in bone regeneration, cardiovascular and cartilage tissue engineering. Its low melting point (around 60 ºC) allows easy modeling in a variety of shapes,

even by 3D rapid prototyping and the low glass transition temperature (-60 ºC) gives flexibility and impact resistance to the semicrystalline polymer [214]. Different combinations of chitosan and PCL have been proposed in the literature, in the form of blends or interpenetrated polymer networks [71, 72, 222].

In some regenerative therapies, the required resorption times of the biomaterial is quite short (in the order of few days) to encompass the degradation of the material to the growth of newly-formed tissue (for instance, in the case of skin regeneration or cornea treatments).

The design of the biomaterial developed in this work is based on a block-copolymer network formed of CmCHT chains, a water-soluble polymer, cross-linked with PCL blocks (a hydrophobous, biodegradable polymer). The hypothesis was that the cleavage of PCL chains via hydrolytic or enzymatic degradation would deliver CmCHT chains that would simply dissolve in aqueous media. The cross-linking reaction was carried out between aldehyde end groups from PCL and amino groups from CmCHT in a Schiff's reaction [223]. Dialdehyde end-capped poly(ε-caprolactone) (aPCL) was used as a cross-linker. The aPCL was synthesized using a Swern oxidation reaction [224] from PCL-diol. Polymer networks with different proportions of aPCL were synthesized.

The physico-chemical properties of the synthesized polymer networks were analyzed. The equilibrium water content, thermal degradation and crystallinity were some characterizations used to verify the cross-linking.

The degradation profiles in hydrolytic and enzymatic conditions (Lipase and Lysozyme) were tested. The degradation was characterized by measuring the remaining weight, equilibrium water content, composition, and molecular weight of the degradation media. Pig mesenchymal stem

cells, MSCs culture in the macroporous membranes, probes the viability, proliferation and fast degradation of the supporting biomaterial during "in vitro" cell culture.

5.3 Materials and methods

5.3.1 Materials

Carboxymethyl chitosan (CmCHT) with a deacetylation degree (DD) of around 90% was obtained from Santa Cruz Biotechnology. The CmCHT was used as received without any purification. The substitution degree of carboxymethyl groups was analyzed with a potenciometric method described in the reference [225] and it is around DS=1.22 ± 0.04 carboxymethyl groups per monomeric unit. The molecular weight was measured [226] and it was around MW=677 kDa with polidispersity index PĐ=2.64. Poly(ε-caprolactone) diol with a molecular weight (Mn) of 2000 Da, chloroform ($CHCl_3$), anhydrous dimethylsulfoxide (DMSO), oxalyl chloride $(COCl)_2$, dichloromethane (DCM), triethylamine (TEA), magnesium sulfate ($MgSO_4$), sodium cianoborohydride, ($NaBH_3CN$) and formic acid, (HCOOH), all analytical grade, were purchased from Sigma–Aldrich.

5.3.2 Methods

5.3.2.1 Synthesis of dialdehyde end-capped poly(ε-caprolactone), (aPCL)

Oxidation of PCL-diol to obtain the dialdehyde end-capped PCL, (aPCL) was carried out following Swern oxidation conditions of Groth *et al.*, [224]. Anhydrous DCM was used like solvent due to the high toxicity that

present the carbon tetrachloride, CCl_4. All reaction vessels and reagents were manipulated in an inert atmosphere.

Oxalyl chloride (0.85 mL; 10 mmol) was mixed in anhydrous DCM (50 mL). The solution was cooled to -47 °C. DMSO (1.5 mL; 0.625 mmol), was mixed with DCM, and slowly added to the oxalyl chloride/DCM solution. PCL-diol (5g; 2.5 mmol) previously dissolved in DCM (16 mL) was added to the cooled solution drop by drop. The mixture was stirred during 3 hours at -47 °C. The catalytic amount of TEA (5.2 ml; 9.3 mmol) was then added and allowed to reach room temperature. The resulting product was diluted in DCM and extracted with HCl 1M and a supersaturated NaOH solution. The extracts were dried with $MgSO_4$. The resulting solution was rotaevaporated and the final product was dissolved in chloroform and reprecipitated with cool diethyl ether and then dried in a vacuum.

5.3.2.2 Synthesis of CmCHT-PCL network

Carboxymethyl chitosan (CmCHT) and dialdehyde end-capped poly(ε-caprolactone) (aPCL) were separately dissolved in formic acid (2% (w/v)). Cross-linkig reaction took place at room temperature. Films with differing initial CmCHT:aPCL weight ratios: 95:5; 90:10; 80:20; 65:35; and 50:50 (w/w) were obtained after evaporation of the solvent in poly(tetrafluor ethylene) (PTFE) molds. The CmCHT-PCL films were carefully separated from the (PTFE) mold and treated with $NaBH_3CN$ 1% (w/v) solution to reduce the (C=N) bond between aldehyde and amine groups from the aPCL and CmCHT respectively. The obtained polymer networks were washed with acetone and water to remove the not bonded polymer chains from the cross-linked network and finally, the networks were dried for 48h in a vacuum oven at 50 °C. The networks were named CmCHT-38, CmCHT-50, CmCHT-66, CmCHT-77 and CmCHT-93 where the number

indicates the mass percentage of CmCHT calculated from thermogavimetric analysis (TGA).

5.3.2.3 Proton Nuclear Magnetic Resonance (1H-NMR) spectroscopy

1H-NMR spectra were recorded at room temperature with a Varian 400 spectrometer (Varian, USA). The samples were dissolved in $CDCl_3$ (δ= 7.28), and tetramethylsilane (TMS) was used as an internal reference.

5.3.2.4 Fourier Transform Infrared Spectroscopy (FTIR)

FTIR spectra of the samples were recorded on a Thermo Nicolet Nexus FTIR, using OMNUC software and the smart diffuse reflectance method. The samples were analyzed as a powder and the reference was dried KBr. The spectra were obtained by continuously accumulating 32 scans in the 500-4000 cm^{-1} range at a 4cm^{-1} resolution.

5.3.2.5 Solid State 13C-NMR spectroscopy (CP/MAS)

Solid-state 13C-NMR (CP/MAS) experiments were carried out on a Bruker Avance III Wide Bore 400 MHz spectrometer at the resonance frequency of 100.6404 MHz using 4 mm double resonance cross-polarization magic angle spinning probe.

Around 100 mg of sample was packed into a 4 mm zirconium oxide rotor with a Kel-F end-cap. CP/MAS 13C-NMR spectrum was acquired with a cross-polarization contact time of 2 ms and a recycle delay of 5s at a MAS speed of 10 kHz. All experiments were carried out at 300 K with high power proton decoupling during acquisition. The spectra were referenciated to α-glycine as external reference.

5.3.2.6 Equilibrium Water Content (EWC)

Water content capacity of the polymer networks was assessed by immersion of the dry samples in deionized water. Samples (N= 3 replicates) ranging between 1-2 mg were immersed in 3 mL of deionized water. The weight of the samples was followed gravimetrically after careful elimination of the superficial water with a piece of filter paper. The equilibrium water content (EWC) was determined by Eq (5.1):

$$EWC(\%) = \frac{m - m_0}{m_0} 100 \quad (5.1)$$

where mo refers to the initial weight in the dry state and m refers to the sample weight after 48h of immersion, once equilibrium was reached. Weight was measured with a balance (Mettler Toledo) with a sensitivity of 0.01 mg.

The equilibrium water content, referred to the hydrophilic component weight, m_{CmCHT}, was determined by Eq (5.2).

$$EWC'(\%) = \frac{m - m_0}{m_{CmCHT}} 100 \quad (5.2)$$

5.3.2.7 Thermogravimetryc analysis

TGA measurements were performed using a TA-Instrument Model SDT-Q600 system. TGA tests were carried out in alumina crucibles where weight samples, between 5 and 10 mg, were heated from 30 ºC to 900 ºC at a heating rate of 10 ºC/min. TGA experiments were performed using a nitrogen flow of 20 mL/min in order to avoid thermoxidative reduction.

The CmCHT proportion in the polymer network was determined by TGA from the residues obtained at 600 °C, RW_{600}, excluding the water loss in the RW_{180} samples (residue measured at 180 °C). Thus, the residue weight of the network, $RW_{network}$, was calculated by applying the Eq (5.3):

$$RW_{network} = \frac{RW_{600}}{RW_{180}} 100 \quad (5.3)$$

The mass fraction of CmCHT, X_{CmCHT}, and PCL blocks, X_{aPCL}, ($X_{CmCHT} + X_{aPCL} = 1$) were calculated by applying the Eq (5.4),

$$RW_{network} = (X_{CmCHT}\, RW_{CmCHT} + X_{aPCL}\, RW_{aPCL})100 \quad (5.4)$$

Where RW_{CmCHT} and RW_{aPCL} are the CmCHT and aPCL residues obtained by applying Eq (5.3) to the pure components.

5.3.2.8 X-ray diffraction

X-ray diffraction spectra of the CmCHT-PCL polymer networks were obtained on a Rigaku Ultima IV X-ray diffractometer in the Bragg-Bentano configuration using the Kα radiation of a Cu anode. The networks were scanned from 2θ=5-70º at a speed of 2º/min. Diffraction patterns were deconvoluted using "PDXL" integrated X-ray powder diffraction software.

5.3.2.9 Differential Scanning Calorimetry (DSC)

Differential Scanning Calorimetry (DSC) was performed in a Pyris DSC8000 from TA Instruments, calibrated with indium and zinc standards in a nitrogen atmosphere. The dry samples (2-10 mg weight) were held at 30 ºC during 1 minute. They were then cooled from 30 to -87 ºC at a cooling rate of -20 ºC/min, held at -87 ºC for 2 min and heated from -87 to 90 ºC at a heating rate of 20 ºC /min, held at 90 ºC for 1 min and cooled and heated again under the same conditions. The final temperature was 30ºC. The degree of crystallinity of the PCL contained in the network was calculated, for both the first and second heating scan, from the area of the melting peak:

$$X_{PCL\,Crist} = \frac{\Delta H_f}{\Delta H_{PCL}\, W_{PCL}} 100 \quad (5.5)$$

Where ΔH_f is the heat of fusion of the polymer network, measured at the first or second heating scans, ΔH_{PCL} is the heat of fusion of the 100% crystalline PCL 139.5 J/g, [227] and W_{PCL} is the PCL weight in the sample, as calculated from composition data.

5.3.2.10 Enzymatic and hydrolytic degradation

Samples with 5 mm of diameter (N=5 replicates at each degradation time) were degraded under hydrolytic or enzymatic conditions. Samples were immersed in a PBS solution to check the hydrolytic degradation (pH=7.4 and 0.02% (w/v) of sodium azide to avoid bacteria proliferation). The enzymatic degradation media was prepared adding 1mg/ml of lysozyme or lipase to PBS (pH=7.4) with 0.02% (w/v) of sodium azide [228]. The temperature was held at 37 ºC during the degradation experiments, and the degradation media was replaced once a week in the hydrolytic degradation and twice a week in the enzymatic degradation. At predefined degradation intervals, samples were extracted from the degradation media, carefully dried with a piece of filter paper and weighed to determine the equilibrium water content by Eq (5.1). Samples were placed in vacuum desiccators at room temperature until a constant weight was reached. The percentage of the remaining weight after degradation was determined by comparison of the weight of the dry sample before the degradation process (m_o), with the weight of the dry sample, m_d, using the following equation Eq (5.6):

$$Remaining\ weight(\%) = \frac{m_d}{m_o} 100 \quad (5.6)$$

5.3.2.11 Gel Permeation Chromatograph (GPC)

Molecular weight distribution of supernatant solutions from enzymatic degradation media were analyzed using a Gel Permeation Chromatographer (GPC), at 35 ºC. Measurements were performed using a Waters Breeze GPC system with a 1525 Binary HPLC pump (Waters Corporation, Milford, MA) equipped with a 2414 refractive index detector and four serial columns of water (Ultrahydrogel 7.8 mm ID x 30 cm). The supernatant solutions were lyophilized to removed the water and obtain a concentrate product, then they was dissolved in 3ml of mili Q water. PBS solution (pH=7.5-7.4) was used as mobile phase at a flow rate of 0.5 mL/min and 100µL injection volume. The calibration curve was prepared using monodisperse PEG poly(ethylene glycol) standard kits (Waters).

5.3.2.12 Cell isolation and sub culture

Mesenchymal stem cells (MSCs) were collected from femora bone marrow obtained from a 4-month-old porcine specimen. Under laminar flow hood femora head was removed and gelatinous bone marrow was collected from medullary cavity. Bone marrow femora was resuspended and homogenized in DMEM GlutamaX supplemented with 10% FBS and 1% penicillin/streptomycin. Cell suspension was centrifuged at 650g for 5 min and supernatant discarded, and repeating once again after going back to resuspended cells. The resulting pellet was again resuspended in culture medium and filtered using a 40µm nylon filter. Cells were seeded in a T75 cm^2 culture flask at $4x10^5$ cells/cm^2 and expanded in monolayer culture until passage 1 with Dulbecco's Modified Eagle's Medium, DMEM GlutamaX (Gibco, UK), supplemented with 10% of fetal bovine serum, FBS (Gibco, UK), 2% penicillin/streptomycin (P/S) (Gibco, UK), 5 ng/mL human recombinant fibroblast growth factor-2 (FGF-2) (Eurobio) and 125

mg/mL amphotericin B (Sigma Aldrich, Spain). Expansion step was repeated twice more until passage 3. Cells were concentrated (at $1.5x10^6$ cells/mL) and cryopreserved in freezing medium (90% FBS with 10% dimethyl sulfoxide). Previous to cell seeding passage 4 was started, cells were unfrozen at 37 ºC in a water bath for 1 min and seeded at $5x10^3$ cells/cm^2 in a T75 cm^2 culture flask.

5.3.2.13 Sample disinfection and membranes cell seeding

Cell culture after undergoing biological degradation (3h, 1, 3 and 6 days from seeding) was assessed in the porous membranes of carboxymethyl chitosan (CmCHT) and poly(ε-caprolactone), CmCHT-77 and CmCHT-50, respectively, with porcine bone marrow MSCs.

Passage 4 cells expanded with DMEM supplemented with 5 ng/mL FGF-2 were detached using trypsine and suspended in free serum DMEM GlutamaX enriched, supplemented with 1% P/S to obtain a final concentration of $5x10^6$ cells/mL. The membranes were cut in circular discs of 6 mm in diameter and then were disinfected with fungicides and broad-spectrum antibiotics treatment (several washes with deionized sterile water, 100 µg/mL of fungizone antimycotic (Fisher, Spain) and 50 µg/mL of ampicilline (Sigma Aldrich, Spain) dissolution. The samples were frozen at -80 ºC and lyophilized under sterile conditions, obtaining the dried samples prior to cell culture.

Cell seeding into the all samples was performed pippeting 20 µL/sample at $5x10^6$ cells/mL on the surface of each membrane and placing them in the incubator 30 min at 37 ºC in a 5% CO_2 atmosphere. Afterward, 1500 µL/sample of medium DEMEN GlutamaX enriched with 10% FBS, 1% P/S and 5 ng/mL FGF-2 was deposited in samples and cultured at 37 ºC in normoxic conditions. Culture medium was changed four days after cell

seeding and samples were collected at 3h, 1, 3 and 6 days.

5.3.2.14 Indirect cytotoxicity assay

Sample cytotoxicity was assed using protocols adapted from the ISO 10993-5 normative. Samples were disinfected following the antibiotic treatment described previously, as negative control was selected polystyrene and as positive control latex that were both sterilized with steam. Samples were weighed and cut following the guidelines of ISO 10993-12 previous to immerse in supplemented DMEM without phenol red for 24 hours at 37 ºC. Cytotoxicity was assessed with L-929 murine fibroblasts that were expanded with DMEM supplemented with 10% of FBS and 1% of P/S and seeded at 10000 cells/well in a 96 well plate. Material liquid extract was added 24 hours after cell seeding. Cell viability was measured 24 hours after initiate the non contact assay. MTT solution at 10% in DMEM media without phenol red was added and incubated 3 hours at 37ºC. MTT solution was removed and precipitated salts were dissolved in Nonidet at 0.1% in isopropanol with 4mM of HCl. Well plate was read at 570nm.

5.3.2.15 DNA Quantification biochemical assay

Sample's DNA content was determined using P7589 Quant-iT Picogreen dsDNA assay kit (Invitrogen). Four samples for each type of membrane were removed at 3h, 1, 3 and 6 days. Samples were washed with/in Dulbecco's phosphate buffered saline, DPBS, and stored in a/an eppendorfs at -80 ºC previous to samples digestion. Samples were digested with proteinase K to release the DNA that was measured with Quant-iTTMPicoGreen® dsDNA Kit following the protocol described in previous works [229-231].

5.3.2.16 Tridimensional cell distribution

Tridimensional cell nucleus distribution was determined by fluorescence with DAPI nuclear staining using a confocal fluorescence microscope mounted on an inverted Zeiss microscope and software Nis-elements (Nikon). Samples were permeabilized with Triton X-100 0.1% and incubated with DAPI solution 20 min previous to mount the samples with Fluorsave Vectashield mounting medium (ATOM) to stain the nucleus. Pictures were taken in 4 randomly selected sample's regions to obtain 3D (Tridimensional) representation of nuclei distribution and cell penetration/colonization depth value.

5.3.2.17 Statistical analysis

Statistical analysis of the data was performed using SPSS software. Differences between the groups with $p<0.05$ were considered statistically significant.

Statistical analysis of cell quantification assay was done by two-way ANOVA for multiple comparisons using Graph-Pad Prism software. In figures, the bars indicate the standard error and asterisk indicate statistically significant differences. In this case statistical significance was laid on $p<0.05$.

5.4 Results and discussion

5.4.1 Synthesis of dialdehyde end-capped Poly(ε-capolactone) (aPCL)

The final product, after Swern funtionalization of PCL-diol, was characterized by 1H-NMR spectroscopy by comparing the spectrum of aPCL with the corresponding PCL-diol, (Figure 5.1).

Both exhibited identical signals corresponding to the polymer backbone with the exception of two new peaks that appear at around 2.5 and 9.5 ppm. These signals are attributed to the methylene neighbor to the aldehyde group (i) and the proton from the aldehyde group (j).

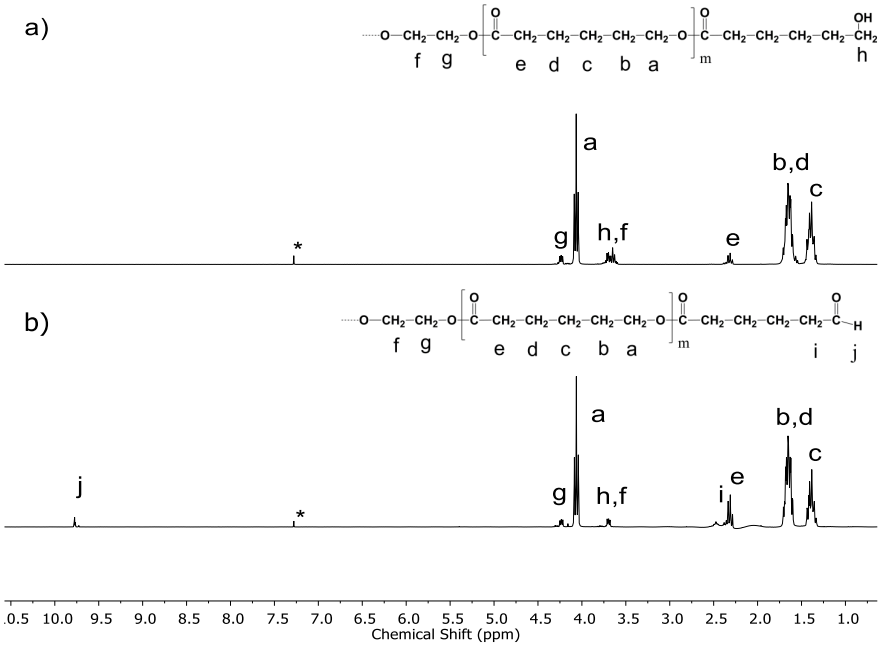

Figure 5.1. 1H-NMR spectra from a) poly(ε-caprolactone) diol, (PCL)-diol and b) Dialdehyde end-capped poly (ε-caprolactone), (aPCL) polymer.

The conversion degree (DC) of the dialdehyde end-capped polymer, (aPCL) was evaluated from the integral of the aldehyde group (j) at 9.78 ppm and taking as a reference the area of the –(CH_2)c- appearing at 1.40 ppm, which is common to the starting PCL-diol and the modified aPCL. Thus, a value of conversion degree (DC) of approximately 40 ± 18% was found. This result is agree with the results reported by Groth *et al.*, [196], where only modest degrees of oxidation between 40 and 60 % were obtained presumably due to the polymer precipitation during the reaction process.

Being this conditions the reaction the high yield of the oxidation, comparing with the others oxidation conditions tested by the author.

aPCL: 1H-NMR (400MHz, $CDCL_3$): δ-1.39 (m, 2H (CH_2)c), 1.65 (m,4H (CH_2)b, d), 2.37 (m, 2H,(CH_2)e), 2.48 (m, (CH_2)i), 3.70 (m,(CH_2)f), 4.06 (t, J=6.7Hz, 2H (CH_2)a), 4.25 (m, (CH_2)g), 9.78 (t, J=1.6Hz, COH).

5.4.2 Cross-linking of CmCHT-PCL network

The CmCHT-PCL polymer networks were obtained by dissolving the desired proportions of aPCL and CmCHT in formic acid at room temperature. A covalent bonding between aldehyde group from aPCL and the amine group from CmCHT, forming a cross-linked network is expected (Figure 5.2). This is a typical reaction of chitosan resulting in Schiff's base formation [223]. The obtained imines (-N=C-) were reduced with $NaBH_3CN$ to obtain a robust cross-linking amine group (-N-C-).

Cross-linking of CmCHT by aPCL is proved by solvent extraction experiments. The non-bonded polymer chains were extracted after network reduction by washing the samples several times with acetone (good solvent for PCL chains) and water (good solvent for CmCHT).

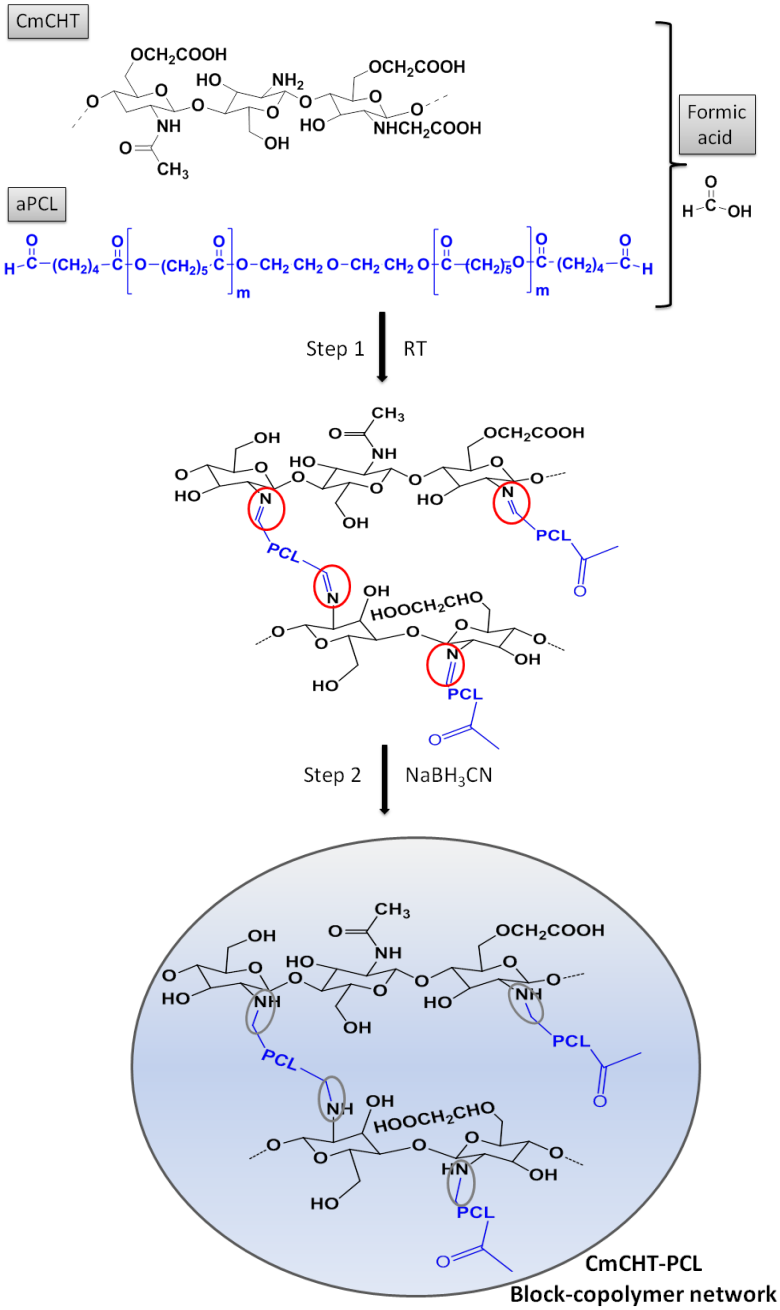

Figure 5.2. Scheme of the cross-linking reaction between CmCHT, (black) and aPCL, (blue). The polymers were dissolved in formic acid at room temperaure (RT). Spet 1: the cross-linking reaction was carried out by Schiff base formation (C=N), (red circle). Step2: Mechanism of reduction to obtain amine group (C-N), (gray circle) with Sodium cyanoborohydride ($NaBH_3CN$).

The remaining weight after reduction and washing was measured gravimetrically (N=3 replicates) (see Table 5.1). The yield of the polymer network insoluble in water and acetone was around 70 ± 3%.

Table 5.1. Remaining weight after: a) $NaBH_3CN$ (reduction) and washes with b) water and c) acetone.

Sample code	Remaining weight after reduction (%)	Remaining weight after washing in water (%)	Remaining weight after washing in acetone (%)
CmCHT-77	72 ± 2	73 ± 1	71 ± 3
CmCHT-66	77 ± 2	75 ± 4	73 ± 1
CmCHT-50	79 ± 4	74 ± 5	71 ± 1
CmCHT-38	84 ± 5	69 ± 4	66 ± 7

Extraction of the unreacted CmCHT starts in the reduction step, in which between 16 and 28% of the initial mass of CmCHT and PCL is extracted depending of the sample composition. After reduction, further extraction of CmCHT with washing in water is not significant. On the other hand the amount of PCL extracted (referring to the initial mass of aPCL) when washing with acetone ranges from 3 ± 7% for CmCHT-77 to 15 ± 4% for CmCHT-38.

5.4.3 Composition and effect of cross-linking on thermal degradation

The fraction of CmCHT was determined from the residue in TGA analysis. This fraction is in good agreement with what was expected from the initial amounts of reactants and the amounts extracted with solvent washing. (Table 5.2).

Table 5.2. Weight residue calculated at 180 °C and 600 °C. Experimental CmCHT proportion obtained from Eq (5.4).

Sample code	Remaining weight measured at 180°C (% ± 1%)	Residue measured at 600°C (% ± 1%)	Initial CmCHT proportion (%)	Measured CmCHT proportion (% ± 2%)
CmCHT	91	45		
CmCHT-93	90	32	90	93
CmCHT-77	90	35	95	77
CmCHT-66	93	31	80	66
CmCHT-50	96	25	65	50
CmCHT-38	95	20	50	38
aPCL	99	3		

For the CmCHT polymer, the thermal degradation occurs in two steps; the first at around 180 °C is attributed to water loss and represents around 5% of the initial weight [108].

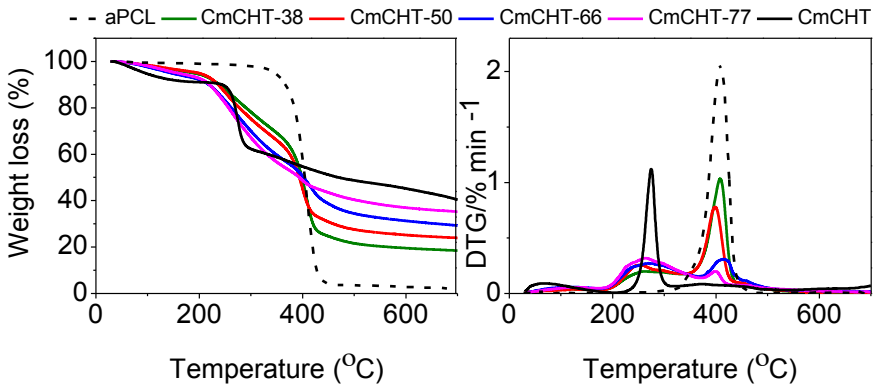

Figure 5.3. TGA and DTG curves of the networks with different compositions and CmCHT and aPCL polymers.

The second step, in the DTG curve, can be observed in a narrow peak between 200 °C and 320 °C, and is due to polymer thermal degradation, followed by a constant mass loss from 320 °C to higher temperatures with

a residual weight of around 45% at 600 °C.

The aPCL polymer presents a single thermal degradation peak between 300 °C-500 °C, and its thermal degradation presented a 3wt% of residue at 600 °C. The weight loss of the polymer networks exhibited a complex profile between 200 °C and 500 °C and showing the main features of the pure components and some differences. Whereas the peak corresponding to PCL thermal degradation maintains its position and decreases in intensity when PCL content decreases, the peak corresponding to CmCHT thermal degradation broadens greatly with small differences among differently composed networks (Figure 5.3b).

The broadening of the temperature interval in which the main degradation of the chitosan chains takes place indicates that an important amount of CmCHT monomeric units is interacting with PCL chains. As expected, when PCL content increases, the polymer network showed less thermal stability and also presented less residue weight than the pristine CmCHT polymer [161]. Although all polymer networks were dried in a vacuum before the TGA experiment, there was a weight loss in the interval from 30 °C to 180 °C due to the presence of some residual water (5-9 wt%).

The weight fraction of CmCHT in the network was lower than the initial proportion, except for CmCHT-93, (Table 5.2). This means that most of the aPCL was cross-linked as can be seen in the composition calculated by TGA.

TGA thermograms also give information on the close interaction between the two components of the network. The thermal degradation of CmCHT presents a narrow peak in the weight derivative and shows a wide process in the networks with an approximate temperature interval between 180

and 380 ºC. This may be related to the new covalent bonding between CmCHT amines and dialdehyde end groups of aPCL.

5.4.4 FTIR spectra

The structural composition of the polymer networks was confirmed by analyzing the FTIR spectra (Figure 5.4). It shows the characteristics peaks of CmCHT at 3400 cm^{-1} (-OH stretch) and 2874 cm^{-1} (-CH- stretching bond). The bands at 1613–1426 cm^{-1} correspond to the carbonyl group (ν -C=O) from amide I and carboxylic acid, respectively, and the band at 1312 cm^{-1} corresponds to C-N stretching, amide II. The intense overlapped peaks from 1200-900 cm^{-1} correspond to several bond vibrations (such as C-O-C, C-O, C-O-H stretching, N-H bending and OH and C=O deformation). The aPCL component (spectrum E in Figure 5.3) shows a band at 1725 cm^{-1} due to the C=O of the ester group, and the characteristic bands of $-CH_2-$ alkyl group that appears between 2952 and 2856 cm^{-1}.

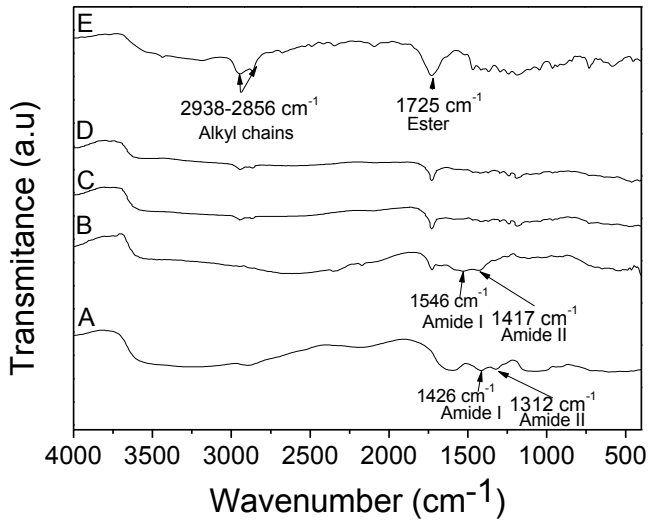

Figure 5.4. FTIR spectra of A) CmCHT, B) CmCHT-77, C) CmCHT-50, D) CmCHT-38 and E) aPCL.

As the PCL content in the polymer networks increased, the intensity of its characteristic peaks at 1725 and 2952-2856 cm^{-1} increased. The broad band observed between 3600 cm^{-1} and 3000 cm^{-1} due to the inter and intra molecular hydrogen bonds of the NH_2 and OH groups of the CmCHT decreases as the PCL content in the network increases. The peaks from amide I and amide II in the polymer networks presented lower intensity than CmCHT still difficult to characterize for CmCHT-50 and CmCHT-38. For CmCHT-77 (spectra B), the amide I and II shifted towards a higher wavenumber with respect CmCHT– indicating the cross-linking between CmCHT and PCL.

5.4.5 Solid State 13C-NMR spectroscopy (CP/MAS)

The cross-linking between aPCL and CmCHT was analyzed by solid state 13C-NMR spectroscopy. Figure 5.5 shows the spectra from pure aPCL and CmCHT polymers and the CmCHT-50, CmCHT-77 and CmCHT-93 samples, in which each peak was identified following the literature for CmCHT polymers. The corresponding signals from each polymer appeared in all solid state 13C-NMR spectra at intensities that varied with the proportion of polymer in the network.

For the cross-linking reaction in which the (-C-N-) linkage was activated: in the 13C solid state NMR spectra the signal corresponding to (-C-N-) linkage was difficult to characterize but the aldehyde group signal that appeared at 202 ppm in aPCL dissapeared in all 13C-NMR spectra of the CmCHT-50, CmCHT-77 and CmCHT-93 networks, indicating the effective cross-linking between the polymers.

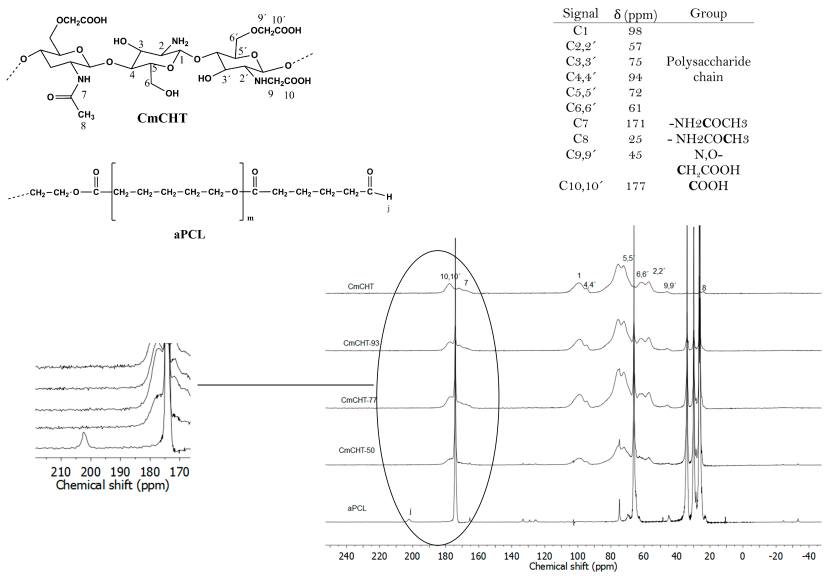

Figure 5.5. Solid state 13C-NMR spectra of carboxymethyl chitosan, (CmCHT), dialdehyde end-capped poly(ε-caprolactone), (aPCL) and their graft copolymers: CmCHT-50, CmCHT-77 and CmCHT-93.

5.4.6 Equilibrium water content (EWC)

The equilibrium water content, EWC, of the polymer networks obtained by Eq.5.1 is shown in Figure 5.6 (black bars). All the obtained polymer networks are hydrogels due to their capacity to host large amounts of water without being solubilized. CmCHT-77 presents a EWC 260 ± 25%. Despite the PCL content increases in the polymer network, the water absorption capacity does not decrease; this indicates that the PCL is forming disperse agglomerates in the network that do not hinder the swelling of the hydrophilic phase. Statistical analysis indicates that there are significant differences between the EWC of CmCHT-77 and the rest of the samples, but there are no significant differences between the EWC of samples CmCHT-66, CmCHT-50, and CmCHT-38.

Figure 5.6, also shows the amount of water referred to the content of

hydrophilic component (grey bars), as it is obtained from Eq (5.2). Except for the case of CmCHT-38, statistical analysis shows no significant change in EWC′. This fact suggests phase separation being the water molecules mainly accommodated in the hydrophilic domains that maintain a similar capacity for water absorption. However, water absorption is significantly lower than that of CmCHT-38 given that it has less hydrophilic component. This effect has been found in other hydrophobic/hydrophilic networks [232, 233] and has been linked with the presence of favored intermolecular hydrogen bonds between polymer chains when there is a larger amount of hydrophilic component, leading to less available sorption sites for water molecules [234].

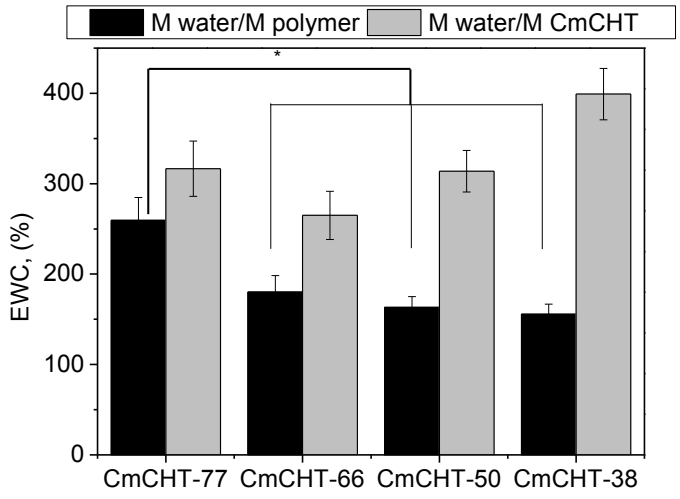

Figure 5.6. Equilibrium water content of the CmCHT-PCL polymer network – referred to the mass of polymer (black bars) and to the mass of hydrophilic component (grey bars).

5.4.7 Miscibility and phase behavior analyzed by XRD and DSC

Figure 5.7 shows the DRX diffractograms of the polymer networks, as well as the pure CmCHT. Diffraction peaks were deconvoluted using non-symmetrical Gaussian peaks (shown in grey in Figure. 5.7). The diffraction

pattern of CmCHT showed two broad and poorly defined peaks around 2θ≈13° and 2θ≈25°. According to the literature [81, 85], the CmCHT has a less ordered structure than CHT and presents two intense peaks around 2θ≈10° and 2θ≈20°. The substitution of the carboxymethyl group breaks the hydrogen bonds between polymer chains and thus decreasing crystallinity. All the polymer networks showed the characteristic diffraction pattern of PCL with peaks at 2θ≈21.3° and 2θ≈23.7°, which correspond to (110) and (200) crystallographic planes, respectively [228].

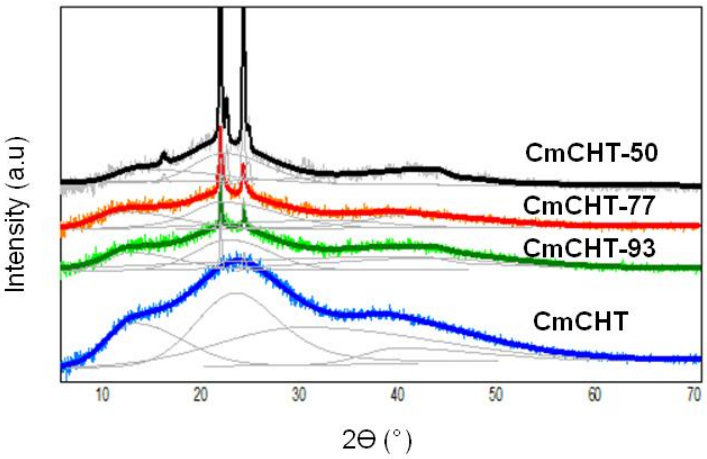

Figure 5.7. Diffractograms of CmCHT-PCL polymer networks.

It is worth noting that even CmCHT-93 with only 7% of PCL presented the characteristic PCL peaks that became better defined as the PCL proportion increased. These results indicate that the PCL domains are large enough to organize the polymer chain in crystalline structures.

Thermal properties were evaluated, by means of DSC experiments following the aforementioned conditions. In Figure 5.8, the second heating scan is represented for all polymer networks and also for pristine polymers.

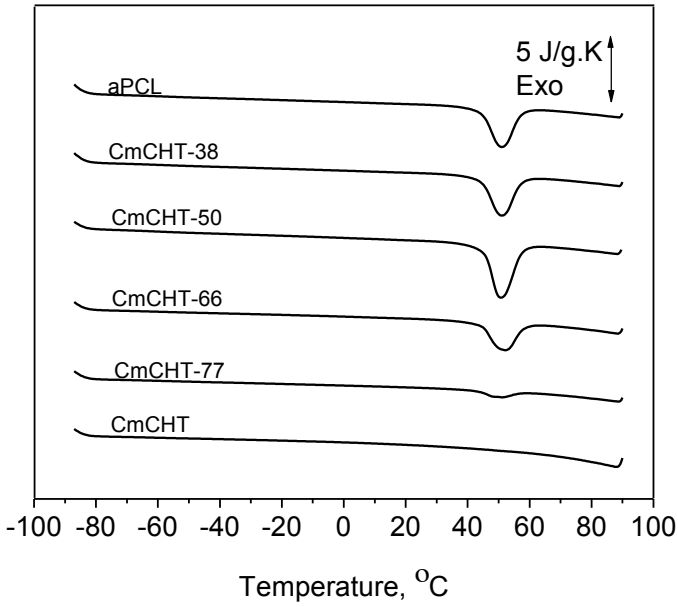

Figure 5.8. DSC thermograms corresponding to the second heating scan at a heating rate of 20°C/min for the polymers networks: CmCHT-77, CmCHT-66, CmCHT-50 and CmCHT-38 – as well as CmCHT and aPCL.

The glass transition temperature (Tg) for the aPCL is around -60 °C. The aPCL polymer shows a melting temperature of Tm≈ 51 °C. However, the CmCHT did not show any characteristic glass transition temperature or melting peak in DSC spectra [215]. All the polymer networks presented the characteristic melting peak corresponding to PCL (around 51 °C). The area of the endotherm increased when the PCL content in the network increased, but the melting temperature showed no significant changes. This confirmed, once again, the phase separation of the polymers in the network.

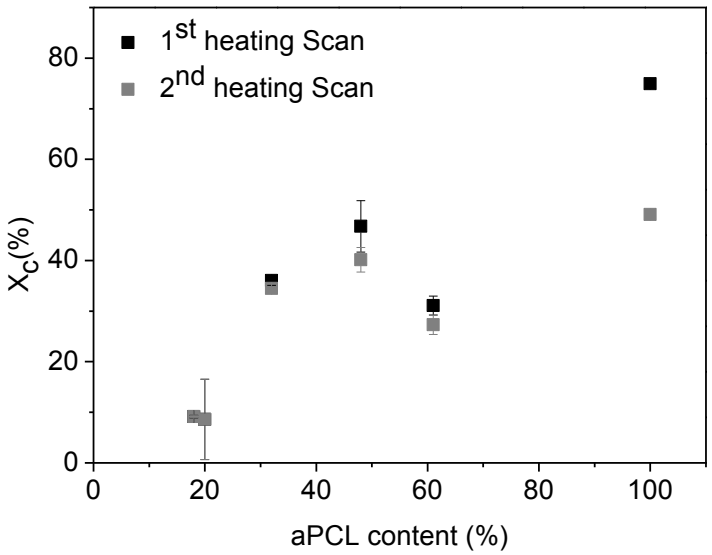

Figure 5.9. Crystallinity fraction of PCL as a function of PCL content for the polymers networks: CmCHT-77, CmCHT-66, CmCHT-50 and CmCHT-38 in both heating scans.

The fraction of PCL that crystallizes in the polymer networks was calculated applying Eq (5.5). The results, calculated from the first and second heating scans, are shown in Figure 5.9. The PCL crystalline fraction in all networks was lower than that corresponding to pure PCL. This feature is due to cross-linking between CmCHT and PCL which hinders PCL chain segment diffusion and incorporation of growing crystals. The pure PCL presented a higher crystallinity in the first than in the second scan. This is attributed to the preparation method, as PCL crystallizes from the solution during solvent casting and the corresponding crystallinity is determined in the first scan – while in the second scan PCL has been crystallized from the melt (after melting during the previous heating scan). However, the polymer CmCHT-PCL networks do not show any difference in crystallinity between the first and second scan. This suggests that when the PCL domains are dispersed in the CmCHT matrix,

melting of the PCL crystals during the first scan produces liquid PCL micro-domains that do not diffuse in the chitosan matrix and that crystals again form on subsequent cooling – in nearly the same way as at the beginning of the measuring cycle.

The block-copolymer network produced by cross-linking of CmCHT chains with dialdehyde end-capped PCL is formed by two very different polymer blocks, one hydrophilic and the other hydrophobic. The polymers used to be immiscible for thermodynamic reasons [149]. The thermodynamic equilibrium criteria drive the polymer blend to phase separation. The case does not differ when the two components of the system are in the form of a network – as happens in interpenetrated polymer networks [235], and even in the case of block-copolymers [209, 210]. In all these cases, the formed phase domains have nanometric dimensions. The same situation is found in block-copolymer networks. Poly(lactide)-poly(2-hydroxyethyl acrylate), PLA-PHEA [236], or poly(ε-caprolactone)-poly(hydroxyethyl acrylate), PCL-PHEA [237] block-copolymer networks present phase separation. Of course, chain connectivity in this kind of two-component polymer system can force compatibility (i.e., homogeneous miscibility of the two components at molecular level). This happens because the increasing cross-linking density of the networks leaves no space available for separated domains [238]. In the case of hydrophilic/hydrophobic systems, the immersion of the material in an aqueous medium induces phase separation – even if the dry system is homogeneous due to the phenomenon of hydrophobic interaction. Our results prove that phase separation takes place in a CmCHT-PCL block-copolymer network. This is clearly revealed by the ability of PCL blocks to crystallize as shown both in the DSC traces of Figure 5.8 and by the XRD difractograms in Figure 5.8. It can be assumed that these PCL

domains must be of nanometric dimensions due to CmCHT-PCL connectivity, and are dispersed in a continuous CmCHT phase – as proved by the water sorption capacity of the networks (around 300% – meaning a great capacity for swelling that a network could not sustain if the hydrophobous PCL phase was continuous).

5.4.8 Hydrolytic and enzymatic degradation tests

The degradation profile of CmCHT-PCL polymer networks was studied under hydrolytic and enzymatic conditions. It is well known that chitosan is enzymatically degraded by lysozyme cleavage of the O-glycosidic bond, and that the PCL can be degraded by lipase [228], and in hydrolytic conditions by the cleavage of the ester groups.

PCL is a polymer susceptible to hydrolytic degradation, but the rate of mass loss when immersed in an aqueous medium is very low [239]. This is because of the high hydrophobicity and high crystallinity of this polymer. Nevertheless, hydrolytic degradation of the CmCHT-PCL networks is very fast when compared with pure PCL, and the degradation of the network must be a product of the cleavage of PCL chains since CmCHT chains are not susceptible to hydrolysis. This behavior can be explained by the dispersion of PCL in nanometric domains dispersed in water-swollen CmCHT; in this way, PCL segments in the network are readily accessible to water molecules – and so to hydrolysis. Thus 80 wt% of the network is degraded in just 28 days in CmCHT-93.

When analyzing the hydrolytic degradation of chain polymers, cleavage of the polymer chains can be monitored by the decrease of the average molecular weight of the polymer and the broadening of the distribution of chitosan molecular weights. It is shown that molecular weight decreases significantly before the material starts loosing weight.

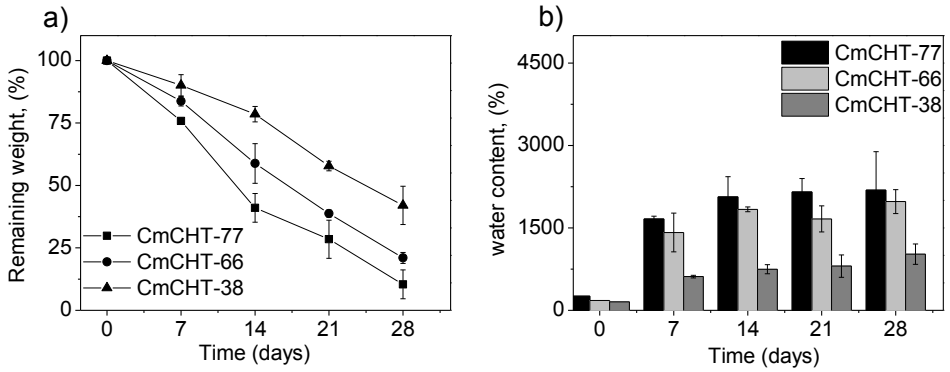

Figure 5.10. Hydrolytic degradation of CmCHT-PCL networks a) remaining weight, and b) water content. The solid lines are a guide.

This kind of analysis is prevented in the case of polymer networks in which molecular weight tends to infinity. Nevertheless, a similar analysis can be performed by measuring the water content of the polymer network since it rapidly increases when the number of effective chains between cross-links decreases, according to Flory-Rehner theory [149]. Interestingly enough, hydrolytic degradation of CmCHT-PCL networks produces a sharp increase of equilibrium water content in the first 5 days of water immersion (Figure 5.10b) multiplying the water sorption capacity by a factor of 7, while the weight loss is still quite moderated. For longer degradation times, weight loss continues while water content keeps around 2000 %.

Figure 5.11 shows the degradation profile of CmCHT-PCL networks in lipase (a) and lysozyme (c). In both cases, the samples that contain the lower amount of PCL blocks (CmCHT-93) degrade faster than the other two compositions (which show no significant differences between them). CmCHT-93 presents a remaining weight of 13 ± 18% after 77 hours in lipase, whereas it presents no remaining weight in lysozyme.

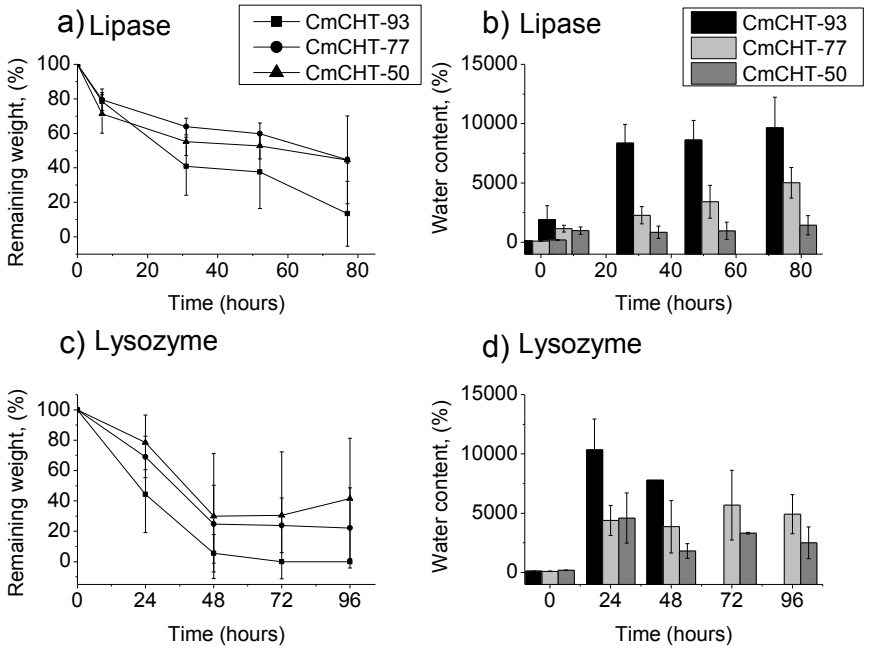

Figure 5.11. Remaining weight and water content as a function of degradation process: a) and b); lipase containing medium; and c) and d) in lysozyme. The solid lines are only guides to the eye.

CmCHT-50 presents a similar remaining weight of 79 ± 70% at 79 hours in lysozyme and 77 ± 50% at 72 hours in lipase conditions. Enzymatic degradation in lipase is much faster in the case of the network than in a PCL homopolymer. Thus, while only 5 wt% of a pure PCL films were lost in 15 days [228], 80 wt% of CmCHT-93 network is degraded in just three days. The water content of the degraded networks was also analyzed. The results (shown in Figure 5.11b and 5.11d) show a result similar to that of hydrolytic degradation with a sharp initial increase of the water content both in lipase and lysozyme conditions. CmCHT-93 presented the highest WC after degradation (as high as 1000% after 20 hours of degradation in both enzymatic media).

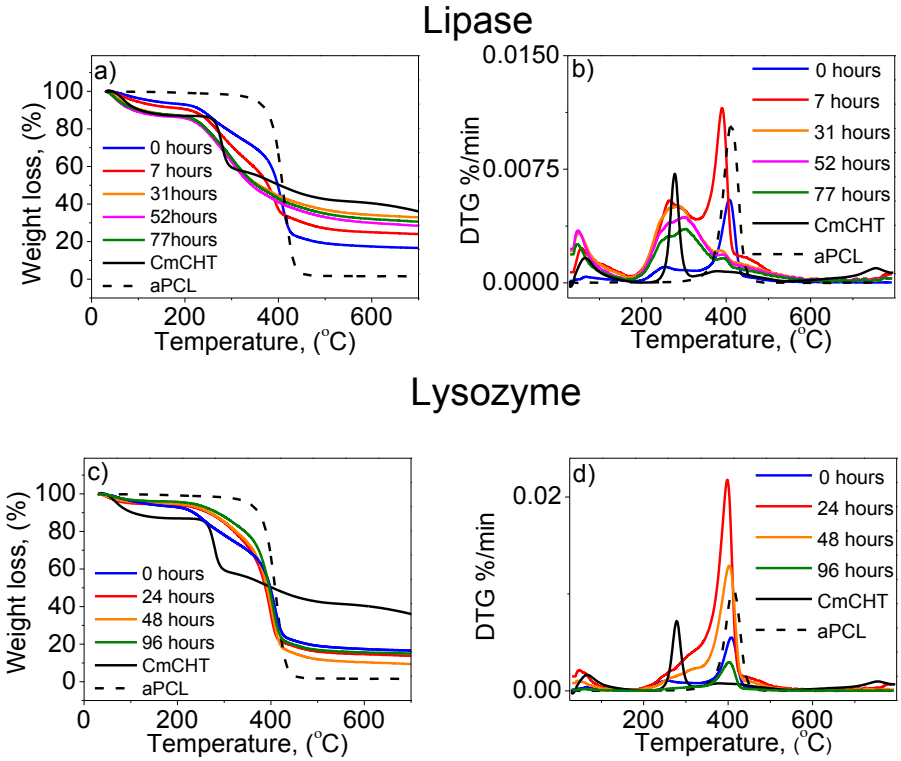

Figure 5.12. TGA a) and c) and DTG b) and c) curves from CmCHT-50 polymer network in both enzymatic media (Lipase, a) and b) and Lysozyme c) and d)).

To further confirm the preferential cleavage of PCL and CmCHT chains in lipase and lysozyme respectively. The degraded networks were analyzed by TGA to evaluate the evolution of network composition during the enzymatic degradation process. Figure 5.12 shows the TGA profiles and the derivative for the CmCHT-50 polymer networks at different degradation times, and the pure components. The samples degraded with lipase (Figure 5.12a and 5.12b) present thermograms that evolve towards the corresponding to pristine CmCHT, indicating that the PCL component is being degraded. In the case of samples degraded in the presence of lysozyme, the TGA trace tends to become more similar to the corresponding pristine PCL as the degradation process advances, indicating that the proportion of CmCHT decreases with degradation time.

It is interesting to characterize the molecular weight of the chain fragments that are delivered from the network as degradation progresses in the enzymatic media. To do this, the supernatants from both enzymatic conditions were analyzed by GPC. The GPC distributions found in the case of CmCHT-50 are shown in Figure 5.13.

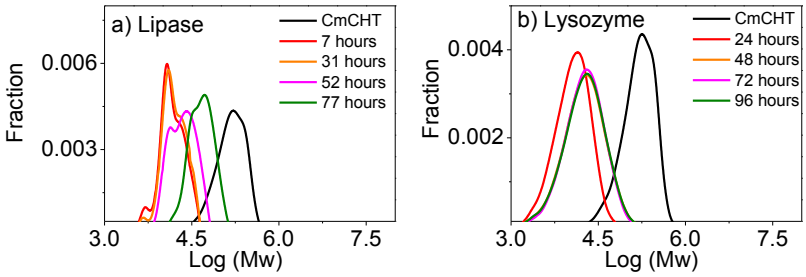

Figure 5.13. Molecular weight distribution in supernatant solution with degradation time of CmCHT-50. a) Lipase and b) Lysozyme respectively.

Interestingly, the degradation in lipase delivers chain fragments (Mw=3x10^4 Da, Mn=2x10^4 Da at 7 hours of degradation) that are much larger than PCL blocks – but shorter than CmCHT original chains (as expected when the cleavage of PCL bridges and CmCHT chains take place). As degradation progresses larger fragments can be detected in the supernatant, but their molecular weight is always lower than that of the original CmCHT chain. Bimodal forms in the molecular weight distribution can be observed in the plots of Figure 5.13a: chain fragments of higher or lower molecular weight are possibly delivered from regions in the network with more or less cross-linking density.

Similar results are found for the networks with other compositions. Nevertheless, during the degradation in lysozyme, the molecular weight of the delivered fragments does not depend significantly on the degradation time, nor on the composition of the network (with values of Mw= 5x10^4 ± 7x10^2 Da, Mn= 2x10^4 ± 5x10^2 Da) and single bell molecular weight

distributions clearly appear (Figure 5.13b).

Thus, polymer chain fragments detected in the degradation medium with molecular weights of between 2 x10^4 and 8 x10^4 Da confirm the hypothesis that cleavage of PCL chains delivers large CmCHT fragments that dissolve in the aqueous medium. Lysozyme acts on CmCHT chains to produce an even quicker degradation, where the molecular weight of CmCHT fragments in the supernatant are of a similar magnitude independently of the degradation time. It seems that CmCHT chains cleavage by lysozyme combines with the hydrolytic degradation of the PCL blocks accelerating the degradation process.

5.4.9 Ciytotoxicity assay

The cell viability obtained with cytotoxicity assay on CmCHT-50 and CmCHT-77 samples, is shown in Figure 5.13. Data showed that samples showed a cell viability over the 70% compared to negative control (polystyrene) pointing that are non-cytotoxic.

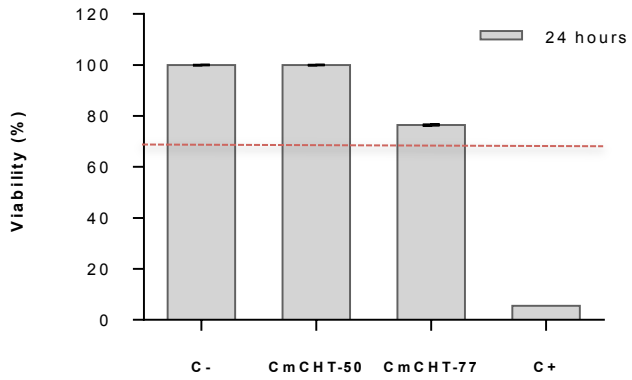

Figure 5.14. Viability of L-929 murine fibroblasts cultured 24 hours in contact with CmCHT-50 and CmCHT-77 membranes, latex (C+) and polystyrene (C-). The bars represent the cell viability (%) ± standard deviation.

5.4.10 MSCs response and membrane degradation during cell culture

Porcine MSCs were seeded into the pores of a microporous membrane made by freeze drying, where the pore size was 51 ± 23 μm for CmCHT-50 and 117 ± 52 μm for CmCHT-77. As shown in Figure 15a the membrane presents large interconnected pores. Cell seeding efficiency and cell proliferation, was analyzed by quantifying the total amount of DNA in the samples (Figure 5.15b). The results reveal that there are no significant differences between the cell seeding efficiency of CmCHT-PCL samples with varying PCL content. Total DNA values show that cell numbers increase after the first day of culture.

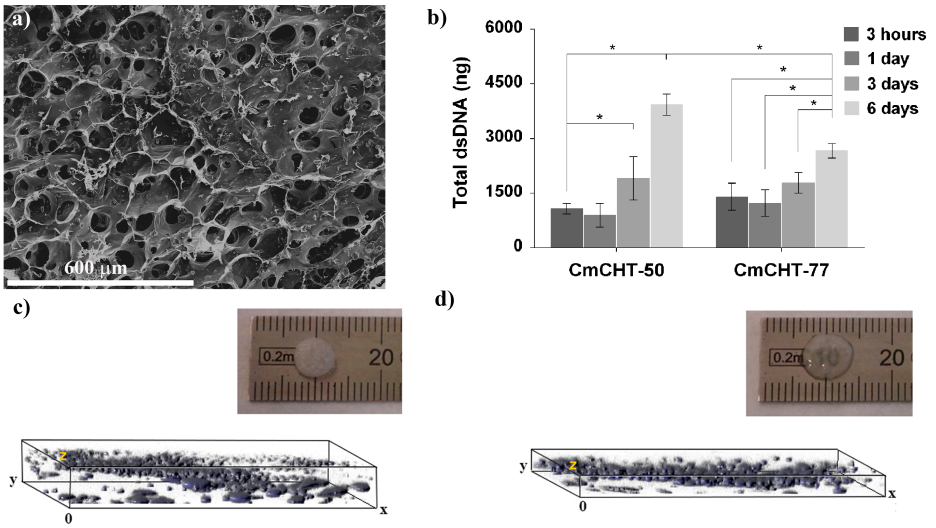

Figure 5.15. a) SEM micrographs of porous membranes CmCHT-50 before cell seeding, b) total dsDNA quantification of the porous membranes CmCHT-50 and CmCHT-77 for 3 hours, 1, 3 and 6 days of culture, c) and d) macroscopic view and tridimensional representation of nuclei distribution (tridimensional cell distribution) of porous membrane CmCHT-50 for 3 hours and 1 day of culture.

Confocal microscopy was used in order to analyze cells distribution inside the pores of the porous membranes. A stack of all the images taken every 10 μm from the surface down to the last cell detected is analyzed. From

these images, the tridimensional cell distribution (shown in Figure 5.15c and 5.15d) and the value of cell penetration depth (see Table 5.3), with the culture time and membranes degradation were characterized. After 3 hours of cell culture, it can be observed (Figure 5.15c and Table 5.3) that most of cells seeded on the surface penetrated into the CmCHT-50 membrane 253 ± 33μm while in CmCHT-77 they enter only up to 163 ± 5μm. This behavior can be explained by the fact that CmCHT-50 present better pore interconnectivity than CmCHT-77.

Table 5.3. Colonization depth value of the porous membranes CmCHT-50 and CmCHT-77 for 3 hours, 1 day, and 3 days of culture. (n= 4 regions for every sample).

	Cell penetration (μm)		
	3 hours	**1 day**	**3 days**
CmCHT-50	253 ± 33	130 ± 50	80 ± 50
CmCHT-77	163 ± 5	40 ± 6	-

Besides, as culture time increases, the membranes are degraded. Membranes of CmCHT-50 can maintain the structure and coherence until 3 days (CmCHT-77 only until day one) after this time point the sample retain the shape but could not be handled (the macroscopic view in Figure 5.15c and 5.15d). For longer culture times, the sample disaggregates and the culture medium becomes translucent. The content of the culture well was moved to a clean one to perform DNA analysis in order to discard the cells that could be adhered to the bottom of the well. Interestingly enough the total DNA value continues increasing up to 6 days culture what can be interpreted in the sense that small fragments of the membrane act as cell carriers and cells continue adhered to the biomaterial particles.

5.5 Conclusions

A new family of CmCHT-PCL networks has been synthesized using aPCL as a cross-linking agent. The main advantage of these networks compared to conventional chitosan is that they present a very fast degradation in cell culture or in enzymatic media while hydrolytic degradation takes longer but it is still much faster than in the pure components of the copolymer network. For CmCHT-77 at three days, only 50% and 20% of the mass is remaining in lipase and lysozyme conditions, respectively. Some 20% of the mass remains at 28 days in hydrolytic conditions. These findings are a consequence of two phenomena. Firstly, the large amount of water absorbed by the networks (despite having a hydrophobous component) facilitates the entrance of water and enzymes, and quickens PCL hydrolysis and CmCHT degradation. Secondly, as the systems are phase separated (XRD and DSC results), the domains rich in CmCHT are easily solubilized – both in enzymatic and hydrolytic conditions. Macroporous membranes made off this copolymer networks can be seeded with MSCs that are viable and proliferate inside the pores. These membranes can be used to deliver cells to the organism in regenerative therapies being resorbed in times of the order of one week.

Chapter 6. Synthesis of highly swellable hydrogels of water-soluble carboxymethyl chitosan and poly(ethylene glycol).

6.1 Abstract*

Highly swellable hydrogels were designed by copolymerization of high molecular weight carboxymethylated chitosan (CmCHT) and poly (ethylene glycol) (PEG) oligomers. The hydrogel swelling capacity can be controlled via the cross-linking density and ranged from 900 to 5600 %.

The hydrogels show good homogeneity with a high-interconnected porosity in the swollen state and with nanodomains rich in CmCHT and others rich in PEGDE. Oscillatory frequency sweep analysis shows a storage modulus of G´=27 kPa for the hydrogel with the highest cross-linking density, which, together with the exhibited enzyme degradability with lysozyme at 59 days indicate that these hydrogels have potential use in delivery systems or soft tissue regeneration.

*The results presented in this chapter is preparing for its publication:
M. A. Gámiz-González, Ulrica Edlund, A. Vidaurre,and J. L. Gómez Ribelles.
Synthesis of highly swellable hydrogels of water-soluble Carboxymethyl chitosan and Poly(ethylene glycol).

6.2 Introduction

The solubility of Poly(ethylene glycol), PEG in water and a wide range of organic solvents in combination with terminal hydroxyl groups are key factors in the successful use to produce PEG block-copolymers and networks with other polymeric materials. PEG presents low levels of protein and cellular adhesion and is a good candidate for drug delivery systems [240] or cell delivery systems for various type of cells [241-244]. Williams *et al.*, synthesized photoencapsulated acrylated PEG with mesenchymal stem cells (MSCs) to produce chondrogenesis in vitro [245]. Poon *et al.* synthesized hydrogels based on dual curable chitosan-graft-poly(ethylene glycol) to cell encapsulation [246].

PEG-based amphiphilic biodegradable hydrogels have been produced by combining PEG with biodegradable hydrophobic polymers such as PLLA, PLGA and PCL [247, 248]. This type of hydrogel presents good mechanical properties with moderate hydrolytic degradation rate and water uptake [248]. PEG can also be combined with hydrophilic polymers such as chitin, chitosan, and collagen, by means of covalent cross-linkers or by functionalization with specific reactive groups.

Our aim was the synthesis of CmCHT-PEG hydrogels which was carried out by cross-linking poly(ethylene glycol) with terminal epoxy groups, the poly(ethylene glycol) diglycidyl ether (PEGDE). The cross-linking mechanism between the two polymers was activated via epoxy-amine and via epoxy-hydroxyl reactions [236]. The reactivity of epoxy groups with amino, hydroxyl, and carboxyl groups has been widely used in developing polymer networks for many different applications [249, 250].

An interconnected macroporous structure was obtained by the freeze-drying method. Due to the insolubility of the hydrogel, the mass fraction of each component was calculated by thermogravimetric analysis. A dynamic

water absorption study showed that the hydrogels have a huge capacity to hold water without dissolving. FTIR and mechanical testing were also carried out in order to characterize the chemical cross-linking and elastic properties of the hydrogels.

6.3 Materials and methods.

6.3.1 Materials.

Poly(ethylene glycol) diglicidyl ether, (PEGDE) with low molecular weight (Mw=500 Da) and sodium hydroxide (NaOH) were purchased from Sigma Aldrich. Carboxymethyl chitosan (CmCHT) with a deacetylation degree (DD) around 90% was obtained from Santa Cruz Biotechnology. The CmCHT was used as received without any further purification. The Substitution degree (DS) was analyzed by a potentiometric method [251] and was found to be DS=1.22 ± 0.04 carboxymethyl groups per monomeric unit.

6.3.2 Methods

6.3.2.1 Size Exclusion Chromatography (SEC)

The Molecular weight of CmCHT was measured by SEC on a Dionex Ultimate-3000 HPLC system (Dionex, Sunnyvale, CA, USA), consisting of three PSS Suprema columns in series (300×8mm, 10μm particle size) with 30Å, 100Å and 1000Å pore sizes, together with a guard column (50×8 mm, 10 μm particle size). The system was equipped with a WPS-3000SL autosampler, an LPG-3400SD gradient pump, a DAD-3000 UV/Vis detector (Dionex, Sunnyvale, CA, USA) and a Waters-410 refractive index detector (Waters, Millford, MA, USA). Pullulan standards with controlled

molecular weights ranging from 342 to 708,000Da (PSS, Germany) were used for calibration [252]. The molecular weight of carboxymethyl chitosan was MW=677kDa with polidispersity index PĐ=2.64.

6.3.2.2 Preparation of CmCHT-PEG hydrogels

A series of CmCHT hydrogels was prepared by cross-linking reaction between CmCHT and PEGDE. The initial mass fraction of the PEGDE (X_{PEGDE}) in each hydrogel is indicated in Table 6.1. A CmCHT solution in NaOH 1.5M (5% (w/v)) was prepared: low molecular weight PEGDE (which is a liquid) was added to the CmCHT solution drop by drop. The solution was homogenized by stirring for 30 min and then cured in an oven at 60 °C until the solvent was fully evaporated (12 hours). The hydrogels were removed from the glass vial and washed several times with deionized water until neutral pH. The samples were freeze-dried at -20 °C for 24h and lyophilized for 48h. The hydrogels were kept in desiccators under vacuum.

6.3.2.3 Morphology

The morphology of each hydrogel was characterized by JSM 5410 Scanning Electron Microscope (JOEL, Ltd., Tokyo, Japan), at a working distance of 15mm and working voltage of 10-15 kV. Samples were fractured after freezing in liquid nitrogen and sputter-coated with gold.

6.3.2.4 Attenuated total reflectance-Fourier transforms infrared spectroscopy, (ATR-FTIR)

ATR-FTIR measurements were performed on a Perkin–Elmer Spectrum 2000 equipped with an attenuated total reflectance (ATR) crystal accessory, within a range of 4000 cm^{-1} to 600 cm^{-1}. A mean of 16 scans at 4

cm^{-1} resolution with atmospheric water and carbon dioxide correction on each sample was recorded and evaluated by the Perkin–Elmer Spectrum software.

6.3.2.5 Water content

The water content of the samples was evaluated as a function of immersion time. The lyophilized samples (N=5 replicates) between 10-15 mg were immersed in 10 mL of deionized water. In order to properly measure water content, the hydrogels were placed in stainless steel baskets with a mesh opening of 0.20 mm and an inner diameter of 30 mm. The basket was carefully dried for each measurement and the water content (WC) was calculated by Eq (6.1), where m_o refers to the dry weight and m_t is the weight in swollen state.

$$WC(\%) = \frac{m_t - m_o}{m_o}\ 100 \tag{6.1}$$

6.3.2.6 Thermogravimetryc Analysis (TGA)

TGA measurements were performed on a TA-Instrument Model SDT-Q600 system. TGA tests were carried out in alumina crucibles in which weight samples of between 5 and 10 mg were heated from 30 °C to 800 °C at a heating rate of 10 °C/min. TGA experiments were performed using a nitrogen flow of 20 mL/min in order to avoid thermoxidative reduction.

The CmCHT proportion in the polymer network was determined by TGA from the residues obtained at 600 °C, RW_{600}, excluding the water loss in the samples (residue measured at 180 °C, RW_{180}). Thus, the weight residue of the network, $RW_{network}$, was calculated by applying the Eq (6.2):

$$RW_{network} = \frac{RW_{600}}{RW_{180}}\ 100 \tag{6.2}$$

The mass fraction of CmCHT, X_{CmCHT}, and PEGDE, X_{PEGDE} were calculated by applying the Eq (6.3),

$$RW_{network} = (X_{CmCHT}\ RW_{CmCHT} + X_{PEGDE}\ RW_{PEGDE})100 \quad (6.3)$$

Where RW_{CmCHT} and RW_{PEGDE} are the CmCHT and PEGDE residues obtained by applying Eq (6.2) to the pure components.

6.3.2.7 Differential scanning calorimetry (DSC)

DSC was performed in a Pyris DSC8000 from TA Instruments calibrated with indium and zinc standards in a nitrogen atmosphere. The dry samples (2-10 mg in weight) were held at 30 °C for 1 minute. They were then cooled from 30 to -87 °C at a cooling rate of -20 °C/min, held at -87 °C for 2 min and heated from -87 to 90 °C at a heating rate of 20 °C /min, held at 90 °C for 1 min and cooled and heated again under the same conditions. The final temperature was 30 °C.

6.3.2.8 Rheological measurements

The mechanical properties of CmCHT-PEG hydrogels (N=5 replicates) were evaluated using a parallel plate rheometer, ARES-G2 Rheometer (TA instruments). The 8 mm diameter hydrogel samples were previously swollen in deionized water. The samples were carefully removed from the Petri dishes in which they were formed and transferred to the bottom plate of the rheometer. The experiments were carried out at room temperature (25 °C). The gap between the plates was adjusted using a normal force of 0.1N. Two different measurements in shear deformation mode were performed: for the frequency sweep test the dynamic modulus (G´) and loss modulus (G´´) were evaluated at 1% shear strain amplitude at frequencies ranging from 0.1 to 10Hz. For the strain sweep tests the module was evaluated at shear strains ranging from 0.1 to 10% at 1Hz.

6.3.2.9 Enzymatic degradation test

Samples with 5 mm diameter samples (N=5 replicates for each degradation time) were degraded under enzymatic conditions. The hydrogels were immersed in the enzymatic degradation media, which was prepared by adding 1mg/mL of lysozyme to phosphate buffer solution, PBS (pH=7.4) with 0.02% (w/v) of sodium azide [4]. The temperature was held at 37 °C during the degradation experiments and the degradation media was replaced twice a week. At predefined degradation intervals, the samples were extracted from the degradation media, carefully dried with filter paper and weighed to determine the equilibrium water content by Eq (6.1). The degraded hydrogels were frozen at -20 °C for 12 hours and lyophilized for 24 hours. The percentage of the weight remaining after degradation was determined by comparing the weight of the dry sample before degradation (m_o) with the weight of the dry sample (m_d) using Eq (6.4):

$$Remaining\ weight\ (\%) = \frac{m_d}{m_o} 100 \quad (6.4)$$

6.3.2.10 Statistics

The data were analyzed by ANOVA using SPSS Statistics 16.0 software, while means were compared by the Tukey-*b* test with the level of significance set at $P<0.05$.

6.4 Results and discussion

6.4.1 Preparation of CmCHT-PEG hydrogels

The CmCHT 5% (w/v) solution in NaOH 1.5 M showed a yellowish color with a pH around 11. When PEGDE was added drop by drop under stirring the solution became translucent, indicating a certain degree of liquid-liquid phase separation. This limits the incorporation of PEG blocks

to the formed block-copolymer network and explains the relatively low PEG content of the resulting material, in spite of the large amount of PEGDE added to the reacting solution. The composition of the resulting network leads to the conclusion that for most of the compositions the hydrogel is formed in the CmCHT-rich phase, while the PEGDE-rich phase is extracted when washing after reaction. Consistent hydrogels were obtained only when PEGDE/CmCHT mass ratio was higher than 75/25. Below this ratio the gel formed could not be handled. Interestingly, at very high PEGDE contents a hydrogel rich in PEG blocks can be obtained, so CmCHT-5 contains just 5% CmCHT. In this case cross-linking reaction seems to have taken place in the PEGDE-rich phase with CmCHT acting as cross-linker. The amount of PEGDE added gives poor control of the final composition of the network, as shown in Table 6.1, but it was possible to obtain a series of block-copolymer networks with varying CmCHT content. Figure 6.1 shows a schema of the reaction mechanism: the result of the cross-linking reaction is a block-copolymer network containing CmCHT and PEG blocks bonded with -C-N- (amine) and –C-O- (ether) linkages. The hydrogels were formed by thermal treatment at 60 °C, since the reaction between the epoxy groups with other reactive groups is slow at room temperature [253].

Pale yellow hydrogels were obtained, removed from the glass vials and washed in water several times until neutral pH, verifying that the pale yellow color had disappeared. The samples were frozen and lyophilized.

The difference in the change of color of the CmCHT solution dissolved in water (clear solution) and basic (yellowish solution) media was attributed to the possible deacetylation mechanism in the CmCHT polymer. It is known that chitosan with different DDs can be obtained from chitin with alkaline media [203]. Similar behavior was observed in the O-acetyl-

galactoglucomanan hydrogels cross-linked with ephychlohydrin in basic media. The colored solution changed as a function of pH [254].

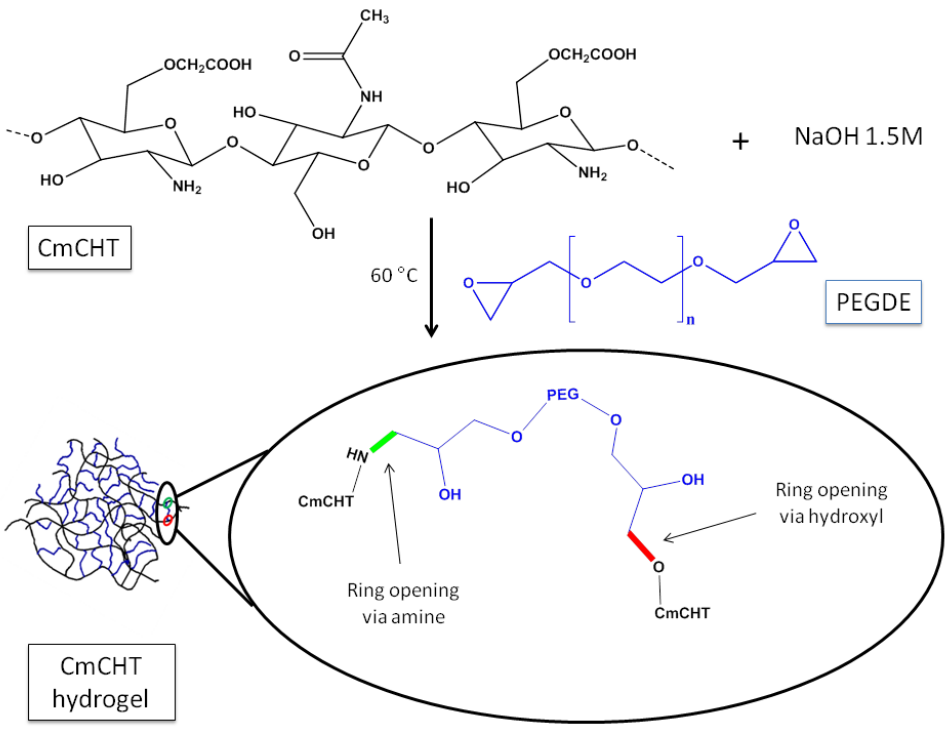

Figure 6.1. Scheme of the cross-linking reaction by ring opening via amine (green bond) and hydroxyl groups (red bond), between CmCHT (black) and PEGDE (blue) polymers.

The mass fraction of CmCHT and PEG blocks in the hydrogel was analyzed by TGA after synthesis and washing. The yield of the reaction as a function of composition was calculated as the mass of the hydrogel obtained ($m_{CmCHT\text{-}PEG}$) with respect to the sum of the initial mass of both polymers ($m_{CmCHT} + m_{PEGDE}$). The values were estimated as being 11 ± 1.20, 7 ± 13 and 63 ± 1 % for CmCHT-89, CmCHT-79, CmCHT-58 and CmCHT-5, respectively. Except for the sample with 0.96 PEGDE starting mass fraction, a low mass fraction of PEGDE remained in the hydrogel,

indicating that the covalent cross-linking had a low yield (see Table 6.1).

Table 6.1. Mass fraction value and sample identification for each synthesized hydrogel of CmCHT-PEG.

Initial mass fraction of PEGDE (X_{PEGDE})	Final mass fraction of PEGDE analyzed by TGA data	Sample Identification
0.72	0.21	**CmCHT-79**
0.75	0.11	**CmCHT-89**
0.94	0.42	**CmCHT-58**
0.96	0.95	**CmCHT-5**

The curing process in epoxy polymers is influenced by the treatment temperature and polymer concentration. In this synthesis, the temperature and polysaccharide concentrations were those specified in [255] to obtain hydrogels from carboxymethyl cellulose (CMC) and PEGDE. A higher yield of hydrogels was obtained than with CmCHT-PEG hydrogels. The main difference between CMC and CmCHT with respect to this cross-linking reaction is the reactive groups in the polymer backbone. While CmCHT have amine, hydroxyl and carboxylic reactive groups, CMC have hydroxyl and carboxylic groups. In basic media the amine group presents lower reactivity than the hydroxyl group [256 -257]. This behavior can be attributed to the N,O-carboxymethyl substitution of the CmCHT [107, 258]. The polymer does not have enough free hydroxyl groups to react with the PEGDE epoxy groups. It is also important to consider that a certain degree of liquid-liquid phase separation could happen.

6.4.2 ATR-FTIR

ATR-FTIR was used to analyze the structural composition of the hydrogels (see Figure 6.2), which were compared with pristine CmCHT [213] and the PEGDE [259] polymer. A variation between the O-H and

N-H stretching peaks appeared, due to the cross-linking between CmCHT and PEGDE. In the reaction new hydroxyl groups appear, due to the epoxy ring opening. This behavior can be observed in the 3200-3500 cm^{-1} range, in which a broader peak appears when the PEGDE content of the hydrogel is increased.

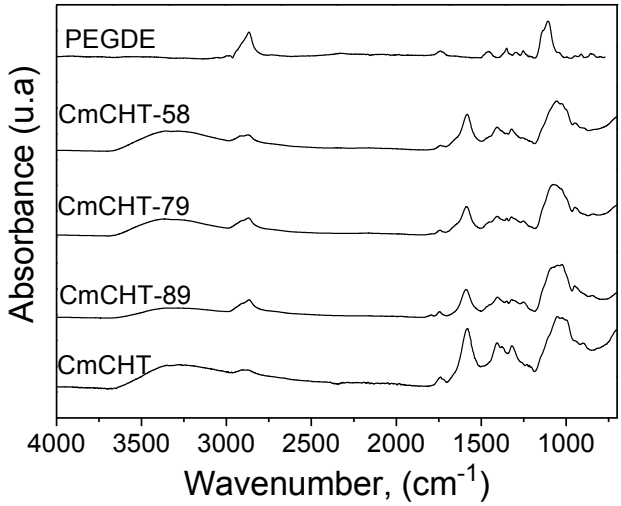

Figure 6.2. ATR-FTIR spectra from CmCHT -PEG hydrogels in the region between 4000 and 750 cm^{-1}.

The new amine bonding appears in the 1244-1246 cm^{-1} range because of the cross-linking due to the opening of the epoxy ring via amine from CmCHT. The cross-linking between the CmCHT hydroxyl groups and the epoxy group can also be observed by the signal that appears at 1036 cm^{-1} and also the broad peak that appears between 1173 and 868 cm^{-1}, attributed to ether cross-linking between hydroxyl and the epoxy ring. At 1741 cm^{-1}, corresponding to the –COOH group of the CmCHT polymer, there were no changes in the different hydrogel compositions, indicating that this group is not involved in the reaction [260].

6.4.3 Water content

The water content of each hydrogel composition was determined by immersing the samples in an excess of deionized water. Water content for the four different compositions as a function of the immersion time is shown in Figure 6.3.

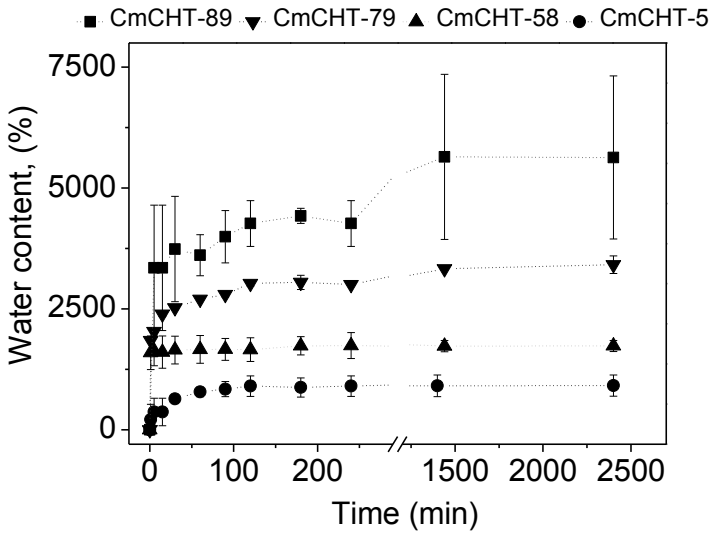

Figure 6.3. Water content curves for the CmCHT-PEG hydrogels with different compositions until reaching equilibrium.

All the hydrogels reached equilibrium before 180 min, except CmCHT-89, which took 300 min to do so. All the hydrogels presented very high water content as both components are hydrophilic polymers. Equilibrium water content was seen to increase as the PEGDE fraction decreased. The Statistical analysis indicates that there are significant differences between the EWC of CmCHT-89, CmCHT-79 and CmCHT-58, but no significant differences between the EWC of samples CmCHT-58 and CmCHT-5. The results revealed that despite having two hydrophilic polymers in the network, cross-linking density is an important factor in determining the water content of the samples. CmCHT-5 equilibrium water content was EWC=900 ± 200%, while the corresponding value for CmCHT-89 was as

high as EWC=5600 ± 1700% mg water with respect to the dry sample.

Repeated swelling-deswelling was carried out to assess the stability of the hydrogel structure. Figure 6.3 shows the two consecutive swelling-cycles of the CmCHT-79 sample in deionized water. This hydrogel composition contained a small amount of PEG blocks with high water content.

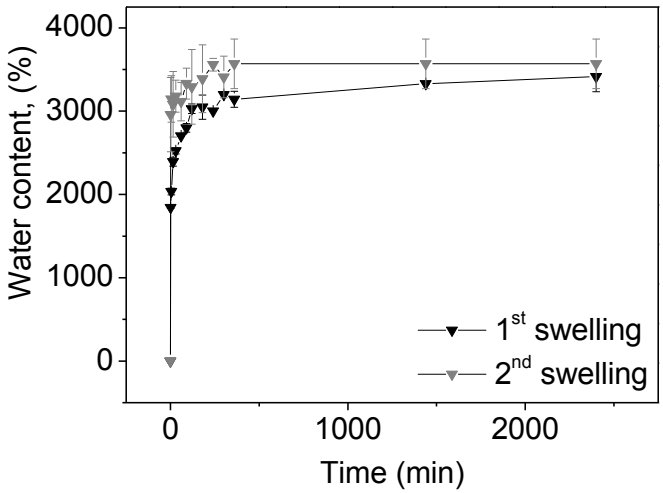

Figure 6.4. Water content curves of CmCHT-79 hydrogel after two consecutive swelling-drying cycles.

Equilibrium water content was EWC=3415 ± 181% after the first swelling and EWC=3569 ± 297% after the second. The samples maintained their shape and dimensions after both swelling cycles, showing that these processes are reversible.

6.4.4 Thermogravimetryc Analysis

The thermal stability of the new hydrogels was studied by TGA and their composition was calculated from the residue measured at 600 ºC. The thermal decomposition of CmCHT can be seen in Figure 6.5. The first

weight loss of around 13 wt%, between 30-190 ºC, is attributed to water loss. The main degradation step appears between 210–310 ºC and a broad shoulder appears around 317-490 ºC, which is more apparent in DTG curves (Figure 6.5b), where it is resolved as a peak with a maximum around Tmax=389 ºC. This could be ascribed to the thermal degradation of the polymer segments without carboxymethyl substitutions. The main peak in the thermal degradation of high DD chitosan CHT takes place between 200 ºC-500 ºC, indicating that the thermal degradation of the CmCHT polymer is less stable than that of chitosan [261]. At higher temperatures there is a peak between 680-766 ºC with a weight loss of around 11wt%. Miranda *et al.*, [261] observed similar behavior in thermal degradation of CmCHT with a peak around 602 ºC, which was attributed to the degradation of the residue produced during the previous thermal decomposition.

PEGDE shows a continuous weight loss at temperatures up to 300 ºC. The low molecular weight of the polymer can explain the loss of short volatile fragments, the main degradation step taking place between 325 and 425 ºC, roughly speaking. The degradation profile of CmCHT-5 is probably more representative of the PEG blocks of the copolymer network, since it has the chain connectivity of the network and the CmCHT content is low enough not to produce changes in the thermogram. In this network a single narrow weight step appears centered around 450 ºC.

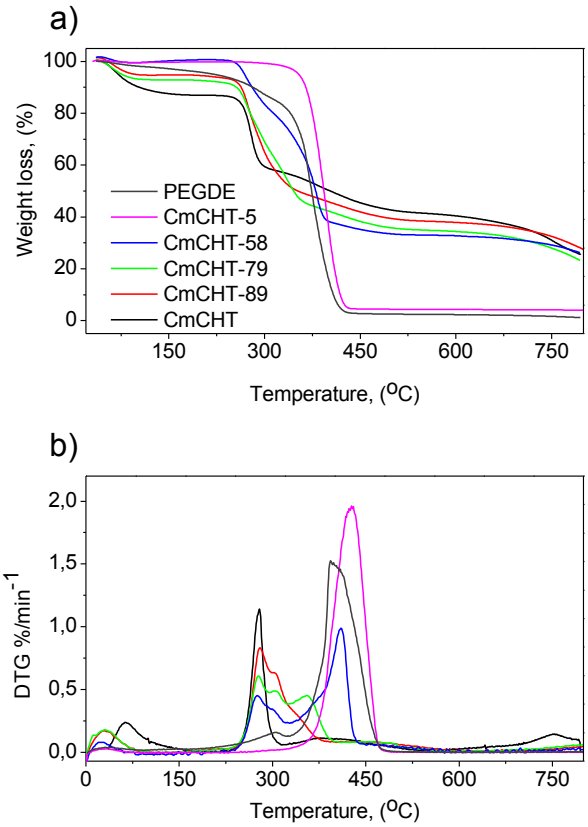

Figure 6.5.a) TGA and b) DTG curves of CmCHT-PEG hydrogels.

The thermal degradation profile of the hydrogels showed the characteristic peaks of pristine polymers. Nevertheless, a clear shift in the position of the PEG peak towards lower temperatures shows the integration of both components in a single network structure. The thermal degradation of the CmCHT-89 presents a Tonset=167 ºC until Tend=561 ºC. The broad peak indicated the interactions between polymer chains, where the thermal degradation temperature range matches with pristine polymers.

6.4.5 DSC

Hydrogel component miscibility was evaluated by DSC tests. CmCHT did not show either glass transition or a melting peak in the DSC

thermograms. On the other hand, PEGDE presented a broad melting peak in the normalized heat flow curve (Figure 6.6a) and an exothermal crystallization peak in the normalized cooling thermogram (Figure 6.6b), with peak temperature Tc=-44.01 ºC. CmCHT-PEG hydrogels did not present any melting or cooling peaks compared with pristine PEGDE. This indicates that the distribution of the polymer chains in the network was homogeneous and that phase separation did not take place in the block-copolymer network. Unlike pure PEGDE polymer, PEGDE chains cannot reorganize to form crystalline domains.

Glass transition was observed in pure PEGDE (Figure 6.6a), with glass transition temperature of Tg_{onset}=-71.10 ºC. CmCHT-5 had a higher glass transition temperature (Tg_{onset} =-46.82 ºC) than pristine PEGDE.

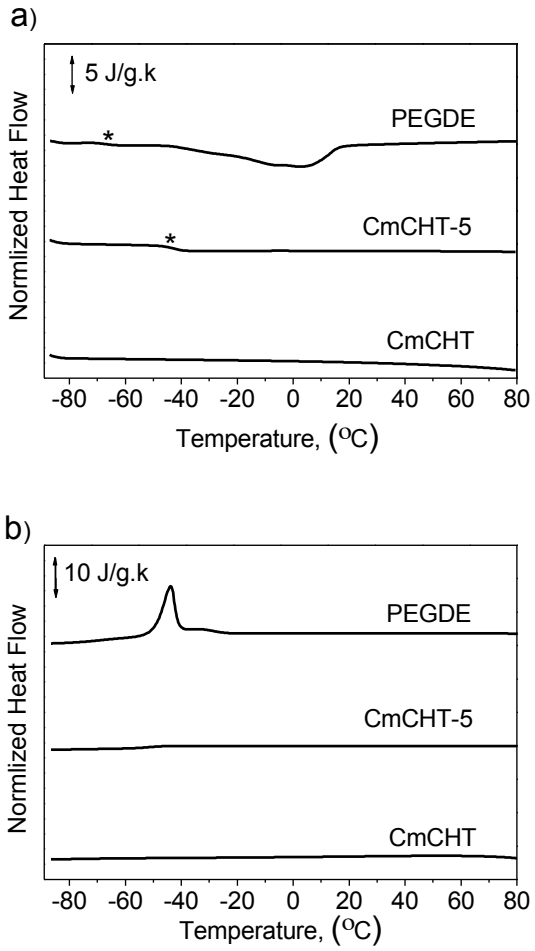

*Figure 6.6. Second a) heating and b) cooling DSC thermograms of the dry hydrogels. The symbol * indicates PEGDE* Tg_{onset}.

6.4.6 Rheological measurements

An oscillatory frequency sweep was carried out to determine the mechanical properties of the hydrogels. Measurement of the shear modulus (G´) was only possible for CmCHT-79 and CMCHT-58 because the rest of the samples were too fragile and disintegrated at the beginning of the test. The G´ values for both samples (see Figure 6.7a) demonstrated that the most cross-linked sample presented a higher storage modulus value (G´=27 ± 9 kPa for CmCHT-58 and G´=14 ± 8 kPa for CmCHT-79 at

1Hz). No noticeable changes were observed in G´ at all sweep frequencies for any sample. The values of the loss moduli (G´´) were lower than G´.

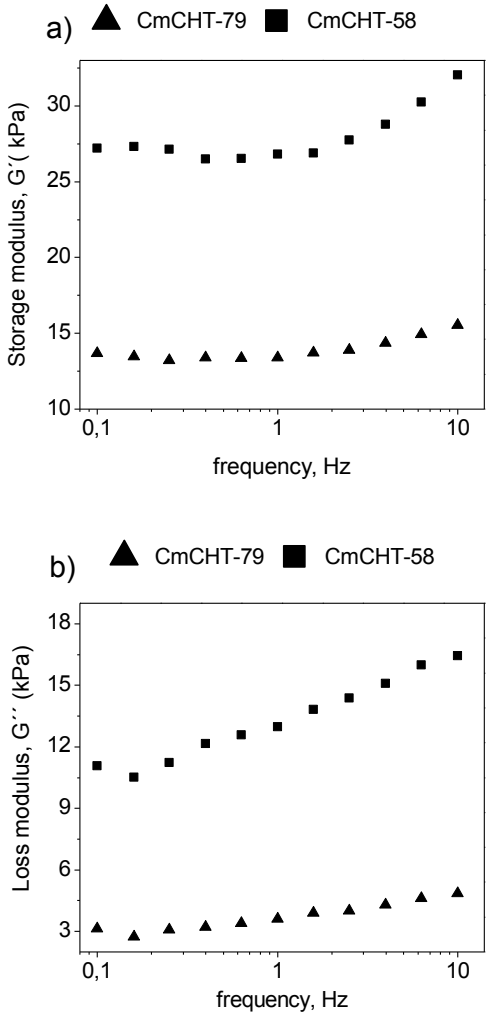

Figure 6.7. Evolution of a) storage modulus (G´) and b) loss moduli, (G´´) as a function of the frequency for hydrogels CmCHT-79 and CmCHT-58.

These results suggest that the hydrogels cross-linked with high PEGDE contents are elastic with low viscosity. This behavior was also observed in hydrogels formed by chitosan cross-linked with genipin, but in this case the difference between G´and G´´ is higher than in the CmCHT-PEG

hydrogels, with a ratio around 100-1000 times higher than G´ [262]. The values of G´ for the hydrogels are in the range of the values used in regeneration of cartilage tissues [263].

6.4.7 Morphology

Hydrogels samples were freeze dried from the swollen state to access the macroporous morphology by SEM. The cross-section of the samples presented an interconnected structure in all the hydrogels, (Figure 6.8).

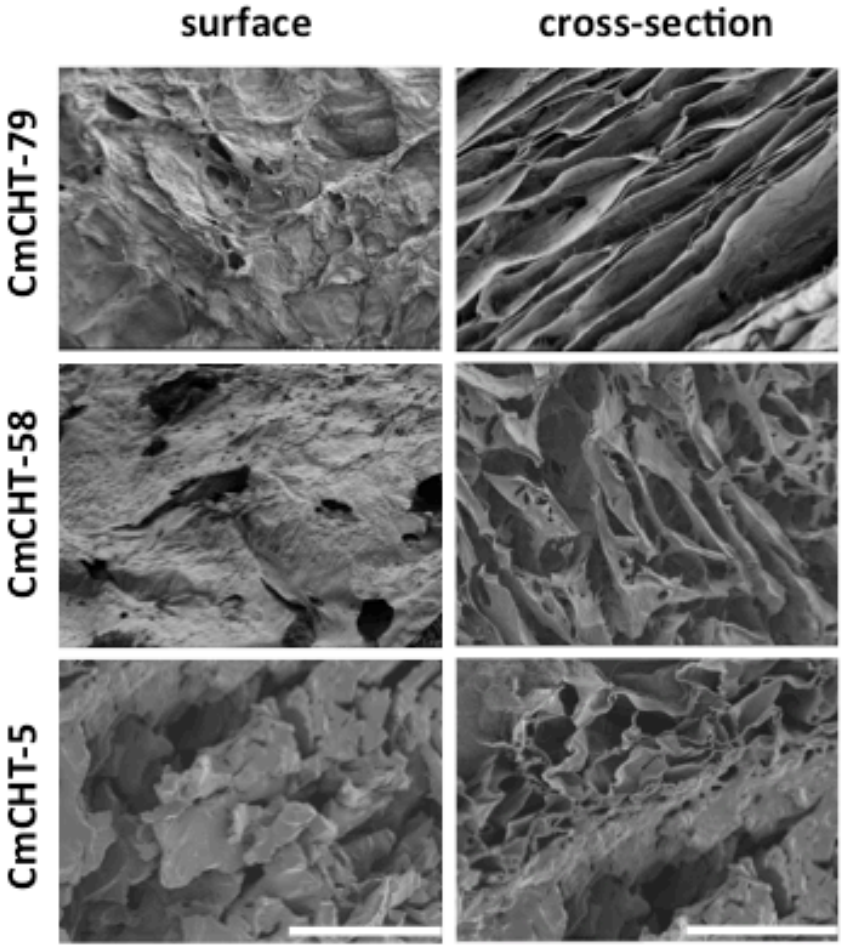

Figure 6.8. Surface and cross-section SEM micrographs of hydrogels with different compositions (100x magnification and scale bars represent 600μm).

CmCHT-79 presented a laminated structure with pore size around 160-70 μm. The CmCHT-58 hydrogel exhibited a more regular porous structure with a pore size distribution from 40 to 100 μm. It is worth noting that the sample with the highest cross-linking density had a smaller pore size than the sample with the lowest density. The surface of the samples was covered by a thin polymer layer (see Figure 6.8), indicating that some solvent had evaporated from the samples before freezing. This phenomenon has been observed in several honeycomb structures of chitosan hydrogels obtained by the freeze-drying method [264].

6.4.8 "In vitro" degradation of the hydrogels

The enzymatic degradation profile of the two extreme compositions (CmCHT-89 and CmCHT-5 hydrogels) was followed by immersing the samples in a PBS solution containing lysozyme. The remaining weight of the hydrogels was followed in the degradation process, Figure 6.9a and 6.9b. Weight loss in both hydrogels was quite small until day 59, when CmCHT-89 (Figure 6.9a) presented a remaining weight of 84 ± 2 % and CmCHT-5 (Figure 6.9b) was 90 ± 8%. In the case of CmCHT-89, the water content (Figure 6.9c) showed a considerable increase (239 ± 55 % at the beginning of degradation) showing that the cleavage of chitosan chains had reduced the effective average molecular weight between cross-links. Nevertheless, in the case of CmCHT-5 (Figure 6.9c) the increase in equilibrium water content is quite modest, around 3700% indicating less cleavage of the PEGDE chains during degradation. After 14 days of degradation the remaining weight was approximately constant for the rest of the time.

The evolution of the CmCHT mass fraction as a function of degradation time was calculated by TGA applying Eq (6.3). CmCHT-89 presented a

higher proportion of CmCHT degradation in the early stages, and the CmCHT fraction fell to 76% after 14 days degradation. The X_{CmCHT} value did not present any important subsequent changes, (Figures 6.9a and 6.9b). For CmCHT-5, no significant variations were observed in the mass fraction throughout degradation.

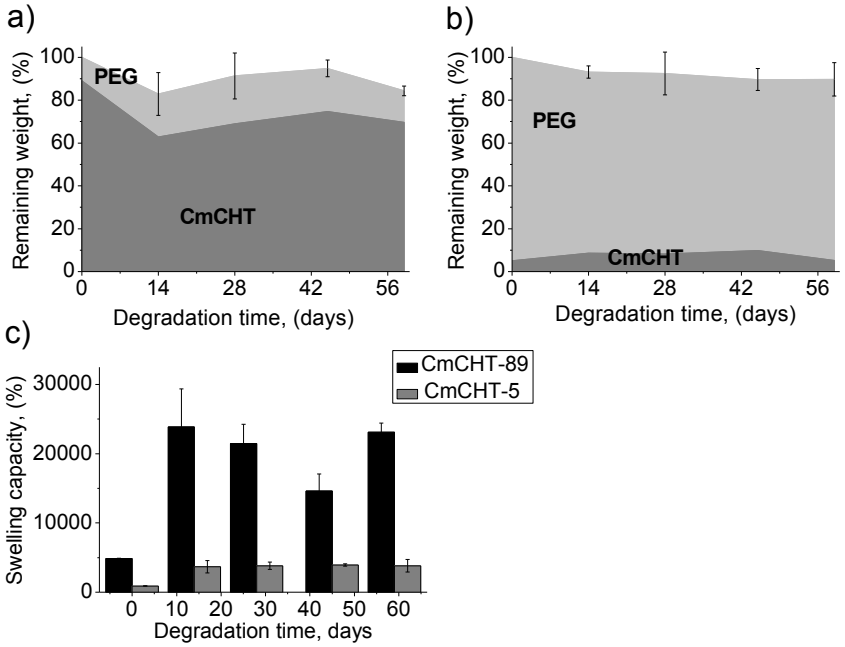

Figure 6.9. Evolution of X_{CmCHT} and X_{PEG} of the hydrogels in enzymatic degradation conditions for a) CmCHT-85, b) CmCHT-5 and c) swelling capacity of both samples.

6.5 Conclusions

Block-copolymer hydrogel networks were synthesized with a large water content capacity (up to 5000%) containing CmCHT and PEG blocks. The cross-linking reaction was seen to take place mainly between the PEGDE epoxy group and the amine and hydroxyl groups of the CmCHT polymers. Chemical cross-linking was confirmed by swelling studies and ATR-FTIR analysis. A double swelling-deswelling process confirmed the stability of

the hydrogels even at a low cross-linking density (CmCHT-79). The mass fraction calculated by the residue measured at 600 °C confirmed that a small fraction of PEGDE was incorporated into the network, which can be explained by a certain degree of immiscibility of the PEGDE and CmCHT in the reacting solution. The rheological measurements showed that these hydrogels had G´ values, ranging from 27 kPa to 14 kPa. The DSC results indicated that both polymers were homogenously distributed with no phase separation, as the PEGDE chains were not able to crystallize even in the sample with the highest PEGDE content (CmCHT-5).

The enzymatic degradation profile of the hydrogels showed a small weight loss in the networks until day 59 of degradation. The cleavage of the CmCHT blocks by lysozyme was detected by the increased water content of the gels for up to 28 days of degradation.

Chapter 7. Conclusions

In this thesis, a series of hydrogels based on chitosan and chitosan derivatives were obtained with tuneable kinetics degradation ranging from a few days to practically biostable. The new materials that are considered to have the most potential for development in tissue engineering applications are networks that combine chitosan or carboxymethyl chitosan with biodegradable polyester and polyether polymers acting as cross linkers. The main conclusions of physico-chemical characterization of chitosan and the synthesized networks can be summarize as follows:

1. Chitosan presented an increase in water content when DD was reduced from 85 to 45 %. This behaviour was explained by the inestability of the crystalline regions, acting as physical cross-linkers, in the presence of water.

2. The thermal stability of chitosans of varying DD was analyzed in dynamic TGA experiments. The activation energy values were obtained by applying "free model" methods such as Ozawa-Flynn-Wall and Kissinger. In all cases the activation energy of the high temperature stage was higher than that corresponding to lower temperatures. The kinetic parameters were used to check different kinetic models. The Sestak Bergreen model was able to fit the experimental thermograms with an activation energy that was in good agreement with the OFW method.

3. Chitosan membranes were obtained by electrospinning. The influence of electrospinning and the subsequent neutralization and cross-linking process were analyzed by thermal analysis. The results showed that the membranes neutralized with sodium hydroxide did not show any solvent traces, unlike the membranes neutralized with ethanol.

4. Chitosan and carboxymethyl chitosan copolymer networks were obtained by cross-linking with end-capped functionalized poly(ε-caprolactone) and with aldehyde groups and poly(ethylene glycol) diglicidyl ether. Although the previous functionalization of poly(ε-caprolactone) gave modest oxidation degrees, the networks presented enough cross-linking points to obtain stable networks.

5. The obtained networks behaved like hydrogels showing high equilibrium water content without dissolving. This behaviour was more pronounced in the networks obtained by hydrophilic polymers (CmCHT-PEG).

6. The carboxymethyl chitosan and poly(ε-caprolactone) networks (CmCHT-PCL) showed a faster kinetic degradation than the pure polymers in both hydrolytic and enzymatic conditions. This behaviour was explained by the hydrophilic domains being accessible to water molecules and, as a consequence, an increased kinetic degradation in the hydrophobic domains.

7. The biological studies of CmCHT-PCL's hydrogels with mesenchymal stem cells (MSCs) revealed that the cells presented cell viability and proliferated as the network was degrading. These hydrogels are suitable materials for tissue engineering applications such as cell delivery systems, which require short degradations times.

8. The biodegradable CHT-PCL's hydrogels are perfect candidates for regeneration of epithelial tissues, which require permeable substitutes whose kinetic degradation is matched with the regeneration of the neotissue.

9. CmCHT-PEG hydrogels presented a hiperporous structure with high water content. The kinetic degradation revealed that these hydrogels are apparently biostable, although the increase in the water content during degradation caused the scission of the polymer chains in the network. These hydrogels can be used as delivery systems in applications where low kinetic degradation is required.

Chapter 8. Bibliography

[1] R. Langer and J. P. Vacanti, "Article science", vol. 260, p. 14, 1993.

[2] F. J. O'Brien, "Biomaterials & scaffolds for tissue engineering," Materials Today, vol. 14, pp. 88-95, 2011.

[3] B. Chan and K. Leong, "Scaffolding in tissue engineering: general approaches and tissue-specific considerations," European spine journal, vol. 17, pp. 467-479, 2008.

[4] B. Dhandayuthapani, Y. Yoshida, T. Maekawa, and D. S. Kumar, "Polymeric scaffolds in tissue engineering application: a review," *International Journal of Polymer Science*, 2011.

[5] T. Dvir, B. P. Timko, D. S. Kohane, and R. Langer, "Nanotechnological strategies for engineering complex tissues," *Nat Nano*, vol. 6, pp. 13-22, 2011.

[6] F. P. W. Melchels, A. M. C. Barradas, C. A. van Blitterswijk, J. de Boer, J. Feijen, and D. W. Grijpma, "Effects of the architecture of tissue engineering scaffolds on cell seeding and culturing," *Acta Biomaterialia*, vol. 6, pp. 4208-4217, 2010.

[7] J. P. Stegemann, S. N. Kaszuba, and S. L. Rowe, "Review: advances in vascular tissue engineering using protein-based biomaterials," *Tissue engineering*, vol. 13, pp. 2601-2613, 2007.

[8] R. Jayakumar, M. Prabaharan, S. Nair, and H. Tamura, "Novel chitin and chitosan nanofibers in biomedical applications," *Biotechnology advances*, vol. 28, pp. 142-150, 2010.

[9] N. Zhu and X. Chen, *Biofabrication of tissue scaffolds*. Intech, 2013.

[10] B.-M. Min, S. W. Lee, J. N. Lim, Y. You, T. S. Lee, P. H. Kang, *et al.*, "Chitin and chitosan nanofibers: electrospinning of chitin and deacetylation of chitin nanofibers," *Polymer*, vol. 45, pp. 7137-7142, 2004.

[11] A. G. Mikos, G. Sarakinos, J. P. Vacanti, R. S. Langer, and L. G. Cima. (1996). "*Biocompatible polymer membranes and methods of preparation of three dimensional membrane structures*," *Patent No US5514378 A*. Massachusetts.

[12] M.-H. Ho, P.-Y. Kuo, H.-J. Hsieh, T.-Y. Hsien, L.-T. Hou, J.-Y. Lai, *et al.*, "Preparation of porous scaffolds by using freeze-extraction and freeze-gelation methods," *Biomaterials*, vol. 25, pp. 129-138, 2004.

[13] K. Whang, C. Thomas, K. Healy, and G. Nuber, "A novel method to fabricate bioabsorbable scaffolds," *Polymer*, vol. 36, pp. 837-842, 1995.

[14] C. X. F. Lam, X. Mo, S.-H. Teoh, and D. Hutmacher, "Scaffold development using 3D printing with a starch-based polymer," *Materials Science and Engineering: C*, vol. 20, pp. 49-56, 2002.

[15] Q. Hou, D. W. Grijpma, and J. Feijen, "Preparation of Porous Poly (ε-caprolactone) Structures," *Macromolecular rapid communications*, vol. 23, pp. 247-252, 2002.

[16] R. Zhang and P. X. Ma, "Porous poly (L-lactic acid)/apatite composites created by biomimetic process," 1999.

[17] A. Revzin, R. J. Russell, V. K. Yadavalli, W.-G. Koh, C. Deister, D. D. Hile, *et al.*, "Fabrication of poly (ethylene glycol) hydrogel microstructures using photolithography," *Langmuir*, vol. 17, pp. 5440-5447, 2001.

[18] S. K. Sarkar and B. T. Lee, "Hard tissue regeneration using bone substitutes: an update on innovations in materials," *The Korean journal of internal medicine*, vol. 30, pp. 279-293, 2015.

[19] F.-M. Chen and Y. Jin, "Periodontal tissue engineering and regeneration: current approaches and expanding opportunities," *Tissue Engineering Part B: Reviews*, vol. 16, pp. 219-255, 2010.

[20] E. A. Abou Neel, W. Chrzanowski, V. M. Salih, H.-W. Kim, and J. C. Knowles, "Tissue engineering in dentistry," *Journal of Dentistry*, vol. 42, pp. 915-928, 2014.

[21] W.-W. Yang and E. Pierstorff, "Reservoir-based polymer drug delivery systems," *Journal of laboratory automation*, vol. 17, pp. 50-58, 2012.

[22] Z. Cao, C. Dou, and S. Dong, "Scaffolding biomaterials for cartilage regeneration," *Journal of Nanomaterials*, p. 4, 2014.

[23] Z. Ge, C. Li, B. C. Heng, G. Cao, and Z. Yang, "Functional biomaterials for cartilage regeneration," *Journal of Biomedical Materials Research Part A*, vol. 100, pp. 2526-2536, 2012.

[24] J. S. Temenoff and A. G. Mikos, "Review: tissue engineering for regeneration of articular cartilage," *Biomaterials*, vol. 21, pp. 431-440, 2000.

[25] D. W. Hutmacher, "Scaffolds in tissue engineering bone and cartilage," *Biomaterials*, vol. 21, pp. 2529-2543, 2000.

[26] J. Mano, G. Silva, H. S. Azevedo, P. Malafaya, R. Sousa, S. Silva, *et al.*, "Natural origin biodegradable systems in tissue engineering and regenerative medicine: present status and some moving trends," *Journal of the Royal Society Interface*, vol. 4, pp. 999-1030, 2007.

[27] R. A. Muzzarelli, F. Greco, A. Busilacchi, V. Sollazzo, and A. Gigante, "Chitosan, hyaluronan and chondroitin sulfate in tissue engineering for cartilage regeneration: A review," *Carbohydrate Polymers*, vol. 89, pp. 723-739, 2012.

[28] M. M. Stevens, "Biomaterials for bone tissue engineering," *Materials today*, vol. 11, pp. 18-25, 2008.

[29] K. Whang, K. Healy, D. Elenz, E. Nam, D. Tsai, C. Thomas, *et al.*, "Engineering bone regeneration with bioabsorbable scaffolds with novel microarchitecture," *Tissue engineering*, vol. 5, pp. 35-51, 1999.

[30] Z. Sheikh, S. Najeeb, Z. Khurshid, V. Verma, H. Rashid, and M. Glogauer, "Biodegradable materials for bone repair and tissue engineering applications,"

Materials, vol. 8, pp. 5744-5794, 2015.

[31] R. Thomson, M. Wake, M. J. Yaszemski, and A. Mikos., (1995),"*Biodegradable polymer scaffolds to regenerate organs*" . Houston: Springer.

[32] S.-S. Kim, M. S. Park, O. Jeon, C. Y. Choi, and B.-S. Kim, "Poly (lactide-co-glycolide)/hydroxyapatite composite scaffolds for bone tissue engineering," *Biomaterials*, vol. 27, pp. 1399-1409, 2006.

[33] T. Shimizu, M. Yamato, Y. Isoi, T. Akutsu, T. Setomaru, K. Abe, *et al.*, "Fabrication of pulsatile cardiac tissue grafts using a novel 3-dimensional cell sheet manipulation technique and temperature-responsive cell culture surfaces," *Circulation research*, vol. 90, pp. e40-e48, 2002.

[34] Y. Liang, W. Liu, B. Han, C. Yang, Q. Ma, W. Zhao, *et al.*, "Fabrication and characters of a corneal endothelial cells scaffold based on chitosan," *Journal of Materials Science: Materials in Medicine*, vol. 22, pp. 175-183, 2011.

[35] U. Kriegebaum, M. Mildenberger, U. D. A. Mueller-Richter, U. Klammert, A. C. Kuebler, and T. Reuther, "Tissue engineering of human oral mucosa on different scaffolds: in vitro experiments as a basis for clinical applications," *Oral Surgery, Oral Medicine, Oral Pathology and Oral Radiology*, vol. 114, pp. S190-S198, 2012.

[36] X. Wang, P. Wu, X. Hu, C. You, R. Guo, H. Shi, *et al.*, "Polyurethane membrane/knitted mesh-reinforced collagen–chitosan bilayer dermal substitute for the repair of full-thickness skin defects via a two-step procedure," *Journal of the Mechanical Behavior of Biomedical Materials*, vol. 56, pp. 120-133, 2016.

[37] N. Nafee, M. Schneider, U. F. Schaefer, and C.-M. Lehr, "Relevance of the colloidal stability of chitosan/PLGA nanoparticles on their cytotoxicity profile," *International journal of pharmaceutics*, vol. 381, pp. 130-139, 2009.

[38] X. Li, K. Nan, S. Shi, and H. Chen, "Preparation and characterization of nano-hydroxyapatite/chitosan cross-linking composite membrane intended for tissue engineering," *International Journal of Biological Macromolecules*, vol. 50, pp. 43-49, 2012.

[39] B. Wang. (2007). *Environmental biodegradation research focus*: Nova Publishers.

[40] H. Homayoni, S. A. H. Ravandi, and M. Valizadeh, "Electrospinning of chitosan nanofibers: Processing optimization," *Carbohydrate Polymers*, vol. 77, pp. 656-661, 2009.

[41] E. P. De Azevedo, "Chitosan hydrogels for drug delivery and tissue engineering applications," *International Journal of Pharmacy and Pharmaceutical Sciences*, vol. 7, 2015.

[42] A. Kaur and G. Kaur, "Mucoadhesive buccal patches based on interpolymer complexes of chitosan–pectin for delivery of carvedilol," *Saudi Pharmaceutical Journal*, vol. 20, pp. 21-27, 2012.

[43] H.-Q. Mao, K. Roy, V. L. Troung-Le, K. A. Janes, K. Y. Lin, Y. Wang, *et al.*, "Chitosan-DNA nanoparticles as gene carriers: synthesis, characterization and transfection efficiency," *Journal of Controlled Release*, vol. 70, pp. 399-421, 2001.

[44] L. Qi, Z. Xu, X. Jiang, C. Hu, and X. Zou, "Preparation and antibacterial activity of chitosan nanoparticles," *Carbohydrate Research*, vol. 339, pp. 2693-2700, 2004.

[45] D. M. García Cruz, J. L. Escobar Ivirico, M. M. Gomes, J. L. Gómez Ribelles, M. S. Sánchez, R. L. Reis, *et al.*, "Chitosan microparticles as injectable scaffolds for tissue engineering," *Journal of Tissue Engineering and Regenerative Medicine*, vol. 2, pp. 378-380, 2008.

[46] C. K. S. Pillai, W. Paul, and C. P. Sharma, "Chitin and chitosan polymers: Chemistry, solubility and fiber formation," *Progress in Polymer Science*, vol. 34, pp. 641-678, 2009.

[47] Q. Yang, F. Dou, B. Liang, and Q. Shen, "Studies of cross-linking reaction on chitosan fiber with glyoxal," *Carbohydrate Polymers*, vol. 59, pp. 205-210, 2005.

[48] V. M. Ramos, N. M. Rodríguez, I. Henning, M. F. Díaz, M. P. Monachesi, M. S. Rodríguez, *et al.*, "Poly(ethylene glycol)-crosslinked N-methylene phosphonic chitosan. Preparation and characterization," *Carbohydrate Polymers*, vol. 64, pp. 328-336, 2006.

[49] R. J. Verheul, S. van der Wal, and W. E. Hennink, "Tailorable Thiolated Trimethyl Chitosans for Covalently Stabilized Nanoparticles," *Biomacromolecules*, vol. 11, pp. 1965-1971, 2010.

[50] M. Fan, Z. Zhang, J. Mao, and H. Tan, "Injectable Multi-Arm Poly (ethylene glycol)/Hyaluronic Acid Hydrogels for Adipose Tissue Engineering," *Journal of Macromolecular Science, Part A*, vol. 52, pp. 345-352, 2015.

[51] C. Santos, P. Seabra, B. Veleirinho, I. Delgadillo, and J. L. da Silva, "Acetylation and molecular mass effects on barrier and mechanical properties of shortfin squid chitosan membranes," *European Polymer Journal*, vol. 42, pp. 3277-3285, 2006.

[52] A. Baxter, M. Dillon, K. D. Anthony Taylor, and G. A. F. Roberts, "Improved method for i.r. determination of the degree of N-acetylation of chitosan," *International Journal of Biological Macromolecules*, vol. 14, pp. 166-169, 1992.

[53] N. Kubota, N. Tatsumoto, T. Sano, and K. Toya, "A simple preparation of half N-acetylated chitosan highly soluble in water and aqueous organic solvents," *Carbohydrate Research*, vol. 324, pp. 268-274, 2000.

[54] X. Kong, "Simultaneous determination of degree of deacetylation, degree of substitution and distribution fraction of –COONa in carboxymethyl chitosan by potentiometric titration," *Carbohydrate polymers*, vol. 88, pp. 336-341, 2012.

[55] J. Du and Y.-L. Hsieh, "Nanofibrous membranes from aqueous electrospinning of carboxymethyl chitosan," *Nanotechnology*, vol. 19, p. 125-707, 2008.

[56] T. Xu, M. Xin, M. Li, H. Huang, S. Zhou, and J. Liu, "Synthesis, characterization, and antibacterial activity of N, O-quaternary ammonium chitosan," *Carbohydrate research*, vol. 346, pp. 2445-2450, 2011.

[57] A. Domard, M. Rinaudo, and C. Terrassin, "New method for the quaternization of chitosan," *International Journal of Biological Macromolecules*, vol. 8, pp. 105-107, 1986.

[58] J. Z. Knaul, S. M. Hudson, and K. A. Creber, "Crosslinking of chitosan fibers with dialdehydes: Proposal of a new reaction mechanism," *Journal of Polymer Science Part B: Polymer Physics*, vol. 37, pp. 1079-1094, 1999.

[59] M. Beppu, R. Vieira, C. Aimoli, and C. Santana, "Crosslinking of chitosan membranes using glutaraldehyde: Effect on ion permeability and water absorption," *Journal of membrane science*, vol. 301, pp. 126-130, 2007.

[60] J. D. Schiffman and C. L. Schauer, "Cross-linking chitosan nanofibers," *Biomacromolecules*, vol. 8, pp. 594-601, 2007.

[61] L. Ma, C. Gao, Z. Mao, J. Zhou, J. Shen, X. Hu, *et al.*, "Collagen/chitosan porous scaffolds with improved biostability for skin tissue engineering," *Biomaterials*, vol. 24, pp. 4833-4841, 2003.

[62] R. A. Muzzarelli, "Genipin-crosslinked chitosan hydrogels as biomedical and pharmaceutical aids," *Carbohydrate Polymers*, vol. 77, pp. 1-9, 2009.

[63] F. L. Mi, H. W. Sung, and S. S. Shyu, "Synthesis and characterization of a novel chitosan-based network prepared using naturally occurring crosslinker," *Journal of Polymer Science Part A: Polymer Chemistry*, vol. 38, pp. 2804-2814, 2000.

[64] F.-L. Mi, H.-W. Sung, S.-S. Shyu, C.-C. Su, and C.-K. Peng, "Synthesis and characterization of biodegradable TPP/genipin co-crosslinked chitosan gel beads," *Polymer*, vol. 44, pp. 6521-6530, 2003.

[65] D. R. Bhumkar and V. B. Pokharkar, "Studies on effect of pH on cross-linking of chitosan with sodium tripolyphosphate: a technical note," *AAPS Pharmscitech*, vol. 7, pp. E138-E143, 2006.

[66] S. H. Lee, S. Y. Park, and J. H. Choi, "Fiber formation and physical properties of chitosan fiber crosslinked by epichlorohydrin in a wet spinning system: the effect of the concentration of the crosslinking agent epichlorohydrin," *Journal of applied polymer science*, vol. 92, pp. 2054-2062, 2004.

[67] S. K. Choudhari, A. A. Kittur, S. S. Kulkarni, and M. Y. Kariduraganavar, "Development of novel blocked diisocyanate crosslinked chitosan membranes for pervaporation separation of water–isopropanol mixtures," *Journal of Membrane Science*, vol. 302, pp. 197-206, 2007.

[68] T. Tojima, H. Katsura, M. Nishiki, N. Nishi, S. Tokura, and N. Sakairi, "Chitosan beads with pendant α-cyclodextrin: preparation and inclusion property to nitrophenolates," *Carbohydrate Polymers*, vol. 40, pp. 17-22, 1999.

[69] T. K. Giri, A. Thakur, A. Alexander, Ajazuddin, H. Badwaik, and D. K. Tripathi, "Modified chitosan hydrogels as drug delivery and tissue engineering systems: present status and applications," *Acta Pharmaceutica Sinica B*, vol. 2, pp. 439-449, 2012.

[70] Y. Lee and W. Chen, "Synthesis and characterization of novel crosslinked PEG-graft-chitosan/hyaluronic acid hydrogel," in *Bioengineering Conference,. IEEE 33rd Annual Northeast*pp. 251-252, 2007.

[71] D. M. G. Cruz, D. F. Coutinho, J. F. Mano, J. L. G. Ribelles, and M. S. Sanchez, "Physical interactions in macroporous scaffolds based on poly (ε-caprolactone)/chitosan semi-interpenetrating polymer networks," *Polymer*, vol. 50, pp. 2058-2064, 2009.

[72] D. M. García Cruz, J. L. Gomez Ribelles, and M. Salmerón Sánchez, "Blending polysaccharides with biodegradable polymers. I. Properties of chitosan/polycaprolactone blends," *Journal of Biomedical Materials Research Part B: Applied Biomaterials*, vol. 85, pp. 303-313, 2008.

[73] J. Kumirska, M. Czerwicka, Z. Kaczynski, A. Bychowska, K. Brzozowski, J. Thoming, *et al.*, "Application of Spectroscopic Methods for Structural Analysis of Chitin and Chitosan," *Marine Drugs*, vol. 8, pp. 1567-1636, 2010.

[74] P. Baldrick, "The safety of chitosan as a pharmaceutical excipient," *Regulatory Toxicology and Pharmacology*, vol. 56, pp. 290-299, 2010.

[75] M. Lavertu, Z. Xia, A. N. Serreqi, M. Berrada, A. Rodrigues, D. Wang, *et al.*, "A validated 1H NMR method for the determination of the degree of deacetylation of chitosan," *Journal of Pharmaceutical and Biomedical Analysis*, vol. 32, pp. 1149-1158, 2003.

[76] W. Wang, S. Bo, S. Li, and W. Qin, "Determination of the Mark-Houwink equation for chitosans with different degrees of deacetylation," *International Journal of Biological Macromolecules*, vol. 13, pp. 281-285, 1991.

[77] K. M. Kim, J. H. Son, S.-K. Kim, C. L. Weller, and M. A. Hanna, "Properties of Chitosan Films as a Function of pH and Solvent Type," *Journal of Food Science*, vol. 71, pp. E119-E124, 2006.

[78] C. Kyung-Hee and K. P. Kwang-hee, "Acid-Base Equilibria and Related Properites of Chitosan," *Bulletin of the Korean Chemical Society*, vol. 4, pp. 68-72, 1983.

[79] H. Sashiwa and Y. Shigemasa, "Chemical modification of chitin and chitosan 2: preparation and water soluble property of N-acylated or N-alkylated partially deacetylated chitins," *Carbohydrate Polymers*, vol. 39, pp. 127-138, 1999.

[80] M. Rinaudo, "Chitin and chitosan: properties and applications," *Progress in polymer science*, vol. 31, pp. 603-632, 2006.

[81] R. J. Samuels, "Solid state characterization of the structure of chitosan films," *Journal of Polymer Science: Polymer Physics Edition*, vol. 19, pp. 1081-1105, 1981.

[82] M. Jaworska, K. Sakurai, P. Gaudon, and E. Guibal, "Influence of chitosan characteristics on polymer properties. I: Crystallographic properties," *Polymer International*, vol. 52, pp. 198-205, 2003.

[83] Y. Zhang, C. Xue, Y. Xue, R. Gao, and X. Zhang, "Determination of the degree of deacetylation of chitin and chitosan by X-ray powder diffraction," *Carbohydrate Research*, vol. 340, pp. 1914-1917, 2005.

[84] M. A. Kobaisi, P. Murugaraj, and D. E. Mainwaring, "Origin and influence of water-induced chain relaxation phenomena in chitosan biopolymers," *Journal of Polymer Science Part B: Polymer Physics*, vol. 50, pp. 403-414, 2012.

[85] M. Gámiz-González, A. Piskin, C. Pandis, C. Chatzimanolis-Moustakas, A. Kyritsis, B. Marí, *et al.*, "Determining the influence of N-acetylation on water sorption in chitosan films," *Carbohydrate polymers*, vol. 133, pp. 110-116, 2015.

[86] S.-H. Lim and S. M. Hudson, "Review of chitosan and its derivatives as antimicrobial agents and their uses as textile chemicals," *Journal of Macromolecular Science, Part C: Polymer Reviews*, vol. 43, pp. 223-269, 2003.

[87] I. K. Park and Y. H. Park, "Preparation and structural characterization of water-soluble O-hydroxypropyl chitin derivatives," *Journal of applied polymer science*, vol. 80, pp. 2624-2632, 2001.

[88] M. D. Buschmann, A. Merzouki, M. Lavertu, M. Thibault, M. Jean, and V. Darras, "Chitosans for delivery of nucleic acids," *Advanced drug delivery reviews*, vol. 65, pp. 1234-1270, 2013.

[89] N. A. Peppas, R. M. Ottenbrite, K. Park, and T. Okano.(2010) *Biomedical applications of hydrogels handbook*.New York: Springer Science & Business Media.

[90] B. D. Mather, K. Viswanathan, K. M. Miller, and T. E. Long, "Michael addition reactions in macromolecular design for emerging technologies," *Progress in Polymer Science*, vol. 31, pp. 487-531, 2006.

[91] G. Ma, D. Yang, Y. Zhou, M. Xiao, J. F. Kennedy, and J. Nie, "Preparation and characterization of water-soluble N-alkylated chitosan," *Carbohydrate Polymers*, vol. 74, pp. 121-126, 2008.

[92] Y. A. Skorik, A. V. Pestov, M. I. Kodess, and Y. G. Yatluk, "Carboxyalkylation of chitosan in the gel state," *Carbohydrate Polymers*, vol. 90, pp. 1176-1181, 2012.

[93] M. Jiang, K. Wang, J. F. Kennedy, J. Nie, Q. Yu, and G. Ma, "Preparation and characterization of water-soluble chitosan derivative by Michael addition reaction," *International Journal of Biological Macromolecules*, vol. 47, pp. 696-699, 2010.

[94] K. Yao, J. Li, F. Yao, and Y. Yin. (2011).*Chitosan-based hydrogels: functions and applications*. [Online]. Retrieved 8 March, 2016, from: http://www.crcnetbase.com/isbn/9781439821152.

[95] W. Sajomsang, S. Tantayanon, V. Tangpasuthadol, M. Thatte, and W. H. Daly, "Synthesis and characterization of N-aryl chitosan derivatives," *International Journal of Biological Macromolecules*, vol. 43, pp. 79-87, 2008.

[96] S. Yamada, S. Yaguchi, and K. Matsuda, "N-Acylation of amides with acid anhydrides by way of dual activation using $MgBr_2 \square OEt_2$," *Tetrahedron Letters*, vol. 43, pp. 647-651, 2002.

[97] S. Hirano, Y. Ohe, and H. Ono, "Selective N-acylation of chitosan," *Carbohydrate*

Research, vol. 47, pp. 315-320, 1976.

[98] V. K. Mourya and N. N. Inamdar, "Chitosan-modifications and applications: Opportunities galore," *Reactive and Functional Polymers*, vol. 68, pp. 1013-1051, 2008.

[99] W. Sajomsang, "Synthetic methods and applications of chitosan containing pyridylmethyl moiety and its quaternized derivatives: A review," *Carbohydrate Polymers*, vol. 80, pp. 631-647, 2010.

[100] K. Kurita, T. Kojima, Y. Nishiyama, and M. Shimojoh, "Synthesis and some properties of nonnatural amino polysaccharides: branched chitin and chitosan," *Macromolecules*, vol. 33, pp. 4711-4716, 2000.

[101] R. F. Borch, "Reductive Amination with Sodium Cyanoborohydride: N, N-Dimethylcyclohexylamine," *Organic Syntheses*, pp. 124-124, 1972.

[102] C. H. Kim, J. W. Choi, H. J. Chun, and K. S. Choi, "Synthesis of chitosan derivatives with quaternary ammonium salt and their antibacterial activity," *Polymer Bulletin*, vol. 38, pp. 387-393, 1997.

[103] H. Tan, R. Ma, C. Lin, Z. Liu, and T. Tang, "Quaternized chitosan as an antimicrobial agent: antimicrobial activity, mechanism of action and biomedical applications in orthopedics," *International journal of molecular sciences*, vol. 14, pp. 1854-1869, 2013.

[104] K. Kurita, Y. Koyama, S.-i. Nishimura, and M. Kamiya, "Facile preparation of water-soluble chitin from chitosan," *Chemistry letters*, pp. 1597-1598, 1989.

[105] F. Feng, Y. Liu, B. Zhao, and K. Hu, "Characterization of half N-acetylated chitosan powders and films," *Procedia Engineering*, vol. 27, pp. 718-732, 2012.

[106] R. A. Muzzarelli, C. Jeuniaux, and G. W. Gooday, "Chitin in nature and technology," in *International Conference on Chitin and Chitosan 1985: Senigallia, Italy)*, 1986.

[107] V. Mourya, N. N. Inamdar, and A. Tiwari, "Carboxymethyl chitosan and its applications," *Adv Mat Lett*, vol. 1, pp. 11-33, 2010.

[108] F. R. de Abreu and S. P. Campana-Filho, "Characteristics and properties of carboxymethylchitosan," *Carbohydrate Polymers*, vol. 75, pp. 214-221, 2009.

[109] R. Muzzarelli and C. Muzzarelli, "Chitosan chemistry: relevance to the biomedical sciences," in *Polysaccharides I*, ed: Springer, 2005, pp. 151-209.

[110] R. Jayakumar, M. Prabaharan, S. Nair, S. Tokura, H. Tamura, and N. Selvamurugan, "Novel carboxymethyl derivatives of chitin and chitosan materials and their biomedical applications," *Progress in Materials Science*, vol. 55, pp. 675-709, 2010.

[111] R. A. Muzzarelli, P. Ilari, and M. Petrarulo, "Solubility and structure of N-carboxymethylchitosan," *International journal of biological macromolecules*, vol. 16, pp. 177-180, 1994.

[112] N. Peppas. (1986). "Hydrogels in Medicine and Pharmacy, Fundamentals, preparation method and structure of hydrogels, Florida: Boca Raton: CRS Press.

[113] J. Berger, M. Reist, J. M. Mayer, O. Felt, and R. Gurny, "Structure and interactions in chitosan hydrogels formed by complexation or aggregation for biomedical applications," *European Journal of Pharmaceutics and Biopharmaceutics*, vol. 57, pp. 35-52, 2004.

[114] F. L. Mi, S. S. Shyu, S. T. Lee, and T. B. Wong, "Kinetic study of chitosan-tripolyphosphate complex reaction and acid-resistive properties of the chitosan-tripolyphosphate gel beads prepared by in-liquid curing method," *Journal of Polymer Science Part B: Polymer Physics*, vol. 37, pp. 1551-1564, 1999.

[115] J. H. Hamman, "Chitosan based polyelectrolyte complexes as potential carrier materials in drug delivery systems," *Marine drugs*, vol. 8, pp. 1305-1322, 2010.

[116] T. Ramasamy, T. H. Tran, H. J. Cho, J. H. Kim, Y. I. Kim, J. Y. Jeon, *et al.*, "Chitosan-based polyelectrolyte complexes as potential nanoparticulate carriers: physicochemical and biological characterization," *Pharmaceutical research*, vol. 31, pp. 1302-1314, 2014.

[117] I. Migneault, C. Dartiguenave, M. J. Bertrand, and K. C. Waldron, "Glutaraldehyde: behavior in aqueous solution, reaction with proteins, and application to enzyme crosslinking," *Biotechniques*, vol. 37, pp. 790-806, 2004.

[118] F.-L. Mi, Y.-C. Tan, H.-C. Liang, R.-N. Huang, and H.-W. Sung, "In vitro evaluation of a chitosan membrane cross-linked with genipin," *Journal of Biomaterials Science, Polymer Edition*, vol. 12, pp. 835-850, 2001.

[119] M. Sahin, N. Kocak, G. Arslan, and H. I. Ucan, "Synthesis of crosslinked chitosan with epichlorohydrin possessing two novel polymeric ligands and its use in metal removal," *Journal of Inorganic and Organometallic Polymers and Materials*, vol. 21, pp. 69-80, 2011.

[120] Y. Hong, Z. Mao, H. Wang, C. Gao, and J. Shen, "Covalently crosslinked chitosan hydrogel formed at neutral pH and body temperature," *Journal of Biomedical Materials Research Part A*, vol. 79, pp. 913-922, 2006.

[121] J. Zhu and R. E. Marchant, "Design properties of hydrogel tissue-engineering scaffolds," *Expert review of medical devices*, vol. 8, pp. 607-626, 2011.

[122] N. Briz, C. Antolinos-Turpin, J. Alió, N. Garagorri, J. Ribelles, and J. Gómez-Tejedor, "Fibronectin fixation on poly (ethyl acrylate)–based copolymers," *Journal of Biomedical Materials Research Part B: Applied Biomaterials*, vol. 101, pp. 991-997, 2013.

[123] A. J. Campillo-Fernández, R. E. Unger, K. Peters, S. Halstenberg, M. Santos, M. S. Sánchez, *et al.*, "Analysis of the biological response of endothelial and fibroblast cells cultured on synthetic scaffolds with various hydrophilic/hydrophobic ratios: influence of fibronectin adsorption and conformation," *Tissue Engineering Part A*, vol. 15, pp. 1331-1341, 2008.

[124] G. G. Ferrer, M. S. Sánchez, J. G. Ribelles, F. R. Colomer, and M. M. Pradas, "Nanodomains in a hydrophilic–hydrophobic IPN based on poly (2-hydroxyethyl acrylate) and poly (ethyl acrylate)," *European polymer journal*, vol. 43, pp. 3136-3145, 2007.

[125] J. Ivirico, M. Salmerón-Sánchez, J. Ribelles, M. M. Pradas, J. M. Soria, M. E. Gomes, *et al.*, "Proliferation and differentiation of goat bone marrow stromal cells in 3D scaffolds with tunable hydrophilicity," *Journal of Biomedical Materials Research Part B: Applied Biomaterials*, vol. 91, pp. 277-286, 2009.

[126] M. Sasatsu, H. Onishi, and Y. Machida, "Preparation of a PLA–PEG block copolymer using a PLA derivative with a formyl terminal group and its application to nanoparticulate formulation," *International journal of pharmaceutics*, vol. 294, pp. 233-245, 2005.

[127] H. Zhao, Z. Liu, S.-H. Park, S.-H. Kim, J.-H. Kim, and L. Piao, "Preparation and characterization of PEG/PLA multiblock and triblock copolymer," *Bulletin of the Korean Chemical Society*, vol. 33, pp. 1638-1642, 2012.

[128] L. Li, N. Wang, X. Jin, R. Deng, S. Nie, L. Sun, *et al.*, "Biodegradable and injectable in situ cross-linking chitosan-hyaluronic acid based hydrogels for postoperative adhesion prevention," *Biomaterials*, vol. 35, pp. 3903-3917, 2014.

[129] H. Sashiwa, N. Yamamori, Y. Ichinose, J. Sunamoto, and S.-i. Aiba, "Michael reaction of chitosan with various acryl reagents in water," *Biomacromolecules*, vol. 4, pp. 1250-1254, 2003.

[130] K. L. B. Chang, M.-C. Tai, and F.-H. Cheng, "Kinetics and products of the degradation of chitosan by hydrogen peroxide," *Journal of Agricultural and Food Chemistry*, vol. 49, pp. 4845-4851, 2001.

[131] Z. Ma, Y. Wu, Y. He, and T. Wu, "A novel protocol for the oxidative degradation of chitosan with hydrogen peroxide catalyzed by peroxomolybdate in aqueous solution," Royal Society Chemistry*Advance.*, vol. 3, pp. 12049-12051, 2013.

[132] M. Nampally, M. G. Rajulu, D. Gillet, T. Suryanarayanan, and B. B. Moerschbacher, "A High Diversity in Chitinolytic and Chitosanolytic Species and Enzymes and Their Oligomeric Products Exist in Soil with a History of Chitin and Chitosan Exposure," *BioMed research international*, vol. 10, p. 1-8, 2015.

[133] H. Zhang and S. H. Neau, "In vitro degradation of chitosan by a commercial enzyme preparation: effect of molecular weight and degree of deacetylation," *Biomaterials*, vol. 22, pp. 1653-1658, 2001.

[134] D. Ren, H. Yi, W. Wang, and X. Ma, "The enzymatic degradation and swelling properties of chitosan matrices with different degrees of N-acetylation," *Carbohydrate Research*, vol. 340, pp. 2403-2410, 2005.

[135] T. Freier, H. S. Koh, K. Kazazian, and M. S. Shoichet, "Controlling cell adhesion and degradation of chitosan films by N-acetylation," *Biomaterials*, vol. 26, pp. 5872-

5878, 2005.

[136] R. J. Nordtveit, K. M. Vårum, and O. Smidsrød, "Degradation of partially N-acetylated chitosans with hen egg white and human lysozyme," *Carbohydrate Polymers*, vol. 29, pp. 163-167, 1996.

[137] S. Pangburn, P. Trescony, and J. Heller, "Lysozyme degradation of partially deacetylated chitin, its films and hydrogels," *Biomaterials*, vol. 3, pp. 105-108, 1982.

[138] N. Bhattarai, J. Gunn, and M. Zhang, "Chitosan-based hydrogels for controlled, localized drug delivery," *Advanced Drug Delivery Reviews*, vol. 62, pp. 83-99, 2010.

[139] M. Dash, F. Chiellini, R. Ottenbrite, and E. Chiellini, "Chitosan—A versatile semi-synthetic polymer in biomedical applications," *Progress in polymer science*, vol. 36, pp. 981-1014, 2011.

[140] J. Kumirska, M. X. Weinhold, J. Thöming, and P. Stepnowski, "Biomedical Activity of Chitin/Chitosan Based Materials—Influence of Physicochemical Properties Apart from Molecular Weight and Degree of N-Acetylation," *Polymers*, vol. 3, pp. 1875-1901, 2011.

[141] M. Mucha and A. Pawlak, "Thermal analysis of chitosan and its blends," *Thermochimica Acta*, vol. 427, pp. 69-76, 2005.

[142] J. F. Mano, "Viscoelastic Properties of Chitosan with Different Hydration Degrees as Studied by Dynamic Mechanical Analysis," *Macromolecular Bioscience*, vol. 8, pp. 69-76, 2008.

[143] S. Ludwiczak and M. Mucha, "Modeling of water sorption isotherms of chitosan blends," *Carbohydrate Polymers*, vol. 79, pp. 34-39, 1/5/ 2010.

[144] M. T. Viciosa, M. Dionísio, and J. F. Mano, "Dielectric characterization of neutralized and nonneutralized chitosan upon drying," *Biopolymers*, vol. 81, pp. 149-159, 2006.

[145] E. Fernandez-Megia, R. Novoa-Carballal, E. Quiñoá, and R. Riguera, "Optimal routine conditions for the determination of the degree of acetylation of chitosan by 1H-NMR," *Carbohydrate Polymers*, vol. 61, pp. 155-161, 2005.

[146] L. Chen, Y. Du, Z. Tian, and L. Sun, "Effect of the degree of deacetylation and the substitution of carboxymethyl chitosan on its aggregation behavior," *Journal of Polymer Science Part B: Polymer Physics*, vol. 43, pp. 296-305, 2005.

[147] S. Bagheri-Khoulenjani, S. M. Taghizadeh, and H. Mirzadeh, "An investigation on the short-term biodegradability of chitosan with various molecular weights and degrees of deacetylation," *Carbohydrate Polymers*, vol. 78, pp. 773-778, 2009.

[148] B. Erman and J. E. Mark. (1997). *Structures and properties of rubberlike networks*: New York:Oxford University Press.

[149] P. J. Flory, "Network Structure and the Elastic Properties of Vulcanized Rubber," *Chemical reviews*, vol. 35, pp. 51-75, 1944.

[150] S. Brunauer, L. S. Deming, W. E. Deming, and E. Teller, "On a Theory of the van der Waals Adsorption of Gases," *Journal of the American Chemical Society*, vol. 62, pp. 1723-1732, 1940.

[151] B. George L, "Clustering of Water in Polymers," *American Chemical Society* vol. 127, pp. 441-450,1980.

[152] M. M. Pradas, J. L. G. Ribelles, A. S. Aroca, G. G. Ferrer, J. S. Antón, and P. Pissis, "Interaction between water and polymer chains in poly(hydroxyethyl acrylate) hydrogels," *Colloid and Polymer Science*, vol. 279, pp. 323-330, 2001.

[153] C. Pandis, S. Madeira, J. Matos, A. Kyritsis, J. F. Mano, and J. L. G. Ribelles, "Chitosan–silica hybrid porous membranes," *Materials Science and Engineering: C*, vol. 42, pp. 553-561, 2014.

[154] C. Pandis, A. Spanoudaki, A. Kyritsis, P. Pissis, J. C. Rodriguez Hernandez, J. L. Gomez Ribelles, *et al.*, "Water Sorption Characteristics of Poly(2-hydroxyethyl acrylate)/Silica Nanocomposite Hydrogels," *Journal of Polymer Science Part B-Polymer Physics*, vol. 49, pp. 657-668, 2011.

[155] M. Monleon Pradas, M. Salmeron Sanchez, G. Gallego Ferrer, and J. L. Gomez Ribelles, "Thermodynamics and statistical mechanics of multilayer adsorption," *The Journal of chemical physics*, vol. 121, pp. 8524-31, 2004.

[156] D. W. Van Krevelen and K. Te Nijenhuis. (2009).*Properties of Polymers*. In: K. T. Nijenhuis. (Ed)," Cohesive Properties and Solubility," (pp. 189-227). Amsterdam: Elsevier,

[157] R. Ravindra, K. R. Krovvidi, and A. A. Khan, "Solubility parameter of chitin and chitosan," *Carbohydrate Polymers*, vol. 36, pp. 121-127, 1998.

[158] S. Dumitriu,(2001). *Polymeric biomaterials*, [Online]. Retrieved 10 February, 2016, from: http://www.crcnetbase.com/isbn/9780203904671.

[159] K. Okuyama, K. Noguchi, T. Miyazawa, T. Yui, and K. Ogawa, "Molecular and crystal structure of hydrated chitosan," *Macromolecules*, vol. 30, pp. 5849-5855, 1997.

[160] F. S. Kittur, A. B. Vishu Kumar, and R. N. Tharanathan, "Low molecular weight chitosans - Preparation by depolymerization with Aspergillus niger pectinase, and characterization," *Carbohydrate Research*, vol. 338, pp. 1283-1290, 2003.

[161] T. Wanjun, W. Cunxin, and C. Donghua, "Kinetic studies on the pyrolysis of chitin and chitosan," *Polymer Degradation and Stability*, vol. 87, pp. 389-394, 2005.

[162] H. L. Friedman, "Kinetics of thermal degradation of char-forming plastics from thermogravimetry. Application to a phenolic plastic," in *Journal of Polymer Science Part C: Polymer Symposia*, pp. 183-195,1964.

[163] H. E. Kissinger, "Reaction kinetics in differential thermal analysis," *Analytical chemistry*, vol. 29, pp. 1702-1706, 1957.

[164] T. Ozawa, "A new method of analyzing thermogravimetric data," *Bulletin of the*

chemical society of Japan, vol. 38, pp. 1881-1886, 1965.

[165] A. A. Jain, A. Mehra, and V. V. Ranade, "Processing of TGA data: Analysis of isoconversional and model fitting methods," *Fuel*, vol. 165, pp. 490-498, 2016.

[166] D. de Britto and S. P. Campana-Filho, "Kinetics of the thermal degradation of chitosan," *Thermochimica acta*, vol. 465, pp. 73-82, 2007.

[167] S. Vyazovkin, A. K. Burnham, J. M. Criado, L. A. Pérez-Maqueda, C. Popescu, and N. Sbirrazzuoli, "ICTAC Kinetics Committee recommendations for performing kinetic computations on thermal analysis data," *Thermochimica Acta*, vol. 520, pp. 1-19, 2011.

[168] F. Bai, W. Guo, X. Lü, Y. Liu, M. Guo, Q. Li, *et al.*, "Kinetic study on the pyrolysis behavior of Huadian oil shale via non-isothermal thermogravimetric data," *Fuel*, vol. 146, pp. 111-118, 2015.

[169] J. H. Flynn and L. A. Wall, "A quick, direct method for the determination of activation energy from thermogravimetric data," *Journal of Polymer Science Part B: Polymer Letters*, vol. 4, pp. 323-328, 1966.

[170] C. Doyle, "Estimating isothermal life from thermogravimetric data," *Journal of Applied Polymer Science*, vol. 6, pp. 639-642, 1962.

[171] S. Vyazovkin and N. Sbirrazzuoli, "Isoconversional Kinetic Analysis of Thermally Stimulated Processes in Polymers," *Macromolecular Rapid Communications*, vol. 27, pp. 1515-1532, 2006.

[172] J. Šesták and G. Berggren, "Study of the kinetics of the mechanism of solid-state reactions at increasing temperatures," *Thermochimica Acta*, vol. 3, pp. 1-12, 1971.

[173] L. S. Guinesi and E. T. G. Cavalheiro, "The use of DSC curves to determine the acetylation degree of chitin/chitosan samples," *Thermochimica Acta*, vol. 444, pp. 128-133, 2006.

[174] Y. S. Nam, W. H. Park, D. Ihm, and S. M. Hudson, "Effect of the degree of deacetylation on the thermal decomposition of chitin and chitosan nanofibers," *Carbohydrate Polymers*, vol. 80, pp. 291-295, 2010.

[175] H. E. Kissinger, "Variation of the peak temperature with heating rate in differential thermal analysis," *Journal Research of the National Institute of Standards and Technology*, vol. 57, pp. 217-21, 1956.

[176] V. Beachley and X. Wen, "Polymer nanofibrous structures: Fabrication, biofunctionalization, and cell interactions," *Progress in polymer science*, vol. 35, pp. 868-892, 2010.

[177] N. Bhardwaj and S. C. Kundu, "Electrospinning: A fascinating fiber fabrication technique," *Biotechnology Advances*, vol. 28, pp. 325-347, 2010.

[178] D. Liang, B. S. Hsiao, and B. Chu, "Functional electrospun nanofibrous scaffolds for biomedical applications," *Advanced drug delivery reviews*, vol. 59, pp. 1392-1412, 2007.

[179] Z.-M. Huang, Y.-Z. Zhang, M. Kotaki, and S. Ramakrishna, "A review on polymer nanofibers by electrospinning and their applications in nanocomposites," *Composites science and technology*, vol. 63, pp. 2223-2253, 2003.

[180] K. Ohkawa, D. Cha, H. Kim, A. Nishida, and H. Yamamoto, "Electrospinning of chitosan," *Macromolecular Rapid Communications*, vol. 25, pp. 1600-1605, 2004.

[181] K. Ohkawa, K.-I. Minato, G. Kumagai, S. Hayashi, and H. Yamamoto, "Chitosan nanofiber," *Biomacromolecules*, vol. 7, pp. 3291-3294, 2006.

[182] V. Sencadas, D. M. Correia, A. Areias, G. Botelho, A. Fonseca, I. Neves, *et al.*, "Determination of the parameters affecting electrospun chitosan fiber size distribution and morphology," *Carbohydrate Polymers*, vol. 87, pp. 1295-1301, 2012.

[183] P. Sangsanoh and P. Supaphol, "Stability improvement of electrospun chitosan nanofibrous membranes in neutral or weak basic aqueous solutions," *Biomacromolecules*, vol. 7, pp. 2710-2714, 2006.

[184] V. Sencadas, D. M. Correia, C. Ribeiro, S. Moreira, G. Botelho, J. G. Ribelles, *et al.*, "Physical-chemical properties of cross-linked chitosan electrospun fiber mats," *Polymer Testing*, vol. 31, pp. 1062-1069, 2012.

[185] Y. Huang, S. Onyeri, M. Siewe, A. Moshfeghian, and S. V. Madihally, "In vitro characterization of chitosan–gelatin scaffolds for tissue engineering," *Biomaterials*, vol. 26, pp. 7616-7627, 2005.

[186] N. M. Julkapli, Z. Ahmad, and H. M. Akil, "X-Ray Diffraction Studies of Cross Linked Chitosan With Different Cross Linking Agents For Waste Water Treatment Application," in *Neutron and x-ray scattering in advancing materials research: Proceedings of the International Conference on Neutron and X-Ray Scattering* pp. 106-111,2010.

[187] C. d. T. Neto, J. Giacometti, A. Job, F. Ferreira, J. Fonseca, and M. Pereira, "Thermal analysis of chitosan based networks," *Carbohydrate Polymers*, vol. 62, pp. 97-103, 2005.

[188] E. Taboada, G. Cabrera, R. Jimenez, and G. Cardenas, "A Kinetic Study of the Thermal Degradation of Chitosan-Metal Complexes," *Journal of Applied Polymer Science*, vol. 114, pp. 2043-2052, 2009.

[189] P.-Z. Hong, S.-D. Li, C.-Y. Ou, C.-P. Li, L. Yang, and C.-H. Zhang, "Thermogravimetric analysis of chitosan," *Journal of Applied Polymer Science*, vol. 105, pp. 547-551, 2007.

[190] P. Novamatrix. (2011). *"Chitosan Biopolymer, Novamatrix"*. Retrieved 9 February, 2012, from http://www.novamatrix.biz/

[191] L. Zeng, C. Qin, L. Wang, and W. Li, "Volatile compounds formed from the pyrolysis of chitosan," *Carbohydrate Polymers*, vol. 83, pp. 1553-1557, 2011.

[192] F. Scheinmann,. (1979). *An introduction to spectroscopic methods for the identification of organic compounds*. Switzerland: Oxford.

[193] A. Pawlak and M. Mucha, "Thermogravimetric and FTIR studies of chitosan blends," *Thermochimica Acta*, vol. 396, pp. 153-166, 2003.

[194] R. E. Kagarise, "Infrared Spectrum of Trifluoroacetic Acid Vapor," *The Journal of Chemical Physics*, vol. 27, pp. 519-522, 1957.

[195] N. Fuson, M.-L. Josien, E. A. Jones, and J. R. Lawson, "Infrared and Raman Spectroscopy Studies of Light and Heavy Trifluoroacetic Acids," *The Journal of Chemical Physics*, vol. 20, pp. 1627-1634, 1952.

[196] G. Botelho, S. Lanceros-Mendez, A. M. Gonçalves, V. Sencadas, and J. G. Rocha, "Relationship between processing conditions, defects and thermal degradation of poly(vinylidene fluoride) in the β-phase," *Journal of Non-Crystalline Solids*, vol. 354, pp. 72-78, 2008.

[197] H. E. Kissinger, "Reaction Kinetics in Differential Thermal Analysis," *Analytical Chemistry*, vol. 29, pp. 1702-1706, 2002.

[198] J. N. Israelachvili, *Intermolecular and Surface Forces: Revised (Third Edition)*. Amesterdam: Elsevier Science, 2011.

[199] R. T. Sanderson.(1983). *Polar Covalence*. Arizona: Academic Press.

[200] J. Berger, M. Reist, J. M. Mayer, O. Felt, N. A. Peppas, and R. Gurny, "Structure and interactions in covalently and ionically crosslinked chitosan hydrogels for biomedical applications," *European Journal of Pharmaceutics and Biopharmaceutics*, vol. 57, pp. 19-34, 2004.

[201] H. Ç. Arca and S. ŞENEL, "Chitosan based systems for tissue engineering Part 1: Hard tissues," Fabad Journal of Pharmaceutical Sciences, vol. 33, pp. 35-49, 2008.

[202] P. M. Kharkar, K. L. Kiick, and A. M. Kloxin, "Designing degradable hydrogels for orthogonal control of cell microenvironments," *Chemical Society Reviews*, vol. 42, pp. 7335-7372, 2013.

[203] M. N. V. Ravi Kumar, "A review of chitin and chitosan applications," *Reactive and Functional Polymers*, vol. 46, pp. 1-27, 2000.

[204] M. Abedalwafa, F. Wang, L. Wang, and C. Li, "Biodegradable poly-epsilon-caprolactone (PCL) for tissue engineering applications: a review," *Reviews On Advanced Materials Science*, vol. 34, pp. 123-140, 2013.

[205] M. Vert, "Aliphatic polyesters: great degradable polymers that cannot do everything," *Biomacromolecules*, vol. 6, pp. 538-546, 2005.

[206] A. Vidaurre, J. M. M. Dueñas, J. M. Estellés, and I. C. Cortázar, "Influence of Enzymatic Degradation on Physical Properties of Poly (ε-caprolactone) Films and Sponges," in *Macromolecular Symposia*, pp. 38-46, 2008.

[207] D. M. Correia, M. Gámiz-González, G. Botelho, A. Vidaurre, J. G. Ribelles, S. Lanceros-Méndez, *et al.*, "Effect of neutralization and cross-linking on the thermal degradation of chitosan electrospun membranes," *Journal of Thermal Analysis and*

Calorimetry, vol. 117, pp. 123-130, 2014.

[208] N. Kil'deeva, P. Perminov, L. Vladimirov, V. Novikov, and S. Mikhaĭlov, "[Mechanism of the reaction of glutaraldehyde with chitosan]," *Bioorganicheskaia khimiia*, vol. 35, pp. 397-407, 2008.

[209] A. S. Aroca, M. M. Pradas, and J. L. Gómez Ribelles, "Macroporous poly(methyl methacrylate) produced by phase separation during polymerisation in solution," *Colloid and Polymer Science*, vol. 285, pp. 753-760, 2007.

[210] A. J. Campillo-Fernández, M. Salmerón Sánchez, R. Sabater i Serra, J. M. Meseguer Dueñas, M. Monleón Pradas, and J. L. Gómez Ribelles, "Water-induced (nano) organization in poly(ethyl acrylate-co-hydroxyethyl acrylate) networks," *European Polymer Journal*, vol. 44, pp. 1996-2004, 2008.

[211] C. R. Huei and H.-D. Hwa, "Effect of molecular weight of chitosan with the same degree of deacetylation on the thermal, mechanical, and permeability properties of the prepared membrane," *Carbohydrate polymers*, vol. 29, pp. 353-358, 1996.

[212] J. Zawadzki and H. Kaczmarek, "Thermal treatment of chitosan in various conditions," *Carbohydrate Polymers*, vol. 80, pp. 394-400, 2010.

[213] H. S. Mansur, A. A. Mansur, E. Curti, and M. V. De Almeida, "Functionalized-chitosan/quantum dot nano-hybrids for nanomedicine applications: towards biolabeling and biosorbing phosphate metabolites," *Journal of Materials Chemistry B*, vol. 1, pp. 1696-1711, 2013.

[214] J. M. Estellés, A. Vidaurre, J. M. M. Duenas, and I. C. Cortázar, "Physical characterization of polycaprolactone scaffolds," *Journal of Materials Science: Materials in Medicine*, vol. 19, pp. 189-195, 2008.

[215] A. K. Mahanta, V. Mittal, N. Singh, D. Dash, S. Malik, M. Kumar, *et al.*, "Polyurethane-Grafted Chitosan as New Biomaterials for Controlled Drug Delivery," *Macromolecules*, 2015.

[216] A. Di Martino, M. Sittinger, and M. V. Risbud, "Chitosan: A versatile biopolymer for orthopaedic tissue-engineering," *Biomaterials*, vol. 26, pp. 5983-5990, 2005.

[217] S. V. Madihally and H. W. T. Matthew, "Porous chitosan scaffolds for tissue engineering," *Biomaterials*, vol. 20, pp. 1133-1142, 1999.

[218] S.-i. Aiba, "Studies on chitosan: 4. Lysozymic hydrolysis of partially N-acetylated chitosans," *International journal of biological macromolecules*, vol. 14, pp. 225-228, 1992.

[219] E. Mirzaei B, A. Ramazani SA, M. Shafiee, and M. Danaei, "Studies on glutaraldehyde crosslinked chitosan hydrogel properties for drug delivery systems," *International Journal of Polymeric Materials and Polymeric Biomaterials*, vol. 62, pp. 605-611, 2013.

[220] V. Crescenzi, A. Francescangeli, A. Taglienti, D. Capitani, and L. Mannina, "Synthesis and partial characterization of hydrogels obtained via glutaraldehyde

crosslinking of acetylated chitosan and of hyaluronan derivatives," *Biomacromolecules*, vol. 4, pp. 1045-1054, 2003.

[221] X. Liu, L. Ma, Z. Mao, and C. Gao.(2011). "Chitosan-based biomaterials for tissue repair and regeneration". In: R.Jayakumar, M. Prabaharan, R.A.A. Muzzarelli (Ed.), *Chitosan for Biomaterials II*, (pp. 81-127). New York: Springer.

[222] D. M. Garcia Cruz, D. F. Coutinho, E. Costa Martinez, J. F. Mano, J. L. Gómez Ribelles, and M. Salmerón Sánchez, "Blending polysaccharides with biodegradable polymers. II. Structure and biological response of chitosan/polycaprolactone blends," *Journal of Biomedical Materials Research Part B: Applied Biomaterials*, vol. 87, pp. 544-554, 2008.

[223] Y. Xin and J. Yuan, "Schiff's base as a stimuli-responsive linker in polymer chemistry," *Polymer Chemistry*, vol. 3, pp. 3045-3055, 2012.

[224] T. Groth, M. Grøtli, W. D. Lubell, L. P. Miranda, and M. Meldal, "HYDRA: A novel hydroxy and amine functionalised resin synthesised by reductive amination of PEG aldehyde and a polyamine," *Journal of the Chemical Society, Perkin Transactions.vol 1*, pp. 4258-4264, 2000.

[225] U. Shinde, M. H. Ahmed, and K. Singh, "Development of dorzolamide loaded 6-O-carboxymethyl chitosan nanoparticles for open angle glaucoma," *Journal of drug delivery,pp.1-15*, 2013.

[226] A. Ibn Yaich, U. Edlund, and A.-C. Albertsson, "Wood hydrolysate barriers: performance controlled via selective recovery," *Biomacromolecules*, vol. 13, pp. 466-473, 2012.

[227] Crescenz.V, G. Manzini, Calzolar.G, and C. Borri, "Thermodynamics of fusion of poly-beta-propiolactone and poly-epsilon-caprolactone - comparative analysis of melting of aliphatic polylactone and polyester chains," *European Polymer Journal*, vol. 8, pp. 449-454, 1972.

[228] I. Castilla-Cortázar, J. Más-Estellés, J. M. Meseguer-Dueñas, J. L. Escobar Ivirico, B. Marí, and A. Vidaurre, "Hydrolytic and enzymatic degradation of a poly(ε-caprolactone) network," *Polymer Degradation and Stability*, vol. 97, pp. 1241-1248, 2012.

[229] C. Antolinos-Turpín, R. M. Román, J. Rodenas-Rochina, J. G. Ribelles, and J. Gómez-Tejedor, "Macroporous thin membranes for cell transplant in regenerative medicine," *Biomaterials*, vol. 67, pp. 254-263, 2015.

[230] T. C. Gamboa-Martínez, J. Ródenas-Rochina, P. R. Tortosa, M. Lebourg, J. G. L. Ribelles, M. S. Sanchez, *et al.*, "Chondrocytes cultured in an adhesive macroporous scaffold subjected to stirred flow bioreactor behave like in static culture," *Journal of Biomaterials and Tissue Engineering*, vol. 3, pp. 312-319, 2013.

[231] J. Ródenas-Rochina, J. L. G. Ribelles, and M. Lebourg, "Comparative study of PCL-HAp and PCL-bioglass composite scaffolds for bone tissue engineering," *Journal of Materials Science: Materials in Medicine*, vol. 24, pp. 1293-1308, 2013.

[232] A. V. Lluch, G. G. Ferrer, and M. M. Pradas, "Biomimetic apatite coating on P (EMA-co-HEA)/SiO_2 hybrid nanocomposites," *Polymer*, vol. 50, pp. 2874-2884, 2009.

[233] A. Rogina, P. Rico, G. G. Ferrer, M. Ivanković, and H. Ivanković, "In Situ Hydroxyapatite Content Affects the Cell Differentiation on Porous Chitosan/Hydroxyapatite Scaffolds," *Annals of biomedical engineering*, pp. 1-13, 2015.

[234] J. Escobar Ivirico, M. Salmerón-Sánchez, J. Gómez Ribelles, and M. Monleón Pradas, "Poly(l-lactide) networks with tailored water sorption," *Colloid and Polymer Science*, vol. 287, pp. 671-681, 2009.

[235] E. S. Dragan, "Design and applications of interpenetrating polymer network hydrogels. A review," *Chemical Engineering Journal*, vol. 243, pp. 572-590, 2014.

[236] R. Sabater i Serra, A. Kyritsis, J. Escobar Ivirico, A. Andrio Balado, J. Gómez Ribelles, P. Pissis, *et al.*, "Structure and dynamics in poly(L-lactide) copolymer networks," *Colloid and Polymer Science*, vol. 288, pp. 555-565, 2010.

[237]J. L. Escobar Ivirico, M. Salmerón Sánchez, R. Sabater i Serra, J. M. Meseguer Dueñas, J. L. Gómez Ribelles, and M. Monleón Pradas, "Structure and Properties of Poly(ε-caprolactone) Networks with Modulated Water Uptake," *Macromolecular Chemistry and Physics*, vol. 207, pp. 2195-2205, 2006.

[238] A. S. Aroca, M. M. Pradas, and J. G. Ribelles, "Effect of crosslinking on porous poly (methyl methacrylate) produced by phase separation," *Colloid and Polymer Science*, vol. 286, pp. 209-216, 2008.

[239] H. Tsuji, T. Ono, T. Saeki, H. Daimon, and K. Fujie, "Hydrolytic degradation of poly (ε-caprolactone) in the melt," *Polymer degradation and stability*, vol. 89, pp. 336-343, 2005.

[240] K. Knop, R. Hoogenboom, D. Fischer, and U. S. Schubert, "Poly (ethylene glycol) in drug delivery: pros and cons as well as potential alternatives," *Angewandte Chemie International Edition*, vol. 49, pp. 6288-6308, 2010.

[241] G. D. Nicodemus and S. J. Bryant, "Cell encapsulation in biodegradable hydrogels for tissue engineering applications," *Tissue Engineering Part B: Reviews*, vol. 14, pp. 149-165, 2008.

[242] J. Elisseeff, W. McIntosh, K. Anseth, S. Riley, P. Ragan, and R. Langer, "Photoencapsulation of chondrocytes in poly (ethylene oxide)-based semi-interpenetrating networks," *Journal of biomedical materials research*, vol. 51, pp. 164-171, 2000.

[243] S. J. Bryant and K. S. Anseth, "Controlling the spatial distribution of ECM components in degradable PEG hydrogels for tissue engineering cartilage," *Journal of biomedical materials research Part A*, vol. 64, pp. 70-79, 2003.

[244] K. L. Spiller, S. A. Maher, and A. M. Lowman, "Hydrogels for the repair of articular cartilage defects," *Tissue engineering part B: reviews*, vol. 17, pp. 281-299, 2011.

[245] C. G. Williams, T. K. Kim, A. Taboas, A. Malik, P. Manson, and J. Elisseeff, "In vitro chondrogenesis of bone marrow-derived mesenchymal stem cells in a photopolymerizing hydrogel," *Tissue engineering*, vol. 9, pp. 679-688, 2003.

[246] Y. F. Poon, Y. Cao, Y. Liu, V. Chan, and M. B. Chan-Park, "Hydrogels based on dual curable chitosan-graft-polyethylene glycol-graft-methacrylate: application to layer-by-layer cell encapsulation," *ACS Applied Materials & Interfaces*, vol. 2, pp. 2012-2025, 2010.

[247] E. Bakaic, N. M. Smeets, and T. Hoare, "Injectable hydrogels based on poly (ethylene glycol) and derivatives as functional biomaterials," *RSC Advances*, vol. 5, pp. 35469-35486, 2015.

[248] S. P. Zustiak and J. B. Leach, "Hydrolytically degradable poly (ethylene glycol) hydrogel scaffolds with tunable degradation and mechanical properties," *Biomacromolecules*, vol. 11, pp. 1348-1357, 2010.

[249] N. Vasylieva, B. Barnych, A. Meiller, C. Maucler, L. Pollegioni, J.-S. Lin, *et al.*, "Covalent enzyme immobilization by poly (ethylene glycol) diglycidyl ether (PEGDE) for microelectrode biosensor preparation," *Biosensors and Bioelectronics*, vol. 26, pp. 3993-4000, 2011.

[250] R. Pauliukaite, M. E. Ghica, O. Fatibello-Filho, and C. M. Brett, "Comparative study of different cross-linking agents for the immobilization of functionalized carbon nanotubes within a chitosan film supported on a graphite□ epoxy composite electrode," *Analytical Chemistry*, vol. 81, pp. 5364-5372, 2009.

[251] H.-C. Ge and D.-K. Luo, "Preparation of carboxymethyl chitosan in aqueous solution under microwave irradiation," *Carbohydrate research*, vol. 340, pp. 1351-1356, 2005.

[252] A. Svärd, E. Brännvall, and U. Edlund, "Rapeseed straw as a renewable source of hemicelluloses: Extraction, characterization and film formation," *Carbohydrate Polymers*, vol. 133, pp. 179-186, 2015.

[253] B. Satheesh, K. Tshai, and N. Warrior, "Effect of Chitosan Loading on the Morphological, Thermal, and Mechanical Properties of Diglycidyl Ether of Bisphenol A/Hexamethylenediamine Epoxy System," *Journal of Composites*, pp.1-8, 2014.

[254] W. Zhao, L. Glavas, K. Odelius, U. Edlund, and A.-C. Albertsson, "Facile and Green Approach towards Electrically Conductive Hemicellulose Hydrogels with Tunable Conductivity and Swelling Behavior," *Chemistry of Materials*, vol. 26, pp. 4265-4273, 2014.

[255] H. Kono, "Characterization and properties of carboxymethyl cellulose hydrogels crosslinked by polyethylene glycol," *Carbohydrate polymers*, vol. 106, pp. 84-93, 2014.

[256] D. Enescu, V. Hamciuc, L. Pricop, T. Hamaide, V. Harabagiu, and B. C. Simionescu, "Polydimethylsiloxane-modified chitosan I. Synthesis and structural characterisation of graft and crosslinked copolymers," *Journal of Polymer Research*, vol. 16, pp. 73-80,

2009.

[257] I. Aranaz, R. Harris, and A. Heras, "Chitosan amphiphilic derivatives. Chemistry and applications," *Current Organic Chemistry*, vol. 14, p. 308, 2010.

[258] M. Rinaudo, P. Le Dung, C. Gey, and M. Milas, "Substituent distribution on O, N-carboxymethylchitosans by 1H and 13C NMR," *International journal of biological macromolecules*, vol. 14, pp. 122-128, 1992.

[259] S. Saladinoa, E. R. Di Leonardoa, M. Salamoneb, D. Mercuric, F. Segattic, and G. Ghersi, "Formulation of Different Chitosan Hydrogels for Cartilage Tissue Repair," *Chemical Engineering Transactions, vol. 38, pp. 505-510, 2014.*

[260] S. Jabeen, S. Saeed, A. Kausar, B. Muhammad, S. Gul, and M. Farooq, "Influence of Chitosan and Epoxy Cross Linking on Physical Properties of Binary Blends," *International Journal of Polymer Analysis and Characterization,vol. 21, pp. 163-174*, 2015.

[261] M. E. S. Miranda, C. Marcolla, C. A. Rodrígues, H. M. Wilhelm, M. R. Sierakowski, T. M. B. Bresolin, *et al.*, "Chitosan and N-carboxymethylchitosan: I. The role of N-carboxymethylation of chitosan in the thermal stability and dynamic mechanical properties of its films," *Polymer International*, vol. 55, pp. 961-969, 2006.

[262] L. Gao, H. Gan, Z. Meng, R. Gu, Z. Wu, L. Zhang, *et al.*, "Effects of genipin cross-linking of chitosan hydrogels on cellular adhesion and viability," *Colloids and Surfaces B: Biointerfaces*, vol. 117, pp. 398-405, 2014.

[263] A. J. Engler, S. Sen, H. L. Sweeney, and D. E. Discher, "Matrix elasticity directs stem cell lineage specification," *Cell*, vol. 126, pp. 677-689, 2006.

[264] H. Tan, C. R. Chu, K. A. Payne, and K. G. Marra, "Injectable in situ forming biodegradable chitosan–hyaluronic acid based hydrogels for cartilage tissue engineering," *Biomaterials*, vol. 30, pp. 2499-2506, 2009.

Chapter 9. Publications

Publications

Related to this thesis

Published articles

D. M. Correia, M. A. Gámiz- González, G. Botelho, A. Vidaurre, J. L. Gomez Ribelles, S. Lanceros-Mendez and V. Sencadas.
Effect of neutralization and cross-linking on the thermal degradation of chitosan electrospun membranes. Journal of Thermal Analysis and Calorimetry 123,130–117 (2014).

M. A. Gámiz-González., A. E. Piskin, C. Pandis., C. Chatzimanolis-Moustakasb, A. Kyritsisb, B. Marí, J. L. Gómez Ribelles., A. Vidaurrea. Determining the influence of N-acetylation on water sorption in chitosan films. Carbohydrate Polymers. 133,110–116 (2015).

Articles under preparation

M. A. Gámiz-González , A. Vidaurre and J. L. Gómez Ribelles. Biodegradable chitosan-poly (ε-caprolactone) copolymer networks.

M. A. Gámiz-González, P. Guldris, C. M. Antolinos Turpín, J. Ródenas Rochinaa, A. Vidaurre,and J. L. Gómez Ribelles. Fast degrading polymer networks based on Carboxymethyl Chitosan.

M. A. Gámiz-González, Ulrica Edlund, A. Vidaurre,and J. L. Gómez Ribelles. Synthesis of highly swellable hydrogels of water-soluble Carboxymethyl chitosan and Poly (ethylene glycol).

Conferences

Gamiz Gonzalez, Mª Amparo; Gómez, Julia; Vidaurre, Ana; Gómez Ribelles, José Luís. Improved biodegradation of CmCHT-PCL networks for biomedical applications.(Poster)
Jornadas: 2015 CIBER-BBN ANNUAL CONFERENCE.
Valencia, (Spain), 30–11–2015.

Gamiz Gonzalez, Mª Amparo; Guldris Padra, Paula; Vidaurre, Ana; Gómez Ribelles, José Luís. Biodegradable cross-linked Carboxymethyl chitosan with Poly(ε-caprolactone) netwroks. (Poster).
I Congreso Biomedicina Predocs. Valencia,(Spain), 28–11–2014.

Gámiz González, Mª Amparo; C Pandis; Christos Chatzimanolis; Vidaurre, Ana; Gómez Ribelles, José Luís; A. Kyritsis. Eco-sustainable Food Packaging Based on Polymer Nanomaterials.(Oral communication)
International Workshop COST Action FA0904. Eco-sustainable Food Packaging Based on Polymer Nanomaterials. Roma, 28–02–2014.

Mª Amparo Gámiz González; Ana Jesús Vidaurre Garayo; José Luís Gómez Ribelles
Characterization and enzymatic degradation of chitosan scaffolds with different degree of deacetylation (Oral communication).
25th European Conference on Biomaterials (ESB 2013). Madrid (Spain), 12–09–2013.

Non- directly related to this thesis

Published articles

Marqués-Gallego P, Gamiz-Gonzalez MA, Fortea-Pérez FR, Lutz M, Spek AL, Pevec A, Kozlevar B, Reedijk J. Quinoxaline-2-carboxamide as a carrier ligand in two new platinum(II) compounds: Synthesis, crystal structure, cytotoxic activity and DNA interaction. Dalton Transactions39, 5152-5158 (2010).

Conferences

Christos Pandis; Christos Chatzimanolis; Mª Amparo Gámiz González; Ana Jesús Vidaurre Garayo; José Luís Gómez Ribelles; Apostolos Kyritsis. Chitosan Electrospun Nanofibers for Gas Sensing Applications.(Poster)
1st International Workshop on Electrospinning for High Performance Sensing (EHPS 2014). Monterotondo, Roma (Italy), 30–04–2014.

Sara Martorell Tejedor; María Sánchez Tello; Noemi Teresa Rojas Lara, Tatiana Carolina Gamboa Martínez, Mª Amparo Gámiz González, JJ Martín Del Llano, Ana Jesús Vidaurre Garayo, Gloria Gallego Ferrer, José

Luís Gómez Ribelles, Carmen Carda Batalla
Tissue Engineerig: Chitosan for Articular Cartilage Regeneration. (Poster)
XVII Congreso Nacional de la Sociedad Española de Histología e Ingeniería Tisular. Logroño (Spain),14–09–2013.

Mª Amparo Gámiz González; Tatiana Gamboa Martínez; Irene Tarraso Urios;Vitor Sencadas; Clarrise Ribeiro; Senentxu Lanceros-Mendez; Ana Jesús Vidaurre Garayo; José Luís Gómez Ribelles.Improvement of cellular adhesion in chitosan electrospun membranes. (Poster).
25th European Conference on Biomaterials (ESB 2013) Madrid (Spain), 12–09–2013.